FEASIBILITY AND BENEFITS OF LAMINAR FLOW CONTROL ON SUPERSONIC CRUISE AIRPLANES

A.G. Powell

McDonnell Douglas Corporation
Douglas Aircraft Company
Long Beach, California 90846

S. Agrawal
T.R. Lacey

McDonnell Douglas Corporation
McDonnell Aircraft Company
St. Louis, Missouri 63166

NASA
National Aeronautics and
Space Administration

Langley Research Center
Hampton, Virginia 23665-5225

FOREWORD

This document covers the contract work performed by the Douglas Aircraft Company and the McDonnell Aircraft Company of the McDonnell Douglas Corporation, on Laminar Flow Control (LFC) under NASA Contract NAS1-18037 entitled "Study of Supersonic Laminar Flow Aerodynamics". This contract is part of an overall effort to improve the energy efficiency of a wide range of airplane types, supported by NASA through its Langley Research Center.

Acknowledgement for their support and guidance is given to Mr. R.D. Wagner, NASA LFC Project Manager, to Mr. D.V. Maddalon, the NASA Contract Manager, and also to Drs. W. Pfenninger, F.S. Collier, and C. Vemuru.

The Douglas personnel primarily responsible for this work were:

Mr. M. Klotzsche	Director, CRAD Programs
Dr. A.G. Powell	Principal Investigator, Aerodynamics
Mr. A.A. Killeen	Aerodynamics
Mr. W.E. Herr	Aerodynamics

The McDonnell personnel primarily responsible for this work were:

Mr. T.R. Lacey	Branch Chief, Aerodynamics Technology
Dr. S. Agrawal	Lead Engineer, Aerodynamics
Mr. T.A. Kinard	Aerodynamics

The McDonnell Douglas Research Laboratories personnel involved in a consultory capacity were:

Dr. A.B. Cain	Scientist, Aerodynamics Research

PRECEDING PAGE BLANK NOT FILMED

CONTENTS

FIGURES

1. SUMMARY

This report details the results of a preliminary investigation into the application of Laminar Flow Control (LFC) technology to Supersonic cruise airplanes. The objectives of this study were: (1) to determine the applicability and realistic benefit potential of LFC technology on a representative supersonic transport, (2) to determine the applicabilty of LFC to other supersonic airplane types, (3) to identify the technical issues critical to supersonic LFC application, (4) to determine how those issues can be addressed through flight and wind-tunnel testing, and (5) to make recommendations for a future development program.

Vehicle types studied include an advanced supersonic transport configuration designed for transpacific range at 2.2 Mach, a Mach 4.0 transport, and two generic supersonic-cruise fighter concepts. These are shown in figure 1.1. Laminar flow control methodologies developed for subsonic and transonic wing laminarization have been applied and in some cases modified; the results are presented in this report.

For the wing of the Mach 2.2 supersonic transport, it was found that attachment line conditions could be made acceptable with moderate suction. Upper and lower surface suction to the control surface hingeline has been found to be the preferred LFC approach due to the large wing chords, the absence of midchord shocks, and the relatively even benefit split between upper and lower surfaces. Suction requirements were found to strongly depend on the wing pressure distribution. Accelerating chordwise pressure distributions were found to be detrimental to laminarization due to associated cross-stream pressure gradients and the resulting boundary layer crossflow. The lowest required suction levels were found for distributions characterized by spatially rapid flow acceleration in the leading edge region followed by a nearly constant-velocity rooftop. Realistic L/D improvements in the range of 12 to 17 percent were found for the DAC Advanced Supersonic Transport.

For the Mach 4 High-Speed Commercial Transport (HSCT) design considered, attachment line conditions were found to prohibit laminar flow. Thermal management and boundary layer stability considerations make this vehicle an impractical candidate for laminarization.

The McAir SF-1107 and SF-1302 generic supersonic cruise fighter configurations were found to be relatively easy to laminarize, but showed small sizing benefits, due to their short mission ranges.

It is concluded that LFC technology is applicable to supersonic cruise airplanes of the Mach 2 class, even ones of large size. No intractable aerodynamic problems have been identified as a result of this study. Several key technical issues, such as contamination avoidance and excresence criteria have been identified, and should be persued further through analysis and research testing in wind tunnels and flight.
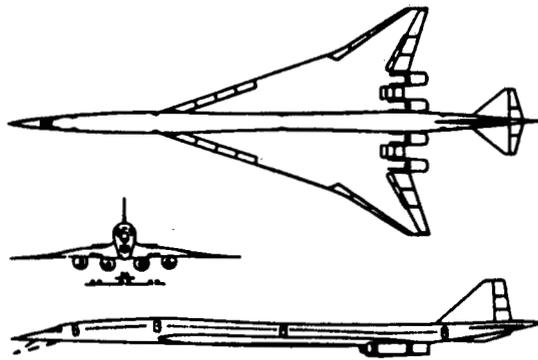
DAC D3233-2.2-1C AST
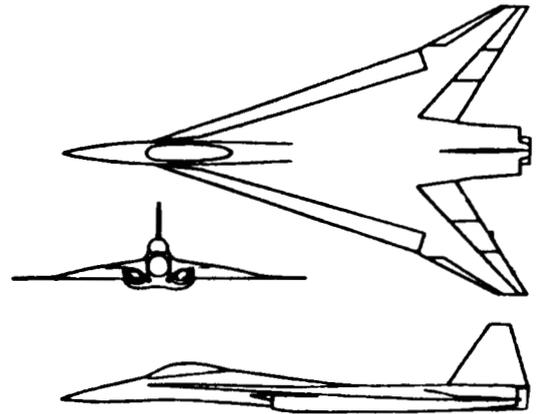
McAIR SF-1302 FIGHTER
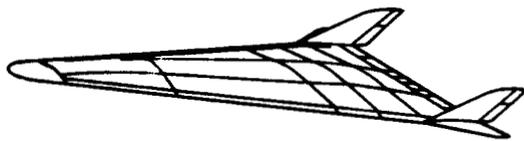
DAC MACH 4 HSCT
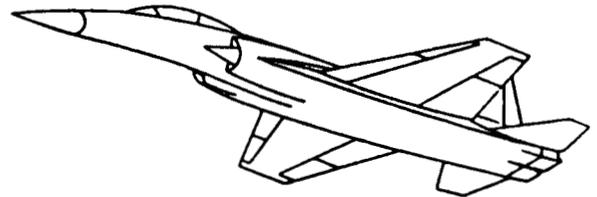
McAIR SF-1107 FIGHTER

Figure 1.1   MDC SUPERSONIC LFC STUDY CONFIGURATIONS

2. INTRODUCTION

The high fuel fractions typical of long range airplanes give increased leverage to cruise drag minimization technologies, such as Laminar Flow Control (LFC), in terms of size, weight, and perhaps even vehicle cost. Current projections show increased traffic for certain distant city pairs, particularly on the Pacific Rim[1]. For many of these, subsonic travel times are sufficiently long to warrant interest in supersonic flight.

Subsonic LFC technology development has been ongoing for many years, and many excellent papers have been written describing progress made in this area[2,3,4]. Improvements in the computation of inviscid and viscous flows and in predicting transition have allowed an expansion of the knowledge base from that of the X-21 program in the early and mid 60s. For example, the NASA Leading Edge Flight Test program established the practicality of systems designed to protect the critical wing leading edge region from contamination in day-to-day service, and demonstrated the efficacy of electron-beam perforated wing skins for boundary layer stabilization using suction[4].

The application of LFC technology to supersonic airplanes has received far less attention. Supersonic wind tunnel investigations have established the feasibility of achieving substantial runs of laminar flow using wall suction[5,6,7]. The effectiveness of the linear theory transition prediction methods has been demonstrated over a wide Mach number range for a variety of geometries[8]. However, the feasibilty and performance benefits of laminarizing supersonic cruise airplanes have not been established.

This report describes a first attempt at addressing the aerodynamic problems associated with applying LFC technology to the wings of supersonic cruise airplanes. The study considered both supersonic and subsonic leading-edge wing designs. The feasibility of laminarizing such wings and the aerodynamic benefits of doing so are addressed.

The process of determining the laminarization potential and benefit for a specific configuration at a particular flight condition requires the accurate computation of both the outer inviscid flowfield and the boundary layer. Specific criteria are applied to determine if the boundary layer can be stabilized and transition delayed to the extent desired. Of the various methods proposed for laminar boundary layer stabilization, low-level wall suction has proven to be the most versatile and practical in most instances. The minimum level of suction required for laminar boundary layer stabilization must be determined, and is a strong function of the pressure distribution imposed by the external flowfield. The iterative procedure involved in the determination of the required suction distribution is shown in figure 2.1.

Current capabilities in laminar flow control have been largely built upon the NASA Langley program to develop laminar boundary layer stability codes such as SALLY[9], MARIA[10], and COSAL[11]. These and other analytical tools available at the time of this study are summarized in figure 2.2.

3
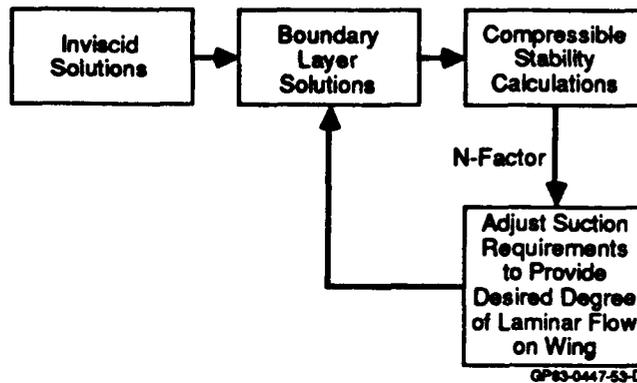
Figure 2.1   PROCEDURE FOR PREDICTING TRANSITION AND SUCTION
LAMINARIZATION REQUIREMENTS

CODE TYPE	DESCRIPTION	USES
OUTER INVISCID FLOW		
FLO-67	EULER WING/BODY, SUBSONIC/SUPERSONIC	PRESSURE DISTRIBUTIONS
BOD-60	EULER WING/BODY, SUBSONIC/SUPERSONIC	PRESSURE DISTRIBUTIONS
SCRAM	EULER WING/BODY, MARCHING SUPERSONIC	INTEGRATED FORCES
BOUNDARY LAYER		
KAUPS-CEBECI	COMPRESSIBLE, LAMINAR ONLY, SUCTION ALLOWED, CONICAL APPROXIMATION TO 3-D	VELOCITY PROFILES FOR STABILITY ANALYSIS
BLP	COMPRESSIBLE, LAMINAR AND TURBULENT 2-D STRIP WITH SUCTION	SKIN FRICTION DRAG, B.L. DISPLACEMENT EFFECTS
LAMINAR BOUNDARY LAYER STABILITY		
SALLY	INCOMPRESSIBLE, T-S AND CF	NOT USED, COSAL PREDECESSOR
MARIA	INCOMPRESSIBLE, APPROXIMATE, STATIONARY CF ONLY	PRELIMINARY SUCTION ESTIMATES
COSAL	COMPRESSIBLE, T-S AND CF	SUCTION MINIMIZATION

Figure 2.2   COMPUTER CODES

4

Of the codes listed, the FLO-67 Euler[12], the Kaups-Cebeci boundary layer[13], and the COSAL boundary layer stability code were used the most extensively. The MARIA crossflow stability code, although incompressible and approximate, was used to identify critical stationary crossflow waves, and to get an initial idea of the suction levels required in the leading-edge region. With the exception of the COSAL code, the application of these codes to the supersonic case required a certain amount of caution and some development, as they were written principally for the transonic case. For the supersonic case, potential codes, such as FLO-22, were excluded, due to their inherent inability to properly account for shock waves.

3. SYMBOLS AND ABBREVIATIONS

A/C   Aircraft, aerodynamic center

α, ALPHA   Angle of attack

AMRAAM   Advanced, Medium Range Air-To-Air Missile

AR   Aspect ratio

AST   Advanced Supersonic Transport

B.L.   Referring to the boundary layer

C   Chord, local wing chord

$\bar{C}$ Average chord, mean geometric chord

CAP   Combat Air Patrol mission

CF   Referring to boundary-layer crossflow or crossflow waves

C_F Skin-friction coefficient

CFX   Skin-friction coefficient component in radial coordinate direction, positive away from virtual tip of tapered wing as used in the Kaups-Cebeci (K-C) code

CFZ   Skin-friction coefficient component in circumferential direction, positive aft from leading edge of tapered wing as used in the K-C code

CP, C_p Pressure coefficient

C_p'' Second derivative of pressure coefficient with respect to X/C.

CPR   Referring to compressor

C_q Suction coefficient: ratio of wall suction massflux to freestream massflux

DAC   Douglas Aircraft Company, Long Beach, Ca.

D   Drag force

D_p Drag due to pressures acting on body

7

D_{ram}	Drag due to destruction of freestream momentum of captured suction air
D_{total}	Total drag force
D_v	Drag due to net effect of viscous shears acting on body
D_w	Drag computed from wake momentum deficit
DELSTX	Boundary layer displacement thickness associated with radial component velocity profile, as used in the K-C code
EM	Energy maneuverability
η, ETA	Semispan fraction ,dimensionless normal coordinate in boundary layer, or efficiency
η_{ps}	Pumping system efficiency: ratio of nozzle thrust power to compressor input shaft power
F	Physical frequency
FF	Fuel fraction: fraction of airplane takeoff gross weight due to fuel
h_{01}	Height in boundary layer at which the crossflow velocity is one-hundredth of its maximum value
h_p, ALT	Pressure altitude
HSCT	High-Speed Commercial Transport
K-C	Referring to the Kaups-Cebeci conical laminar boundary layer code
L.E.	Leading edge of wing
LFC	Laminar Flow Control
L/D	Lift-to-drag ratio
L.S.	Referring to the wing lower surface
λ_1	Leading-edge sweep angle
λ_2	Trailing-edge sweep angle
M	Mach number, million
$\dot{M}$	Mass flowrate
McAir	McDonnell Aircraft Company, St. Louis, Mo.

N, N-factor	Natural log of the ratio of local amplitude to that at the neutral stability point, for a hypothetical boundary layer wave
NL sust	Maximum sustained load factor for given altitude and Mach conditions
NOZ	Referring to exhaust nozzle
P_{in}, P_{pump}	LFC compressor input shaft power
PSFC	Power specific fuel consumption; fuel flowrate per unit of output shaft power
P_s	Specific excess power; maximum available steady-state climb rate at a given Mach number and altitude
PSI, ψ	local orientation angle in a plane parallel to the surface bounding the flow, measured from the direction of the local boundary layer external velocity vector
P_t	Total pressure; isentropic stagnation pressure
q	Dynamic pressure
R, Re	Reynolds number
RC, R_c	Reynolds number based on freestream conditions and local chord
Re_{cf}	Crossflow Reynolds number; Reynolds number based on maximum crossflow velocity, h_{01} as defined above, and local external fluid properties
R_θ, Rtheta	Momentum-thickness Reynolds number; Reynolds number based on freestream velocity, local external fluid properties, and local boundary layer momentum thickness
R_θ N=9	Momentum-thickness Reynolds number at a point where a particular hypothetical boundary layer wave has reached an amplification factor of 9
S, SW	Wing gross planform area
T/C, t/c	Wing section thickness/chord ratio
θ	Local boundary layer momentum thickness, angular coordinate in the K-C code
TOGW	Airplane takeoff gross weight
T-S	Referring to Tollmien-Schlichting waves

TSFC	Engine thrust-specific fuel consumption; fuel flowrate per unit of net thrust
T/W	Airplane thrust/weight ratio
u	Boundary-layer velocity component in the radial direction on a linearly tapered wing; positive away from the virtual wingtip
u''	Second derivative of u with respect to distance measured normal to the local wing surface
U_E, U_e	Radial velocity component at the boundary layer edge
U.S.	Referring to the wing upper surface
w	Boundary-layer velocity component in the circumferential direction on a linearly tapered wing; positive away from the attachment line along an arc at fixed distance from the virtual wingtip
v, V	Boundary layer local total velocity, generalized velocity, or freestream velocity
v	Local crossflow velocity; boundary layer velocity component in a direction perpendicular to the total edge velocity
V_E	Total boundary layer edge velocity
V_e	LFC pumping system exit velocity
V_i	LFC pumping system inlet velocity
V_{fs}, U_{fs}	Freestream velocity
v_{max}	Maximum crossflow velocity
WEUFS	Velocity ratio W_E/U_{fs}, as used in the K-C code
W/S	Airplane wing loading
W.T.	Referring to wind tunnel
X/C	Local chord fraction
XLENC	Wavelength/chord ratio, as used in the COSAL code
y	Distance in a direction normal to the wing surface
$Y_{.95}$	distance y above the wing surface at which the boundary layer total velocity is .95 of its edge value

SL/MAX   Referring to maximum thrust conditions at sea level

20/MAX   Referring to maximum thrust conditions at 20 kft

30/MAX   Referring to maximum thrust conditions at 30 kft

4. LAMINARIZATION CONSIDERATIONS

The external and boundary layer flows over a swept wing are highly three-dimensional. On a swept wing there are many mechanisms which can cause early transition of the boundary layer. These are summarized in figure 4.1. The first category is what Morkovin calls "bypass mechanisms"[14]. This includes freestream turbulence, surface excresences, noise, vibration, and pre-existing turbulence created at points upstream. The absence of these mechanisms is a prerequisite for laminar flow to exist, so they are listed first. From a practical standpoint, wing surface contamination from accreted insect remains and bird droppings pose a potentally great threat to laminarization. The penalties increase inversely with aspect ratio, since turbulent wedges caused by accreted excrescences occupy larger areas on low aspect wings.

Along the attachment line of a swept wing, where the normal flow stagnates, there exists a boundary layer caused by the spanwise flow. If the leading-edge radius and sweep are constant, this boundary layer will have congruent mean flow profiles at all span stations. This boundary layer can be stable as a laminar layer, can be laminar but unstable to disturbances, or can be turbulent. If the laminar boundary layer is unstable to disturbances, turbulence from some point inboard can propagate outward along the leading edge, making laminar flow over the affected part of the wing impossible. Boundary layer waves can also cause transition in the flow along the attachment line. This is the Tollmien-Schlichting mechanism, and is discussed below. A useful stability criterion given by Bacon and Pfenninger[15] for an attachment line boundary layer is the value of the momentum-thickness Reynolds number, R_θ. Typical critical values used in the transonic regime are 100, as the upper limit for a stable laminar attachment line, and 240 as the upper limit for a laminar attachment line in the absence of disturbances.

Boundary layer crossflow - i.e. twisted velocity profiles caused by cross-stream pressure gradients, is a common condition in regions of acceleration on a swept wing and is a potential cause of early transition. Consider the projection of such a twisted velocity profile onto a plane at some arbitrary azimuthal direction, but parallel to the surface, as shown in figure 4.2. For large angles relative to the external flow direction, approaching 90 degrees, these projected profiles can be highly inflectional. Such profiles are known to be unstable, amplifying boundary layer waves in the direction of the inflected profile. These "crossflow waves" are actually co-rotating vortices within the boundary layer. They can rapidly grow to sufficient strength to influence, and interact with their neighbors, causing transition.

13

The Tollmien-Schlichting waves observed in 2-D and axisymmetric flows result from a type of instability which can exist in the absence of pressure gradients. The instability mechanism has been described by Morkovin as a resonance between local and instantaneous pressure and vorticity fields within the boundary layer. This "viscous-tuned" mechanism does not require inflectional velocity profiles, but is very sensitive to profile shape, particularly in the near-wall region, with more convex profiles being more stable than weak ones. Stabilizing the boundary layer against this mechanism requires generally lower wall suction than for the inflectional crossflow mechanism. The temperature and viscosity profiles created by viscous heating in high-speed flows weaken the mechanism substantially, lowering suction requirements still further. Favorable streamwise pressure gradients result in full profiles, so are stabilizing unless they are associated with significant cross-stream gradients, as is typically the case with swept wings. Presumably, in a three-dimensional flow this mechanism applies to component profiles as well as streamwise ones, muddling the traditional distinction between T-S and crossflow waves. Like crossflow waves, when T-S waves grow to the point of interacting with their neighbors, transition is imminent.

The distinction between crossflow and Tollmien-Schlichting waves is of much less practical importance, in the author's view, than the distinction between "inflectional" and "viscous-tuned" instability mechanisms as described by Morkovin, owing to the potentially large differences in wall suction required for boundary layer stabilization, and the effects of Mach number. Inflectional instability, such as found in 3-D flows in regions of strong boundary layer crossflow and in 2-D flows in regions of adverse pressure gradient, is known to require higher suction levels to suppress than does viscous-tuned instability on a 2-D flat plate at the same Reynolds and Mach number. As noted above, the temperature and viscosity profiles in high-speed boundary layers have a significant stabilizing effect on the viscous-tuned instability mechanism, but have much less effect on the inflectional mechanism[14]. This is because the viscous-tuned mechanism depends exclusively on conditions in the near-wall region, whereas the inflectional mechanism depends on conditions which can exist much higher up in the boundary layer. In the near-wall region the effect of suction on profile shape is largest, and the effect of Mach number on local temperature (and viscosity) is highest.

Gortler vortices are counter-rotating, streamwise vortices which are caused by a centrifugal instability mechanism due to concave streamwise wall curvature. These too can intensify to the point of causing transition. They are not a problem if the wall curvature is convex or flat.

The wings of supersonic cruise airplanes can be divided into two types, in terms of the value of the leading edge normal component of Mach number: those whose leading-edge-normal Mach numbers are less than one are said to have subsonic leading edges, while those whose leading edges are exposed to supersonic normal flow are said to have supersonic leading edges.

The sigificance of this distinction is that for the subsonic leading edge, pressure information of a wing section's imminent approach is signalled from stations inboard and upstream, allowing the air to change direction gradually and pass around the leading edge isentropically. For a lifting wing, the upwash caused by stations inboard and upstream of a wing section can be capitalized upon. Essentially this allows low pressures to act on forward facing surfaces, giving potentially much lower drag due-to-lift at supersonic speeds[16]. For wings having supersonic leading edges, this so-called "leading-edge thrust" is absent, giving the drag coefficient a tangent dependence on angle of attack, similar to a separated flat plate in subsonic flow. Compromises to low-speed performance and handling cause most supersonic cruise wing designs to be a combination of these two types.

Subsonic and supersonic leading-edged wings are compared in figure 4.3, in terms of laminarization issues. Of the two, the supersonic leading-edged wing has much more favorable conditions at the leading edge, due to the very small radius. The fact that sweep plays only a small role in the drag due-to-lift of this type of wing means that the leading-edge sweep does not have to be large. The attachment line travel with angle of attack is very small, so it is very easy to satisfy the attachment line momentum thickness Reynolds number criterion of Bacon & Pfenninger over a wide angle of attack range. Any leading-edge acceleration region would be extremely short in physical length, so stationary crossflow would not be expected to present problems. The chordwise pressure distribution for a section in a supersonic leading-edged wing is largely driven by the streamwise contour: slab-sided sections, such as the modified double wedge, give stepped pressure distributions with narrow regions of acceleration between the steps, and convex surfaces give smoothly accelerating pressure distributions. In the absence of sweep, an accelerating chordwise pressure distribution acts to stabilize boundary layer velocity profiles and extend laminar run. For the swept wing case, any chordwise pressure gradient has an associated cross-stream component, so boundary layer destabilization by crossflow is a potential problem.

For the subsonic leading-edged wing, the attachment line has high sweep (inside the Mach cone) and nonzero leading-edge radius. This could give rise to unacceptably large values of attachment-line momentum-thickness Reynolds number, requiring locally high suction levels[15]. The acceleration immediately downstream of the attachment line takes place in the most highly swept region of the wing, resulting in potentially powerful boundary-layer crossflow. High levels of suction may be required in this region as a result. For a Subsonic leading edge, the drag penalty for leading-edge bluntness is small. The use of a blunt leading-edge gives freedom in designing the wing pressure distribution to minimize total suction flow while providing for structurally desirable local section thickness, and additional room for suction ducting.

OBSTACLES TO LAMINARIZATION

1. "BYPASS" MECHANISMS : SEPARATION
                        NOISE
                        ROUGHNESS (BUGS, ICE, etc)
                        WAVINESS
                        etc

2. ATTACHMENT LINE : TURBULENCE PROPAGATION
                     LAMINAR STABILITY

3. CROSSFLOW WAVES (INFLECTIONAL INSTABILITY)

4. T-S WAVES (VISCOUS INSTABILITY)

5. GORTLER VORTICES (CONCAVE FLOW REGIONS)

Figure 4.1   OBSTACLES TO LAMINARIZATION
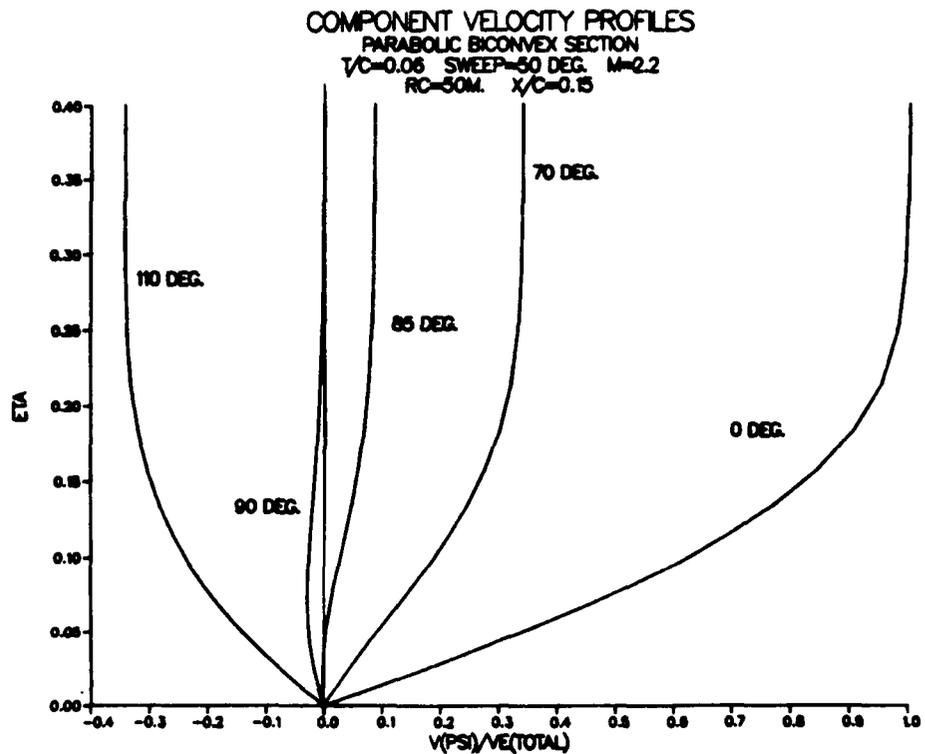
Figure 4.2   COMPONENT VELOCITY PROFILES

16
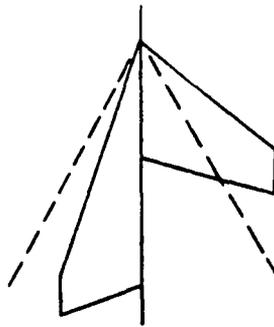
CONSIDERATION	SUBSONIC LEADING EDGE	SUPERSONIC LEADING EDGE
LEADING-EDGE THRUST	YES	NO
HI-SPEED A/C SHIFT	NO	YES
LOW-SPEED AERO CHAR.	POOR	BETTER
SWEEP	HIGH	LOWER
LEADING EDGE	BLUNT	SHARP

Figure 4.3   LEADING EDGES - SUBSONIC VS. SUPERSONIC

For a subsonic leading edge, the sweep must increase with design Mach number. This reduces low-speed wing lift-curve slope and maximum lift, and increases yaw-roll coupling, all of which is undesirable. There exists, therefore, an upper Mach number limit for which an all-subsonic-leading-edged wing is acceptable. Compromise with low speed characteristics have caused most of the recent study wings, including the Mach 2.2 DAC AST, to have a subsonic inner panel and supersonic outer panel. The span fraction of the leading edge sweep break typically decreases as design Mach number is increased.

If laminarization were found to be feasible for supersonic leading edges only, the drag due-to-lift disadvantage would have to be counted against LFC, and the resulting net gain would probably be small or nonexistent. For this reason, the laminarization of wings with subsonic leading edges has been given high priority in this study.

5. DAC AST WING — LFC FEASIBILITY

The Douglas Advanced Supersonic Transport (AST) configuration, shown in the upper left-hand corner of figure 1.1, is one of several developed under NASA contract in the mid- to late 1970s[17]. It was designed as a transpacific (5750 nm), high capacity (308 passengers) airplane intended to cruise at Mach 2.2. It featured four underwing variable cycle engines with mixed-compression conical inlets and an efficient cranked arrow wing with leading- and trailing-edge flaps for low speed operation. Extensive use was made of superplastic formed and diffusion bonded (SPF/DB) titanium in the wing structure. The wing leading edge has a sweep break station at 70% semispan, with a subsonic (71 deg.) leading edge inboard of the break, and supersonic (61.5 deg.) leading edge outboard. The entire wing is cambered and twisted for minimum pressure drag due-to-lift under cruise conditions. The lower sweep of the outer panel gives improved low-speed performance and handling at minimal compromise to supersonic cruise efficiency, while avoiding the large structural span of an all-subsonic leading-edged wing. The wing trailing edge also has a sweep break. The aft-swept trailing edge was found to offer a performance advantage over an unswept or negatively swept trailing edge due to a favorable interaction with the closing fuselage afterbody. Laminar flow control was not considered in the original design. The specific configuration used in this study, designated the D3233-2.2-1C, was chosen as a baseline, since its geometry and performance characteristics were well documented[18].

Some of the potential laminarization problems presented by the AST wing as a candidate for LFC are shown in figure 5.1. Despite the relatively small leading-edge radius, the high leading-edge sweep of the inboard wing could make attachment line laminarization difficult. Concave curvatures exist on the wing lower surface near the leading edge, so there was a potential for Gortler instability. The leading-edge sweep outboard of the sweep break is such that the normal component of Mach number at cruise is only 1.03, giving rise to a detached or lambda-type shock on the lower surface at the leading edge. It seemed doubtful that a laminar boundary layer could survive this abrupt deceleration. The low absolute pressure of the air, especially over the wing upper surface, coupled with the high freestream massflux at cruise, could cause the ducting for the suction air to be unduly large.

The first step in determining the prospects for laminarizing a wing is to get a solution for the inviscid flowfield. Although linear small-disturbance methods were used in the design of the wing, these methods were found to lack the necessary accuracy and resolution, particularly in the leading-edge region. Inboard of the leading-edge sweep break, where the leading edge is subsonic, the small-disturbance methods could not allow or properly account for spatially rapid pressure variations. For the outboard panel, which had a supersonic leading edge, it is necessary to correctly account for the leading-edge shock. Compressible Euler codes have the ability to model these effects. Two advanced-grid Euler codes, BOD-60[19] and FLO-67[12], were used in this analysis. The BOD-60 code is an improved version of Jameson's FLO-58 Euler. Both codes have the capability of computing mixed subsonic and supersonic flows, an important feature in the low supersonic regime.

19

ATTACHMENT LINE INSTABILITY

GORTLER VORTICES

LAMBDA-SHOCK

EXCESSIVE SUCTION VOLUME FLOWS & LARGE DUCTING

BODYSIDE TURBULENT WEDGE
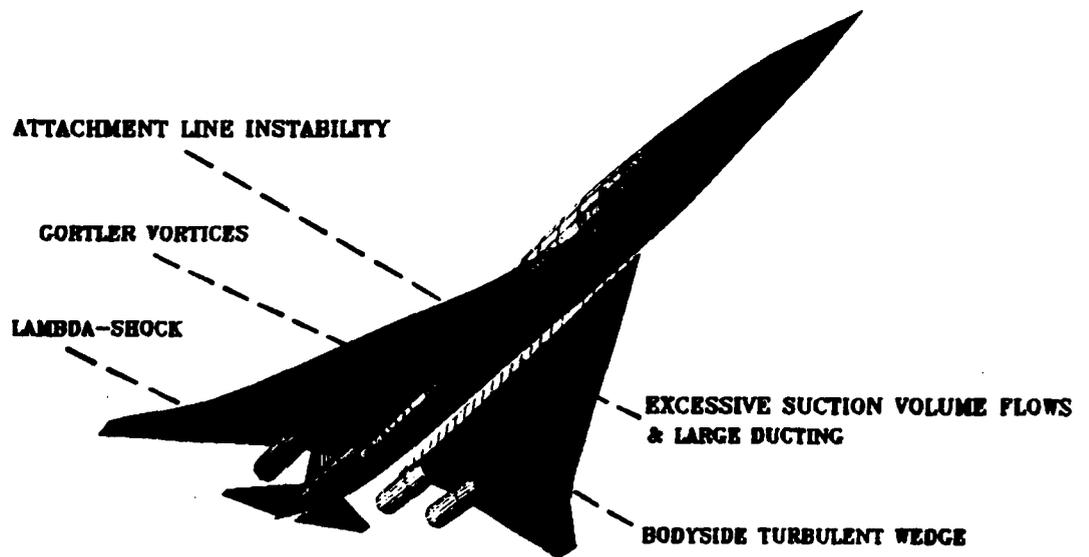
Figure 5.1   DAC MACH 2.2 AST POTENTIAL LAMINARIZATION PROBLEMS

Direct comparisons were made with supersonic wind-tunnel data for an earlier AST configuration, and are shown in figures 5.2A through 5.2F for the BOD-60 code, and figures 5.3A through 5.3F for the FLO-67. Considering the scale of the wind-tunnel model (2 ft. span), the agreement for both codes was judged to be acceptable. The computed pressure distributions were found to be reasonably well resolved and smooth in the leading-edge region and elsewhere. A schematic representation of the AST wing planform, with BOD-60 pressure distributions at the span stations used in the boundary layer analyses is shown in figure 5.4.

Conditions along the leading-edge attachment line are critical to the achievement of laminar flow on a wing. Criteria for the existence of laminar flow along the attachment line were established at low speed by Bacon and Pfenninger[15], and use a Reynolds number based on the laminar momentum thickness: if R_Θ is less than 100, the laminar attachment line boundary layer is stable; if R_Θ is greater than 240, T-S waves can grow and spontaneously transition the boundary layer. For R_Θ between 100 and 240, established turbulence will propagate, but the attachment line will remain laminar in the absence of disturbances. The value of R_Θ is increased by sweep, leading edge radius, and unit Reynolds number, but can be reduced with suction. In this study it was assumed that these criteria apply to the supersonic case. This assumption is felt to be conservative in view of the known effect of viscous heating in stabilizing the boundary layer. The development of attachment line criteria valid throughout the Mach number range is an important objective for the research program recommended· in section 12.

20
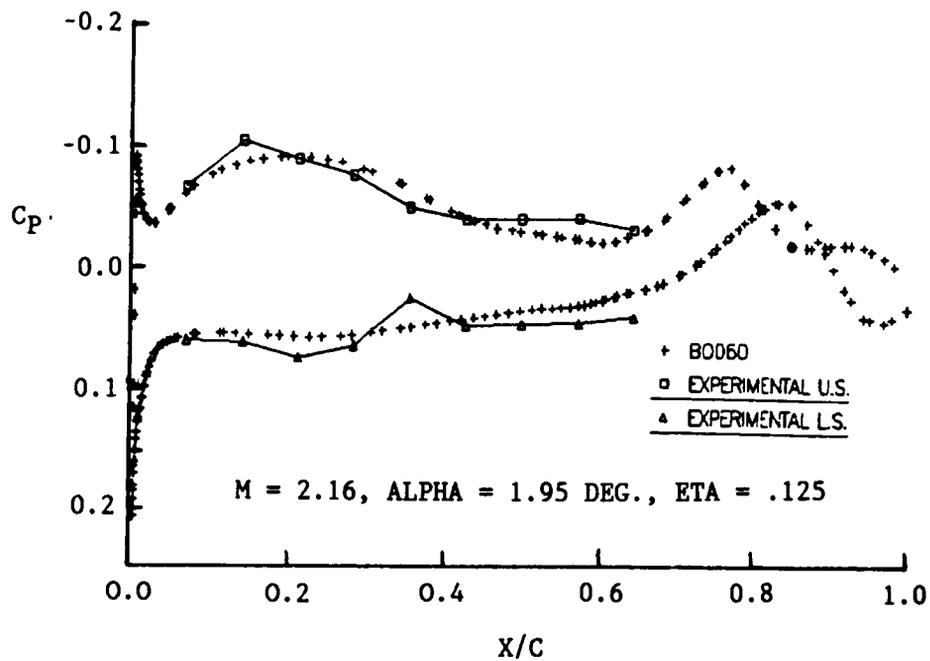
Figure 5.2A   BOD-60 EULER vs. W.T. TEST DATA
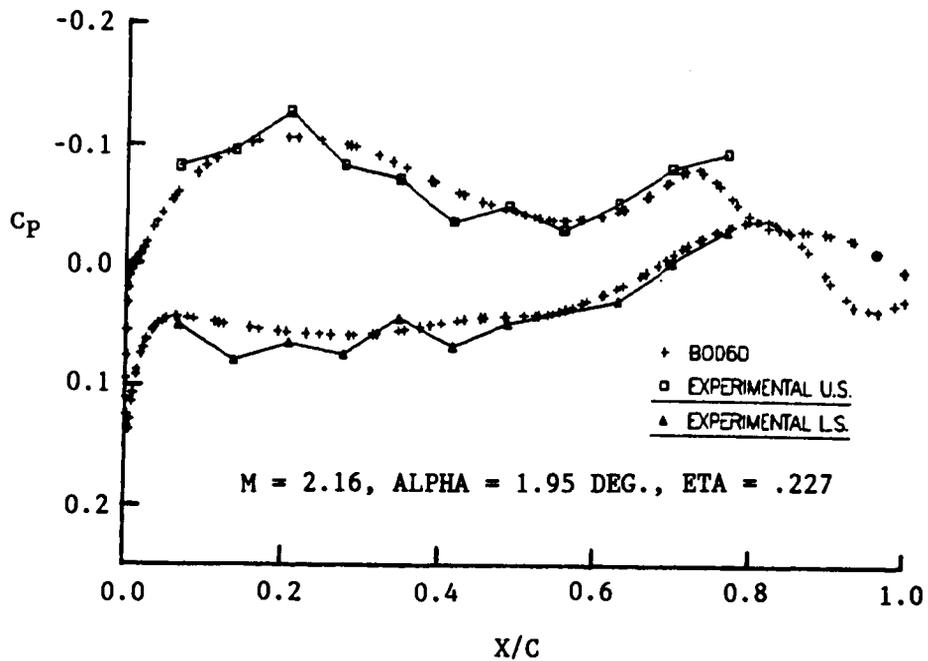
Figure 5.2B   BOD-60 EULER vs. W.T. TEST DATA

21
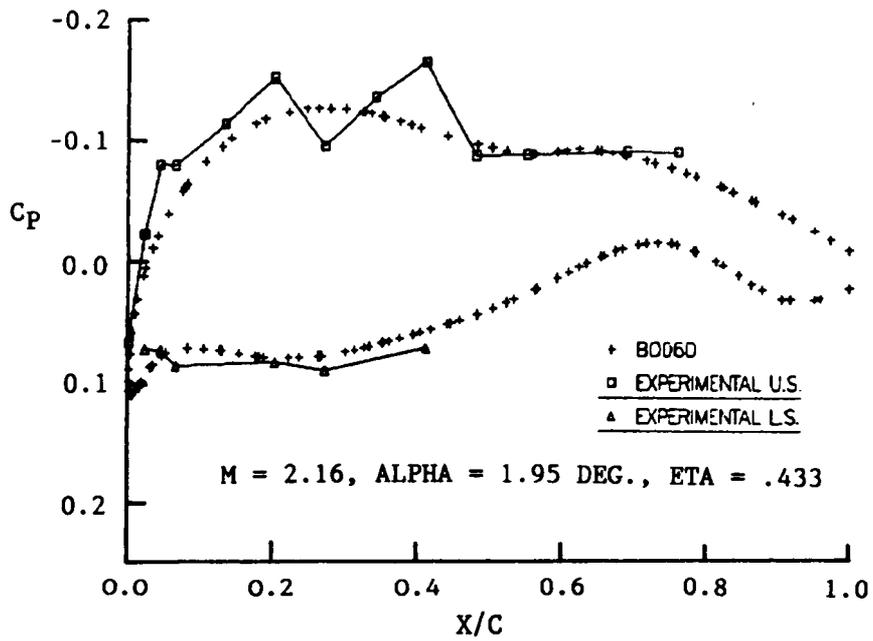
Figure 5.2C   BOD-60 EULER vs. W.T. TEST DATA
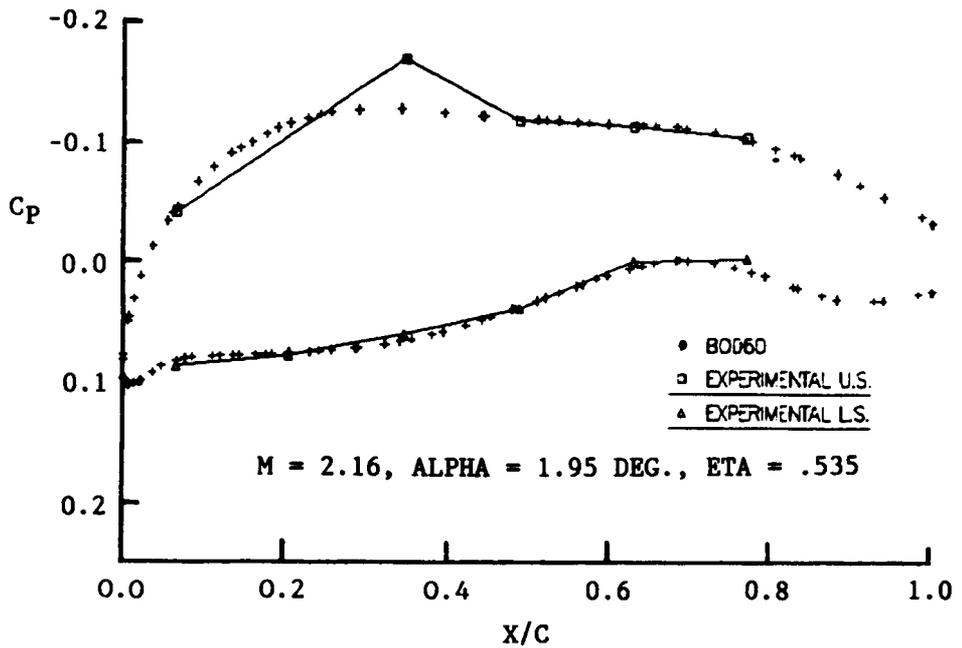
Figure 5.2D   BOD-60 EULER vs. W.T. TEST DATA
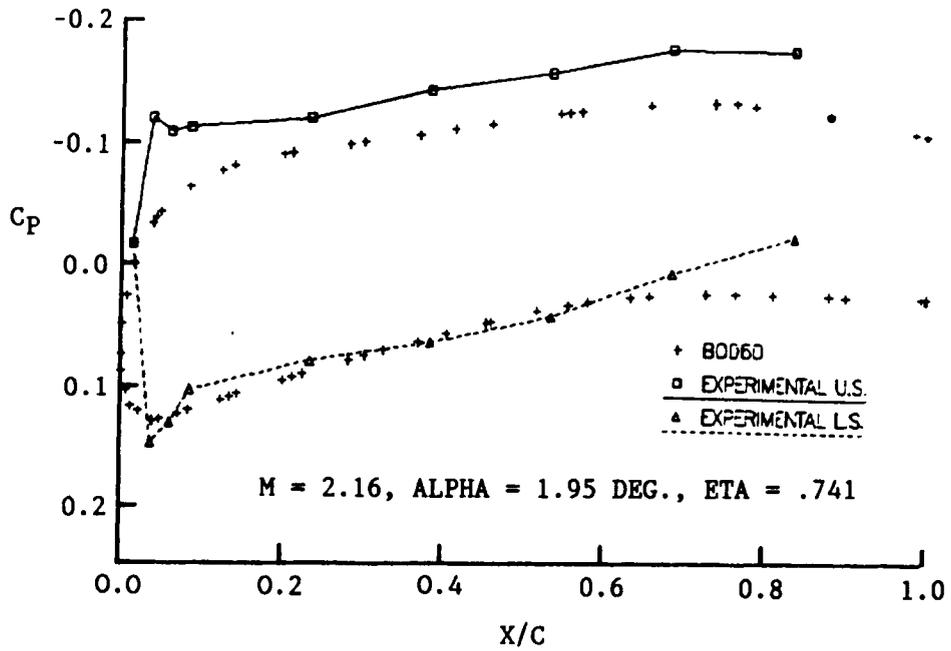
Figure 5.2E   BOD-60 EULER vs. W.T. TEST DATA
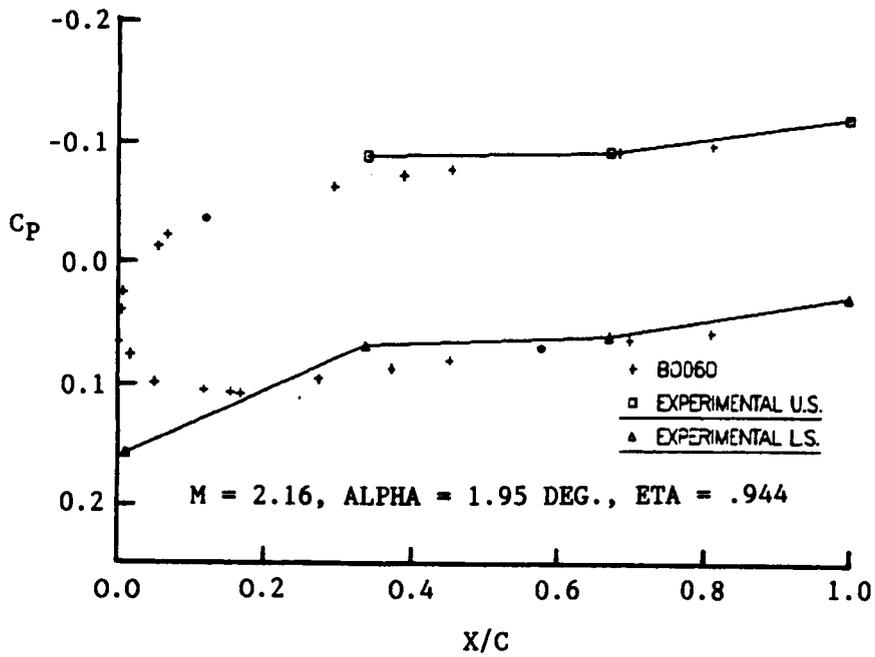
Figure 5.2F   BOD-60 EULER vs. W.T. TEST DATA
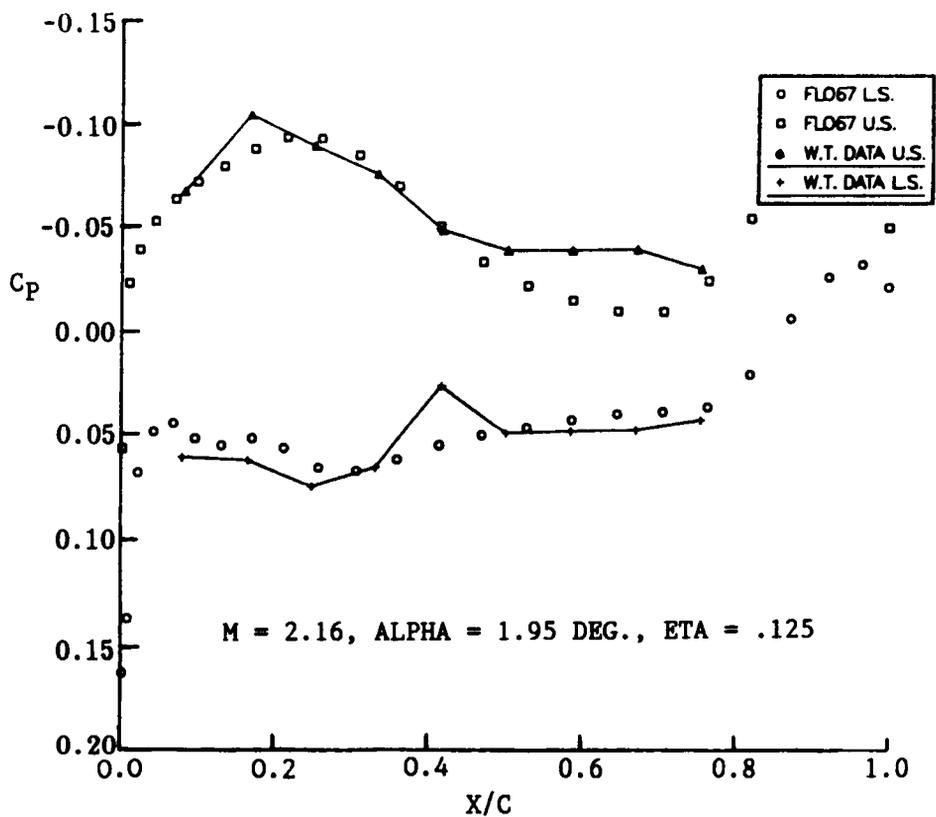
Figure 5.3A FLO-67 EULER vs. W.T. TEST DATA
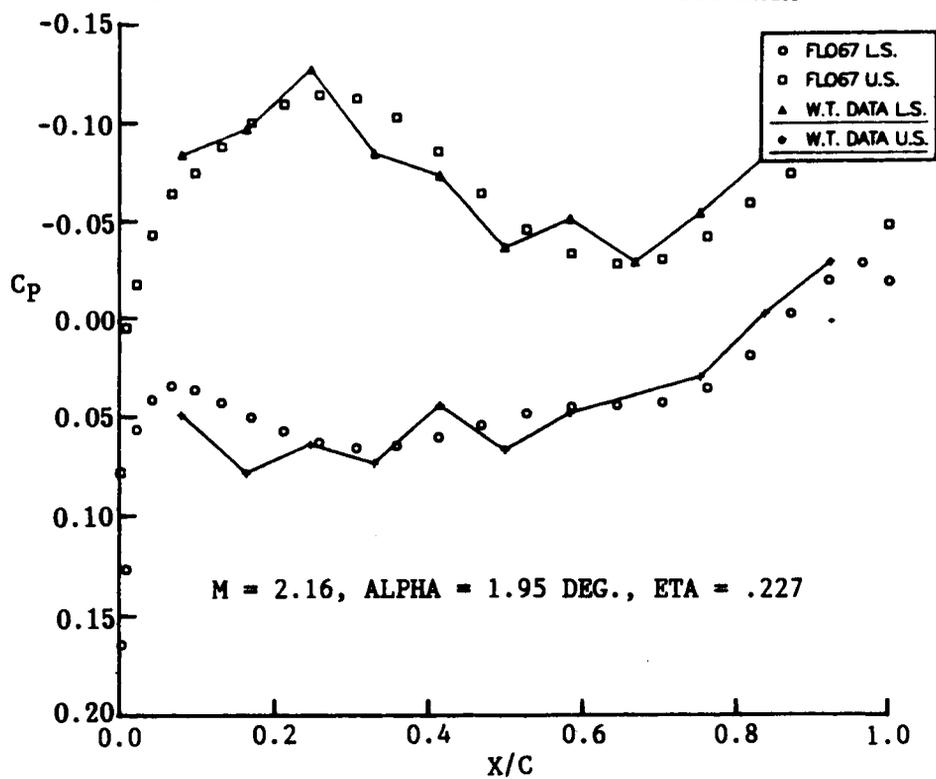
Figure 5.3B   FLO-67 EULER vs. W.T. TEST DATA

24
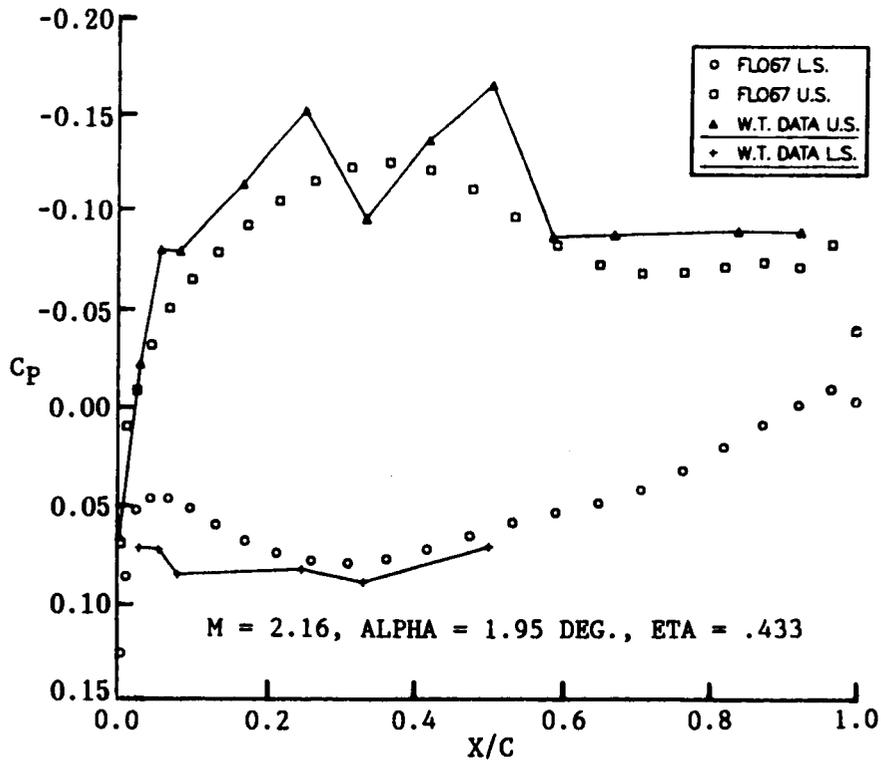
Figure 5.3C . FLO-67 EULER vs. W.T. TEST DATA
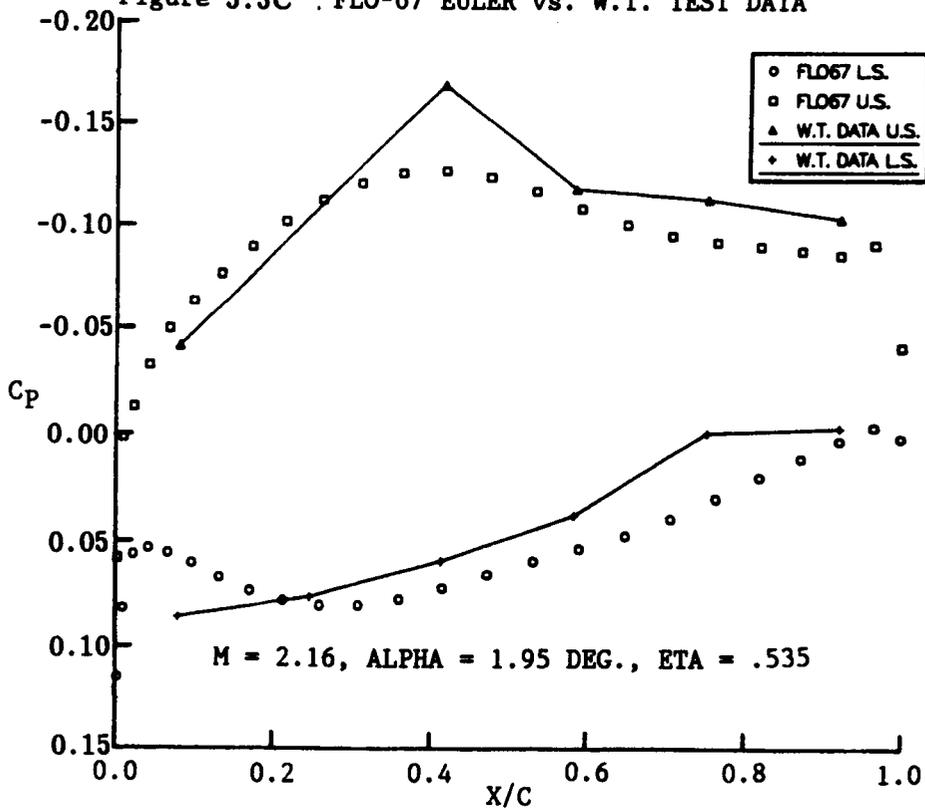
Figure 5.3D FLO-67 EULER vs. W.T. TEST DATA

25
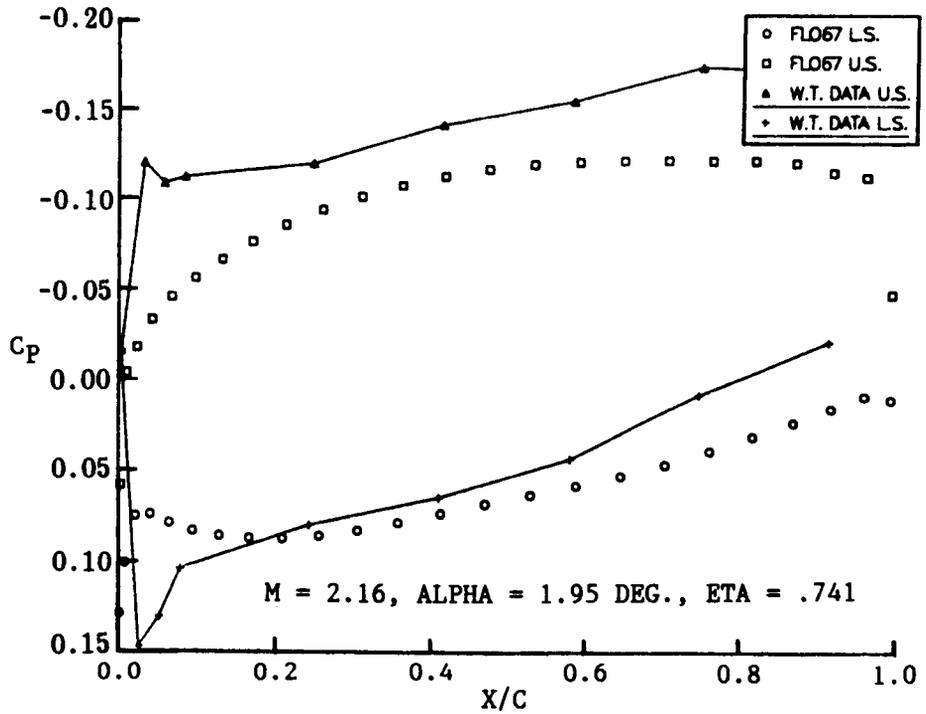
Figure 5.3E   FLO-67 EULER vs. W.T. TEST DATA
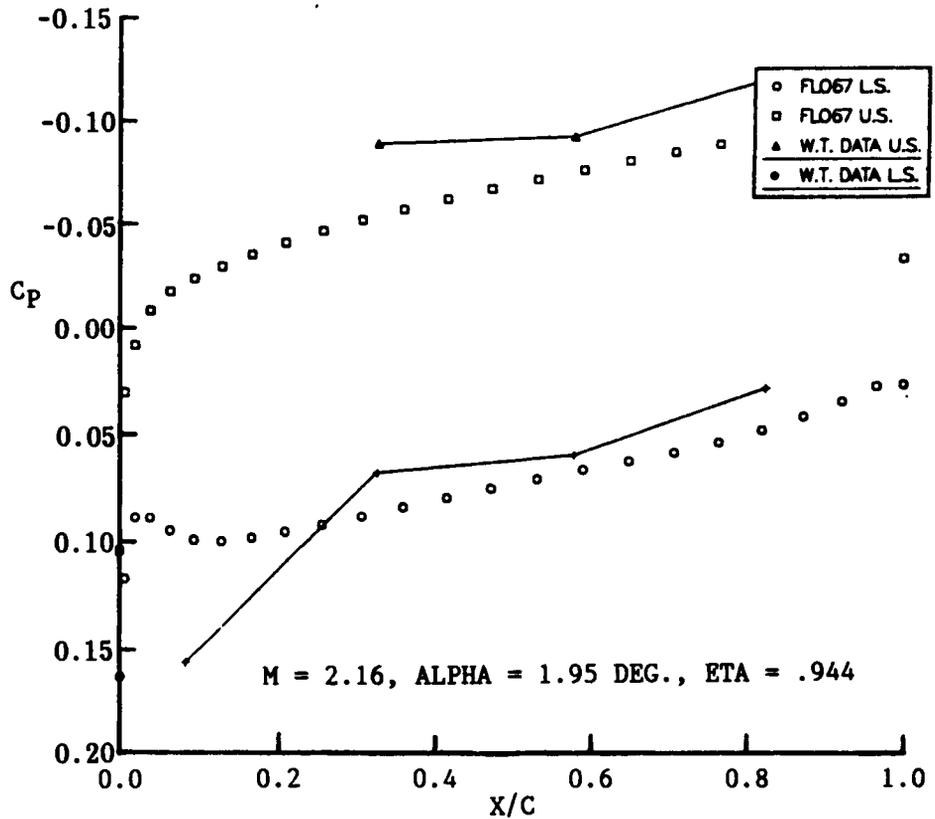
Figure 5.3F   FLO-67 EULER vs. W.T. TEST DATA
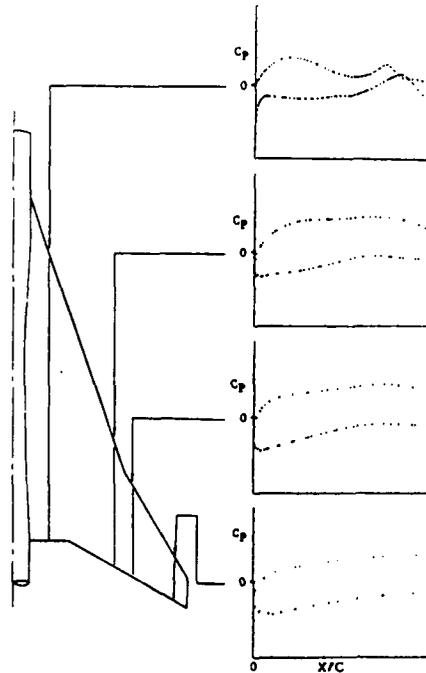
Figure 5.4   AST WING STATIONS FOR B.L. STABILITY ANALYSIS

Both the BOD-60 and FLO-67 Euler solutions were used in the computation of R_θ for the two inboard span stations. These are shown as a function of suction level in figure 5.5. At each station, the differences in R_θ are due to the computed attachment line locations, which are near the relatively sharp leading edge in the FLO-67 solution, but below and behind it in the BOD-60 solution. Of the two, the FLO-67 solution is more representative of the proper attachment line location at the design point. According to either solution, attachment line R_θ values allowing laminar flow can be achieved with moderate suction. R_θ was computed using a newly developed algorithm that allows the attachment line C_p values to differ from their simple-sweep attachment line values. The new approach uses the computed or measured attachment line C_p, and the fact that the leading-edge-normal velocity component at the attachment line is zero, to compute the local effective sweep angle at which the flow approaches the leading edge. This effective sweep is then used in the calculation of leading-edge normal velocity for each of the two points straddling the attachment line. The resulting normal velocity gradient is then used in the formula for R_θ given by Bacon and Pfenninger.

The wing lower surface inboard of the leading edge break featured an extensive region of streamwise concavity, and there was concern that Gortler instability could cause early transition in this region. Stationary, counter-rotating Gortler vortices are due to centrifugal instability, and can form in a laminar boundary layer in regions of concave flow curvature. However, recent theoretical and experimental investigations[20,21] have indicated that the presence of boundary layer crossflow can destroy Gortler vortices.

27
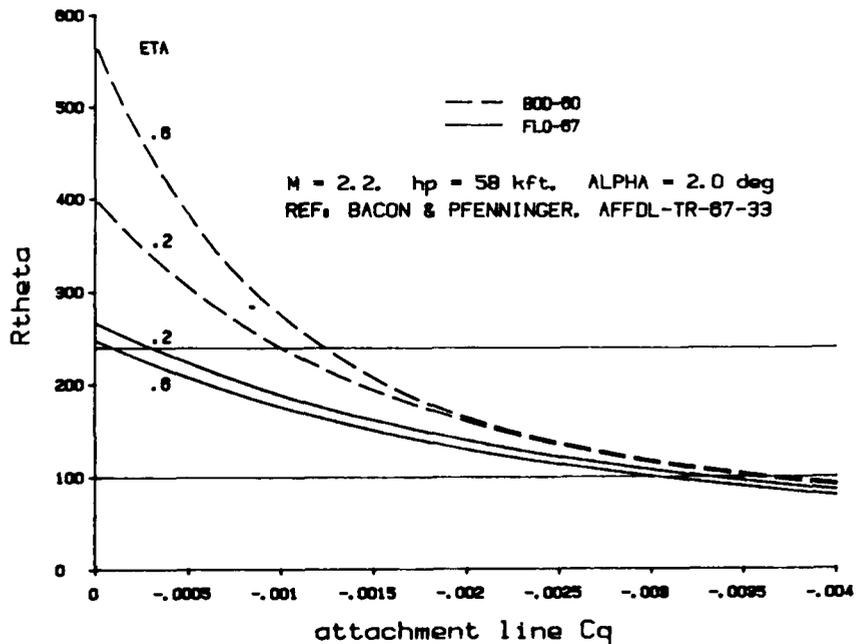
Figure 5.5   ATTACHMENT LINE CONDITIONS - INBOARD AST WING

Figure 5.6 shows the definition of the crossflow Reynolds number, the value of which serves as a rough criterion for Gortler vortex destruction, per reference 20. If this Reynolds number exceeds 45, Gortler vortices of one rotational sense have been raised up out of the boundary layer, where they decay rapidly, while those of opposite sense are converted to crossflow waves. Calculations were done on the lower surface of the AST wing in the concave region. The average crossflow Reynolds number was found to be 84, over twice that required to destroy Gortler vortices. It is thus concluded that Gortler instability does not pose a threat to laminarization on this wing.

Collier et al[22] have pointed out that the concave curvature does provide an additional mechanism for crossflow wave amplification that is not accounted for in the current production version of the COSAL[11] boundary layer stability code. This effect was not considered.

Suction requirements for laminarization were determined by boundary layer stability analysis, employing the NASA MARIA[10] and COSAL codes. The large chordlengths of the AST wing precluded serious consideration of a hybrid laminarization scheme. A full-chord suction scheme was adopted, with transition targeted for the control-surface hingeline. The low cruise lift coefficient of approximately 0.10, coupled with the low ambient pressure at the initial cruise altitude of 58 kft means that the density differences between upper and lower wing surfaces might be expected to compensate somewhat for the differences in velocity, so that the upper/lower laminarization benefit split would be more even than for the subsonic case. Calculations have since borne this out; the computed benefit split is approximately 3/7 upper, 4/7 lower.

B.L. CROSSFLOW: VELOCITIES WITHIN THE BOUNDARY LAYER ARE NOT PARALLEL TO THE EXTERNAL FLOW.
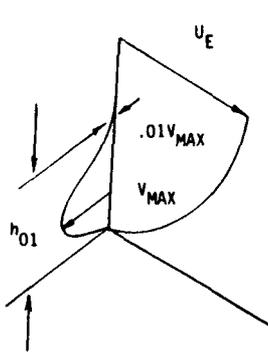
$$Re_{CF} = \frac{h_{01} \, V_{max}}{\nu}$$

Re > 45 => COMPLETE CONVERSION OF
GORTLER VORTICES TO
CROSSFLOW WAVES.
REF. COLLIER & MALIK
AIAA-87-1412

FOR DAC AST, AVERAGE Re_{CF} = 84
IN L.S. CONCAVE REGION.

Figure 5.6   CONVERSION OF GORTLER VORTICES TO CROSSFLOW WAVES

It is therefore important to laminarize both wing surfaces if possible. The major concern here was the suction volume flow, and the required size of internal ducting.

Both boundary layer stability codes use the conical laminar boundary layer code of Kaups and Cebeci[13] to generate velocity profiles. Since this code was written for the subsonic and transonic cases, it is not surprising that some modifications, both to the code and the way it is used, were found to be necessary for supersonic application. Fortunately, the modifications were small, and were confined to three areas: velocity overshoots, supersonic leading edges, and near-wall symmetric oscillations.

The Kaups-Cebeci code uses a conical wing approximation to solve the three-dimensional flow on straight tapered wings, in which profiles are assumed to be similar on rays from a virtual wingtip. The coordinate system used in the program is shown in figure 5.7. The modified versions of the code used with the MARIA and COSAL codes contained statements prohibiting velocity overshoots in which w/W_E or u/U_E exceed unity below the boundary layer edge. Such overshoots are known to occur in supersonic boundary layers near a wing leading edge[23]. The overshoot prohibition was, in certain cases, creating velocity profiles that were not smooth, resulting in artificial eigenvalues in the stability analysis. These statements were removed.

29
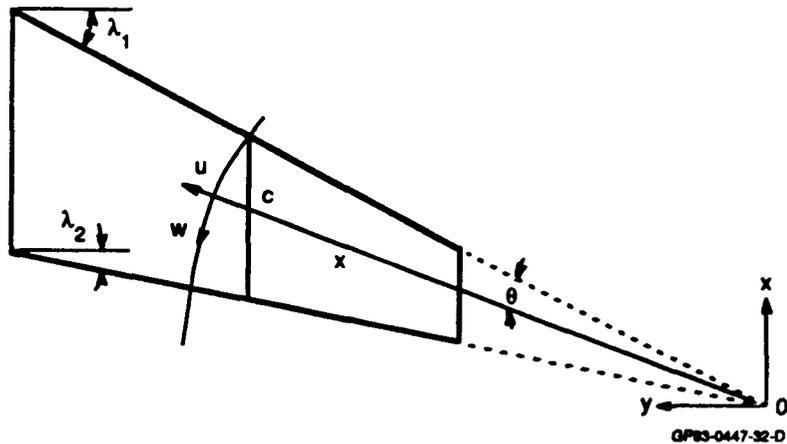
Figure 5.7   POLAR COORDINATE SYSTEM USED IN THE K-C CODE

The supersonic leading edge case presented problems in that the boundary
layer code was not designed to deal with the total pressure losses caused by
leading-edge shocks, nor did it have the option of a wedge flow or flat plate
starting solution. The only starting solution needed for the subsonic
swept-wing case is the infinite swept cylinder attachment line. The
leading-edge shock problem was dealt with outside of the boundary layer
program by assuming that the shock is detached slightly from the leading
edge, and that all streamlines entering the boundary layer pass through the
leading-edge-normal part of the shock. Since the leading edge is swept,
oblique shock relations are used to calculate the correct total external
velocities at each station, based on the computed (nonisentropic) pressure
coefficients. The boundary layer code expects the flow to be isentropic, so
equivalent isentropic pressure coefficients are then computed from the total
external velocities. A simple program, written in IBM BASIC-A, was used to
make these calculations. A listing is given in appendix B. The problem of
curved shock waves and the resulting velocity and total pressure gradients
found downstream is much more complicated. This effect was not accounted
for.

Although low supersonic pressure drag demands a sharp leading edge
outboard of the break, the only existing starting solution in the
Kaups-Cebeci boundary layer code is that of a swept cylinder attachment
line. This solution, which assumes that the leading edge is to some degree
blunt, was still found to be usable. Computational points were bunched in
the leading edge region in order to provide for a spatially rapid but smooth
acceleration from the attachment line C_p.

30

This gives rise to leading edge crossflow which is not fundamental to the stability of the boundary layer if the leading edge is reasonably sharp. However, the stability consequences of this short acceleration region were found to be addressable by using the MARIA stability code to separate the very short wavelength stationary crossflow waves amplified in the leading edge region from the longer waves amplified by the basic pressure distribution. The wavelengths and amplifications of those waves generated in the rapid acceleration region varied directly with the physical length of the region, so the length was simply adjusted downward until the resulting waves were so short and little amplified as to die off in the first 10% chord or so. This made them readily distinguishable from those arising from the airfoil's basic pressure distribution, as shown in figure 5.8. With the very thin boundary layers in the attachment line region, not many computational points were available for stability calculations. This was considered acceptable, since the profiles giving rise to the longer wavelengths generally were adequately resolved. Once the wavelengths of the most amplified crossflow waves were found using MARIA, the COSAL stability code was used to compute their amplifications. Even at Mach 2.2 the MARIA code was found to do a good job of identifying the most amplified stationary crossflow waves.
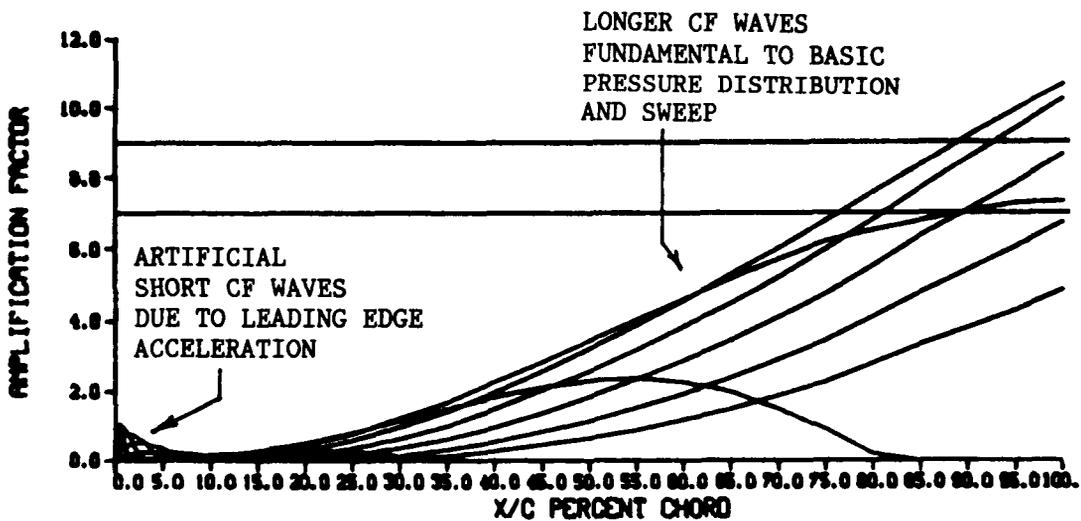
Figure 5.8   STATIONARY CROSSFLOW WAVES - SUPERSONIC L.E.
USING ATTACHMENT LINE STARTING SOLUTION
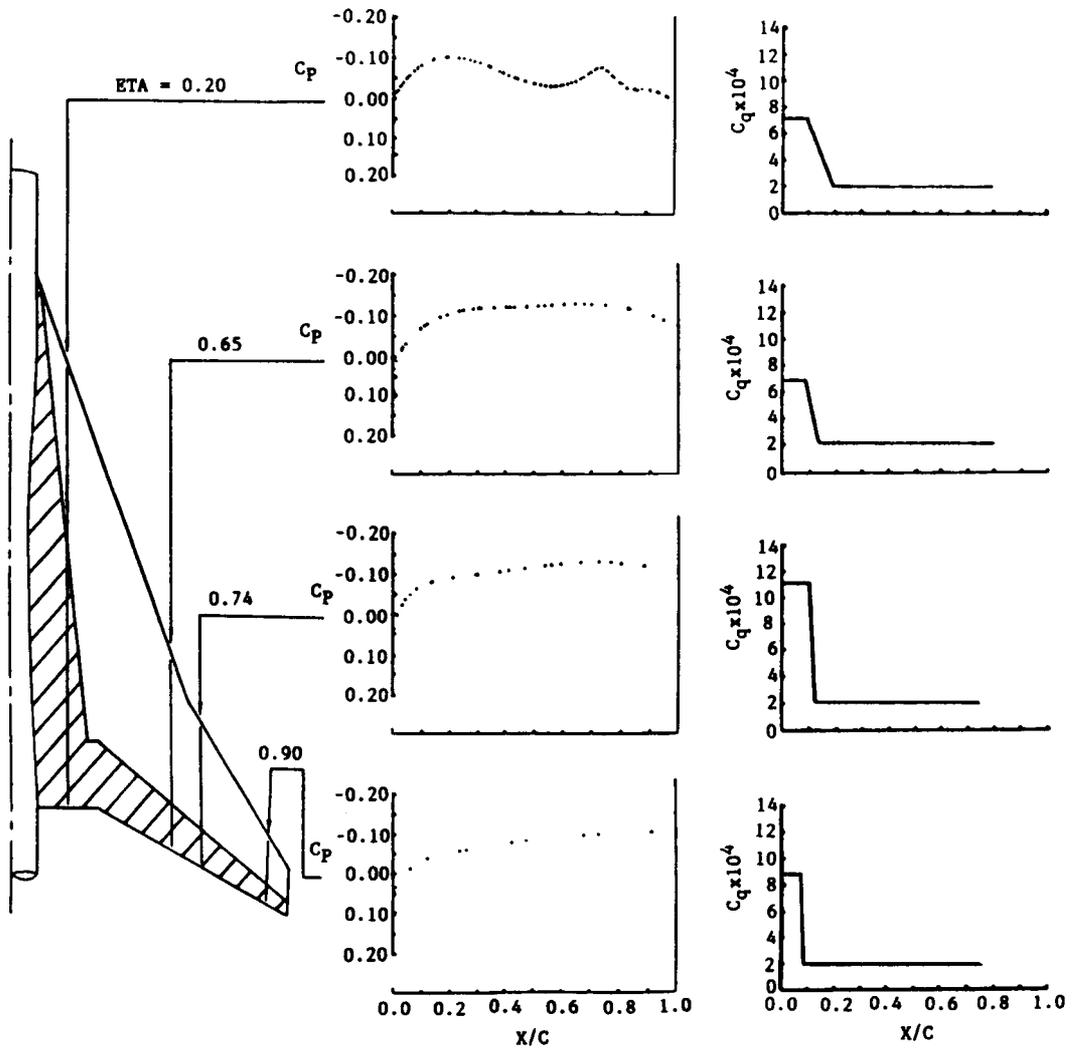
Figure 5.9 LFC FEASIBILITY ON ORIGINAL AST WING
UPPER SURFACE SUCTION DISTRIBUTIONS
(M = 2.16, ALPHA = 1.95 deg, h_P = 58 kft)

Small near-wall oscillations were observed in the computed velocity profiles in the vicinity of Mach 2 and above. These oscillations were found to be symmetric station-to-station, and are a result of the manner in which the equations of motion are solved. In the iteration scheme, the momentum and continuity equations are solved, then the energy equation is solved externally and used to update the fluid properties prior to the next continuity-momentum loop. This procedure is efficient and works well in the transonic regime, but the larger variation of temperature with total velocity at the higher Mach numbers causes the inherently lagging fluid properties to affect the solution. The problem was visible as a sawtooth variation in wall skin friction station-to-station. Modifications were made to the code to correct this problem, but comparisons of stability characteristics computed with and without the code modification showed no differences.

For the feasibility analysis, the required suction levels were determined conservatively. The suction required to prevent excessive growth of stationary crossflow waves in the leading edge region was determined using the MARIA code, then the adequacy of the levels was checked using COSAL. An N-factor of 9 was taken as critical. For the conditions of this study, the MARIA code always erred on the conservative side of COSAL, indicating larger stationary crossflow amplifications for a given suction level. The adequacy of an assumed suction level of C_q = -.0002 over the rooftop was also verified using COSAL. Both stationary and nonstationary crossflow waves, as well as T-S waves were computed. All boundary layer wave growth was small due the conservatively high suction levels. Since the object here was to demonstrate feasibility, not minimize suction, these results are not presented. Figures 5.9 and 5.10 show the upper and lower wing surface laminar regions, pressure coefficients and suctions. The hatched regions indicate turbulent flow. On both surfaces a 6 degree bodyside turbulent wedge was assumed, based on extrapolated subsonic data. This value is in agreement with the correlation of Fischer[24] at Mach 2.2.

The leading-edge sweep angle on the outboard panel was such that the normal Mach number is only 1.03. On the lower surface, at the cruise angle of attack, the local flow-deflection angle was too high for an attached shock to exist. The result was a strong adverse pressure gradient in the leading-edge region which prevented laminarizing the lower surface outboard of the leading-edge break. Therefore, no suction was used on the lower surface in the tip region. The station immediately inboard of the break is laminar, but the required suction is considerably larger than at the inboard station. This is due to the stronger favorable gradient, and underscores the strong dependence of required suction on pressure distribution.

33

ETA = 0.20

C_P

0.65

C_P

0.74

C_P

0.90

C_P

$C_q \times 10^4$

$C_q \times 10^4$

X/C

TURBULENT DUE TO
ADVERSE PRESSURE GRADIENT
IN LEADING EDGE REGION

TURBULENT DUE TO
ADVERSE PRESSURE GRADIENT
IN LEADING EDGE REGION

X/C
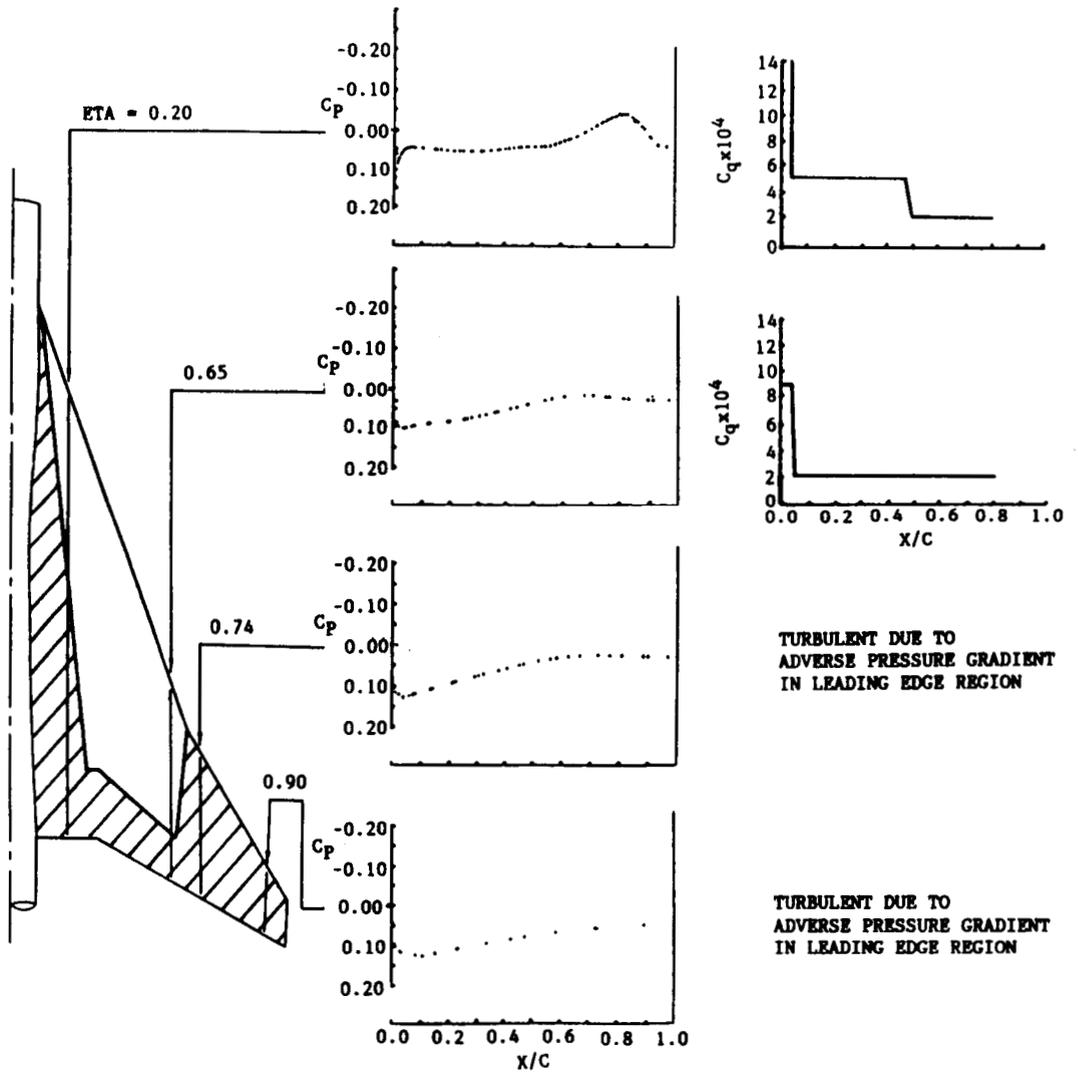
Figure 5.10   LFC FEASIBILITY ON ORIGINAL AST WING
LOWER SURFACE SUCTION DISTRIBUTIONS
(M = 2.16, ALPHA = 1.95 deg, h_p = 58 kft)

34

In order to establish the feasibility of fitting the suction ducting into the wing, the suction distribution was integrated over the wing area to determine the total suction flow. The low average pressure, particularly on the wing upper surface, makes the penalty for large skin pressure drops rather large in term of duct volume. A total pressure loss of 10% was assumed for the skin, and no loss was assumed in the ducting. In practice, the skin pressure drop is set by design. Strictly for the purpose of establishing the feasibility of providing the required suction capacity within the available wing volume, the suction air was assumed to pass internally through the wing root at maximum massflux, i.e. a ducting Mach number of 1.0,. The resulting duct area as a fraction of wing footprint area is shown in figure 5.11. The small (3%) area fraction is very encouraging. In a practical system, ducting Mach numbers would probably not be allowed to exceed 0.2 to 0.3, so the actual ducting size would be accordingly larger. This amounts to a factor of 2 to 3 on duct area.

Although the analysis described above identified no intractable aerodynamic problems that would preclude the successful application of LFC to the DAC AST wing, the original wing is far from an optimum design from a laminarization standpoint. In the benefit analysis to follow, it was not deemed appropriate to analyze this wing, since it was felt that large improvements in required suction flow and laminar area fraction could be made if the wing were redesigned.

WING FOOTPRINT AREA = 366 sqft
MINIMUM DUCT AREA = 10 sqft
(ONLY 3% OF FOOTPRINT)

Figure 5.11   THEORETICAL MINIMUM SUCTION DUCT AREA AT WING ROOT

The original AST wing had two problems: The lower surface wingtip could not be laminarized, and the acceleration of flow to the rooftop level in the leading edge region typically took place over too great a surface distance. This aggravates the crossflow instability problem, and requires large amounts of suction to overcome. A modified wing was developed to solve these problems. The original and modified planforms are shown in figure 5.12. Bluntness was added to the inboard wing leading edge, and the wingtip was unswept to 50 degrees. The lower sweep allowed an attached shock to exist on the lower surface at cruise angle of attack. These modifications did not degrade the wing's drag due-to-lift characteristics over the baseline, nor did they significantly worsen conditions along the attachment line. It was assumed that any changes in volume wave drag could be compensated for by re-area ruling the fuselage.

One major concern with the blunted leading edge was that the attachment-line momentum-thickness Reynolds number would be increased to such an extent as to make laminarization of the new wing impossible. R_θ calculations were made based on FLO-67 solutions for the original and modified wings. A comparison at the 20 and 60 percent span stations is show in figure 5.13 over a range of attachment line suction coefficients. Laminarization is still possible, but increased suction on the attachment line would be necessary to achieve the same R_θ values as the original wing. In either case it is necessary to keep the leading edge and wing clean, since turbulent wedges pose a very serious threat to the realization of LFC benefit on low-aspect, highly swept wings. According to this analysis, the blunted leading edge of the modified wing does not present an intractable attachment line problem for laminarization.
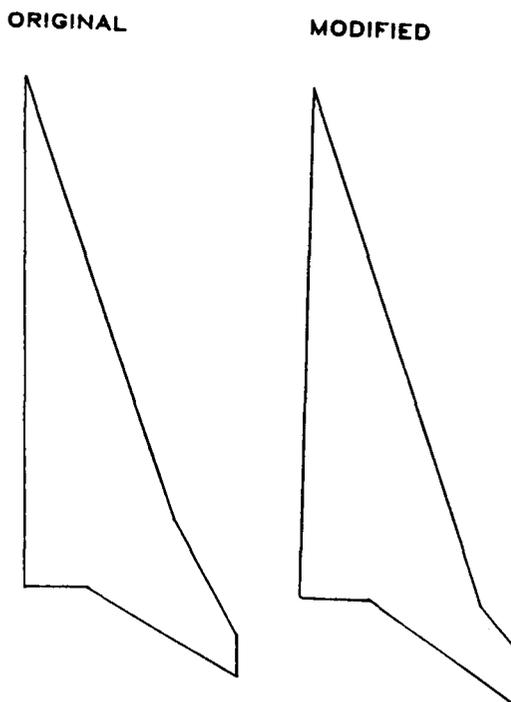
ORIGINAL   MODIFIED

Figure 5.12   LFC PLANFORM MODIFICATION

36

M = 2.2. hp = 58 kft. ALPHA = 2.0 deg
REF: FLO-67. BACON & PFENNINGER AFFDL-TR-67-33
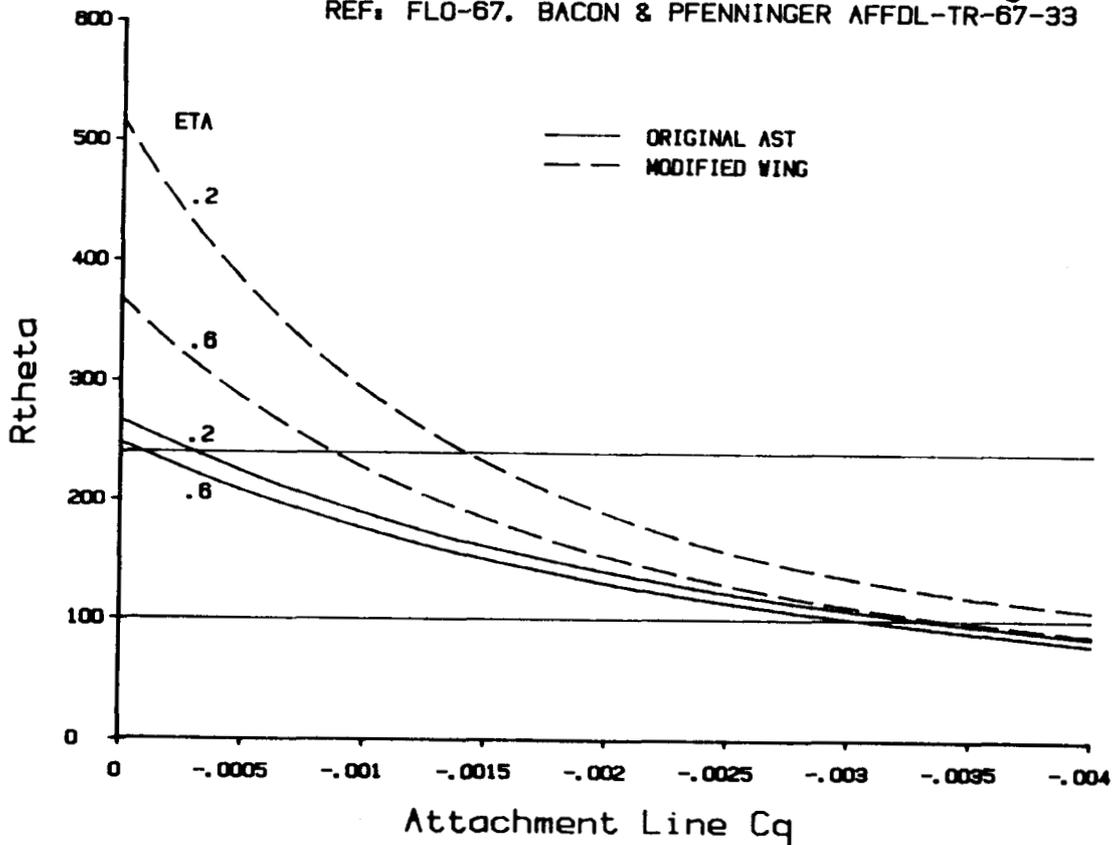
Figure 5.13 ATTACHMENT LINE CONDITIONS -
ORIGINAL AND MODIFIED AST WINGS

One concern with the highly swept leading edges is that of the variation of R_θ with angle of attack, particularly if the local radius of curvature varies rapidly with surface distance in the region of cruise attachment line travel. This variation of attachment line location with angle of attack is typically largest in the vicinity of the sweep break. Calculations of zero-suction R_θ were made for angles of attack from 0 to 3 degrees for both original and modified wings, based on the FLO-67 solutions. These are shown in figure 5.14. The 63% span station was chosen for comparison because of the above, and because it is on the inboard, highly swept region of both original and modified wings. It should be noted that the uncertainties in computed R_θ are greater for the original wing, due to numerical problems near the sharp leading edge in the FLO-67 solution. However, the trend of minimal R_θ variation over this angle of attack range is clear.

37
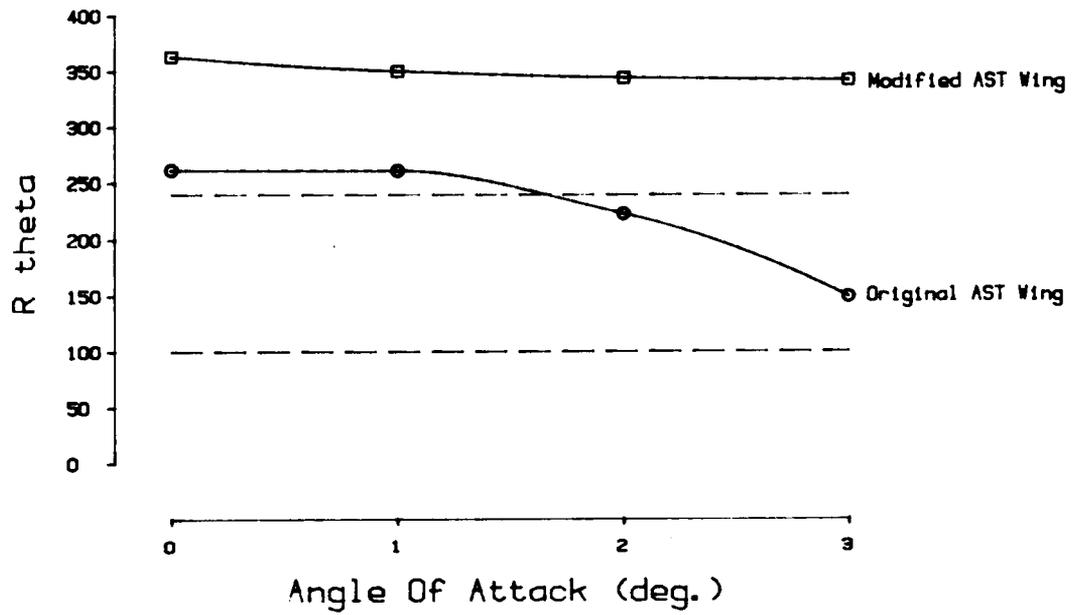
Figure 5.14   ZERO-SUCTION ATTACHMENT LINE MOMENTUM THICKNESS
REYNOLDS NUMBER AS A FUNCTION OF ANGLE OF ATTACK

6. MODIFIED AST WING – LFC BENEFIT

In order to maximize LFC benefit, it is important to minimize the suction flow, since this relates directly to suction system size, weight, and power requirements. Suction minimization is done through an iterative procedure in which complete boundary layer stability calculations are performed using COSAL for various trial suction levels. COSAL has three commonly-used options for computing boundary layer stability, all of which compute the amplification of waves of constant frequency. Option 1, commonly called the maximum amplification method, conducts a search in waveangle and wavelength for the most amplified wave, at each chordwise station. Option 5 holds wavelength constant, and searches through waveangle for the most amplified wave. Option 6 holds waveangle constant, searching through wavelength for the most amplified wave. For this study it was felt that options 5 and 6 were the most physically realistic, so these options were used exclusively. In order to be conservative, the option giving the higher amplification was used. Typically this meant that option 6 was used for average waveangles less than about 85 degrees, and option 5 was used at higher average waveangles. Boundary-layer transition is correlated to the so-called amplification factor, N, which is the natural logarithm of the ratio of the local integrated amplification rate to a reference amplitude of the wave taken at the point of neutral stability. A growing body of experimental evidence supports values in the range of 8-12 for a wide variety of flows[8]. A value of 9 has been taken as indicating transition. This value was chosen to allow reasonable estimates of suction requirements to be made; more conservative values of 5 to 7 are typically used in the design process.

The procedure used in determining the minimum suction distribution starts with the attachment line. The R_θ criterion is satisfied by the application of an appropriate suction level over the region of expected cruise attachment line travel. In the attachment-line region and immediately downstream, the boundary layer is most unstable to stationary, or very nearly stationary crossflow waves. The MARIA code is useful in identifying the most amplified wavelengths of the stationary waves, and for a first estimate of the required suction levels. The COSAL code is then used to better determine the crossflow amplifications, and to iterate the suction to the minimum required level. In the leading-edge region, increased suction causes a decrease in the wavelength/chord ratio of the most amplified or critical waves, due to thinning of the boundary layer and changes in the profile shapes. This must be recognized in finding the minimum suction level. Fortunately, MARIA does an excellent job of identifying the critical waves, even under the conditions of this study. In the region downstream of the leading edge, where travelling waves are favored, the determination of minimum suction is much more complicated, since the waveangle and frequency of the most amplified wave vary with the suction level, and no inexpensive guidance is available.

The reason for the variation of critical wave frequency and angle with suction is best explained with reference to figure 6.1. This figure shows component velocity profiles with and without suction in a region of weak crossflow. Profiles are shown for various angles, PSI, relative to the external flow direction. In the figure, the crossflow is a result of using an airfoil having a constant favorable chordwise pressure gradient in a swept wing. With no suction (solid lines) the 70, 85, and 90 degree component profiles show inflection. Inflectional profiles are unstable, and the rate of amplification of boundary layer waves in a particular direction depends on the stability characteristics of the component profile in that direction. Note that the elevation of the inflection point above the surface increases with angle. With suction applied (dashed lines), all of the profiles are changed, but the inflection persists only for the higher angle profiles (85 and 90 degrees). This is consistent with the observed shift of the critical wave to higher waveangles as suction is increased, and explains why the stationary (nearly 90 degree) crossflow waves require the highest suction levels to subdue.
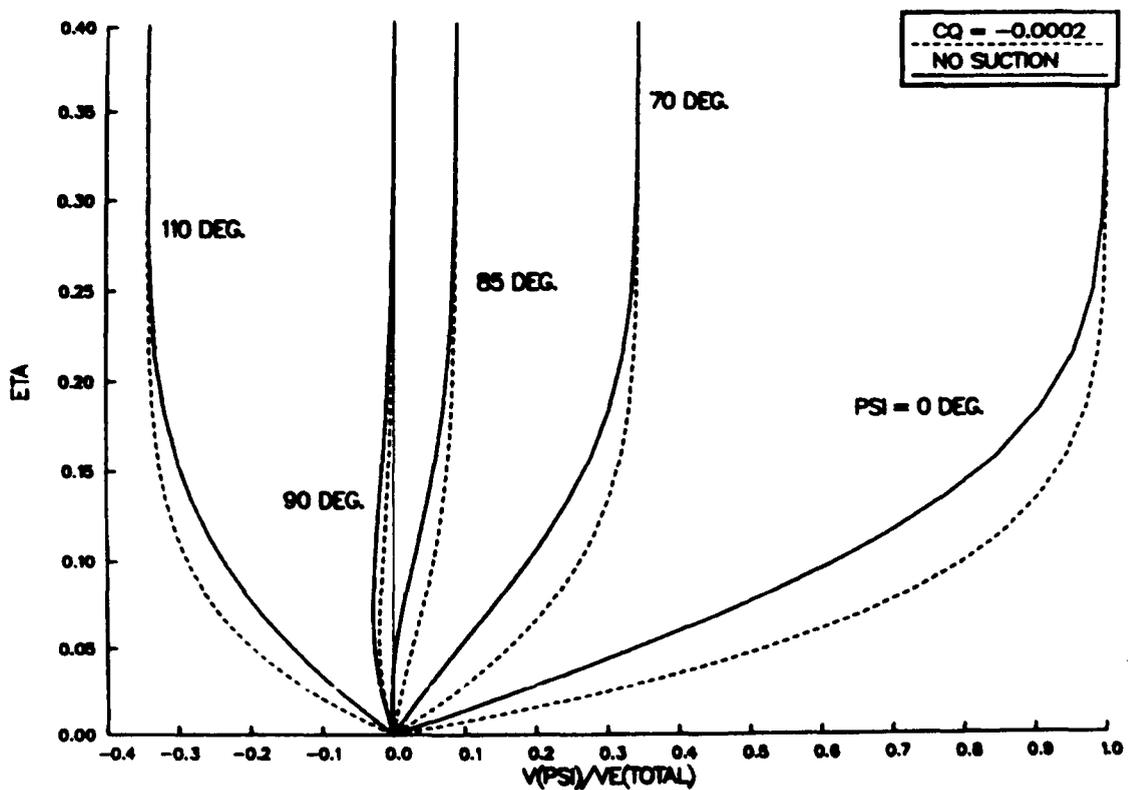
Figure 6.1 TYPICAL COMPONENT VELOCITY PROFILES
IN A REGION OF WEAK CROSSFLOW

Chordwise pressure distributions computed using FLO-67 are given is figure 6.2 for three span stations. Comparison of these pressure distributions with those of the original wing (figures 5.3A-5.3F) illustrates the success of the redesign. These pressure distributions were used in the stability analyses with the intent of minimizing the required suction. Final suction distributions for the LFC-modified AST wing are given in figures 6.3 and 6.4 for upper and lower surfaces, respectively, for the three span stations investigated.
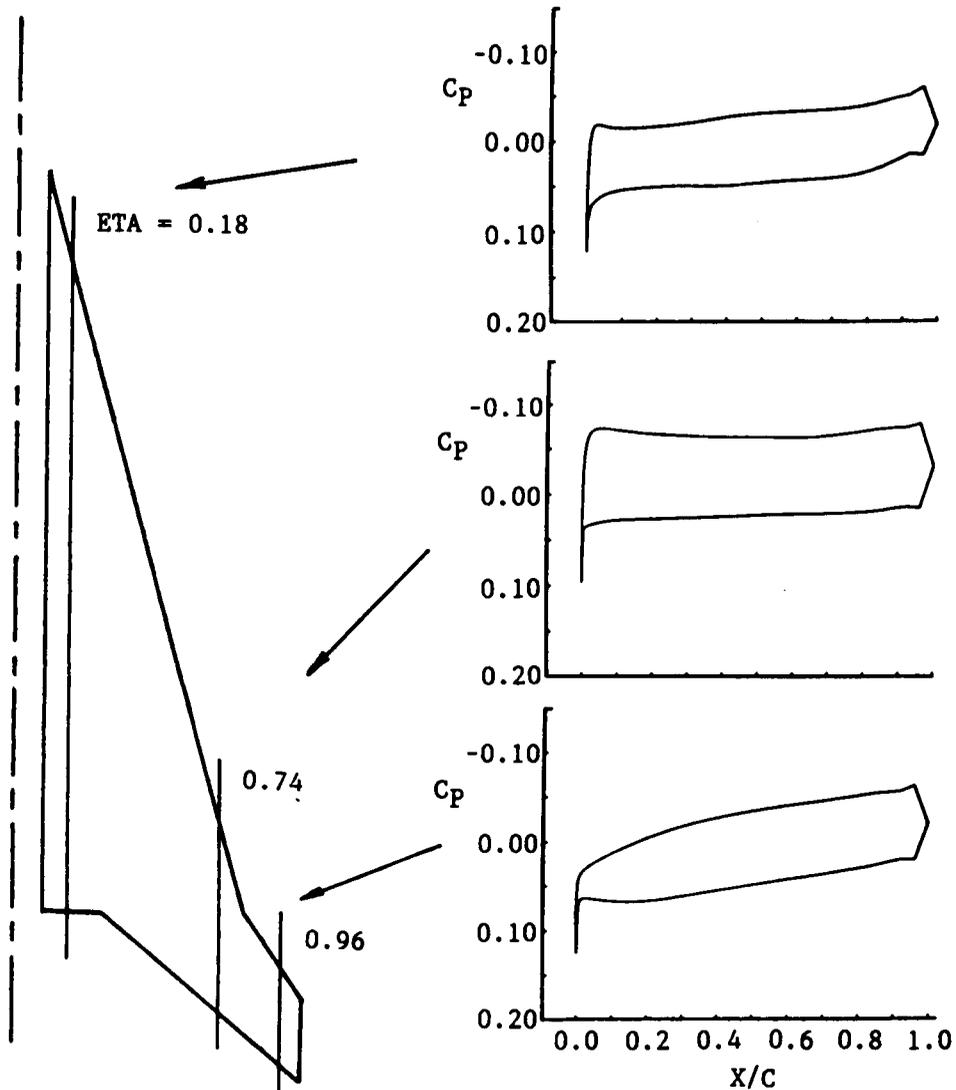
Figure 6.2   CHORDWISE PRESSURE DISTRIBUTIONS -
             MODIFIED AST WING

41

ETA = 0.18

0.74

0.96

C_P

$C_q \times 10^4$

X/C
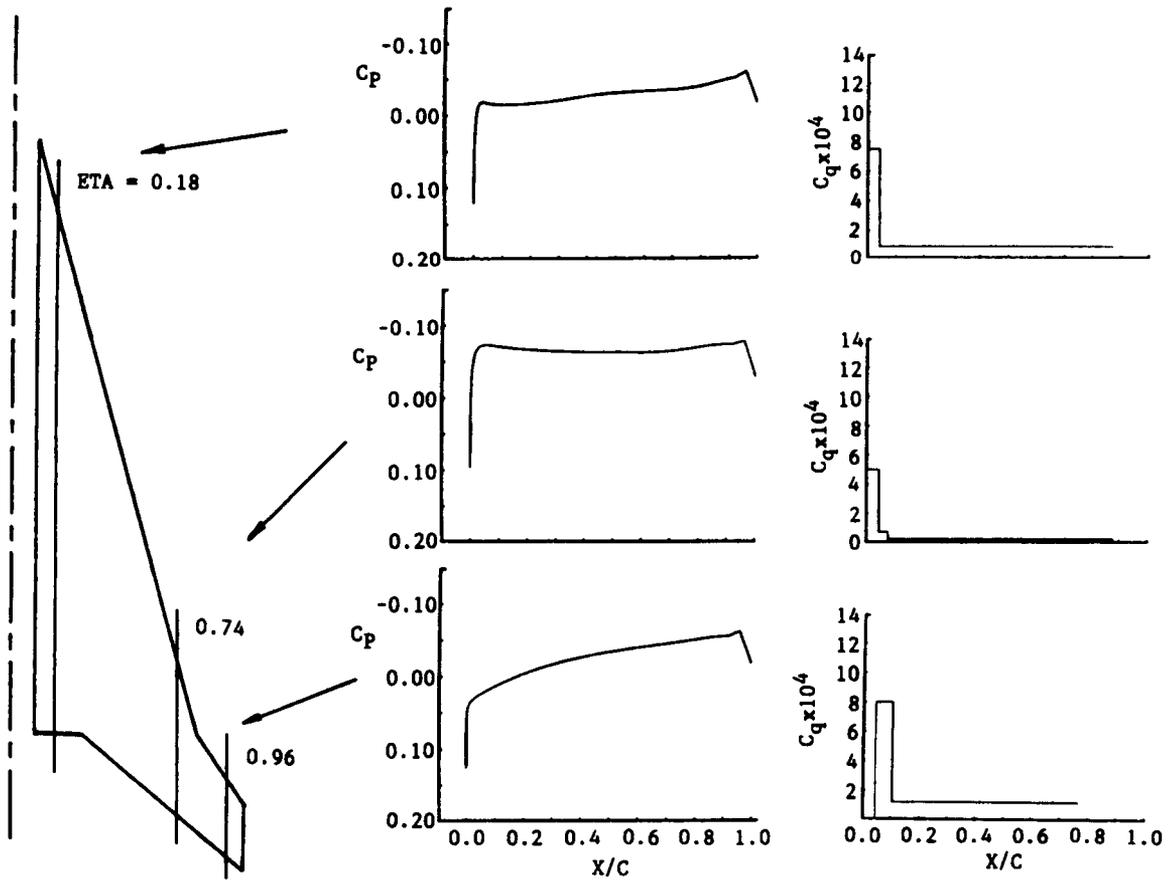
Figure 6.3 UPPER SURFACE FINAL SUCTIONS -
MODIFIED AST WING

ETA = 0.18

C_P

-0.10
0.00
0.10
0.20

$C_q \times 10^4$

14
12
10
8
6
4
2
0

0.74

0.96

C_P

-0.10
0.00
0.10
0.20

$C_q \times 10^4$

14
12
10
8
6
4
2
0

C_P

-0.10
0.00
0.10
0.20
0.0 0.2 0.4 0.6 0.8 1.0
X/C

$C_q \times 10^4$

14
12
10
8
6
4
2
0.0 0.2 0.4 0.6 0.8 1.0
X/C
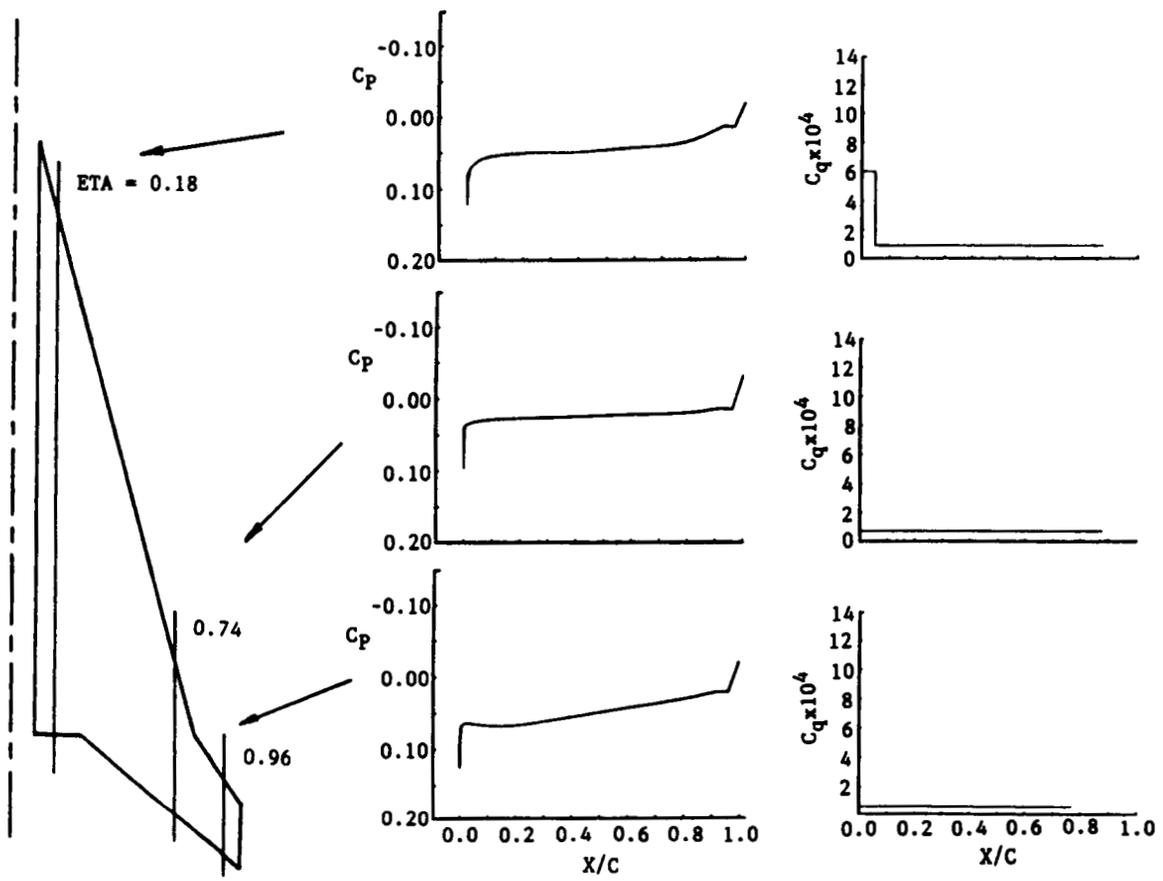
Figure 6.4   LOWER SURFACE FINAL SUCTIONS -
MODIFIED AST WING

43

Figures 6.5A through 6.7 highlight typical boundary layer stability results taken, after extensive iterative analysis, at the final suction levels. Figures 6.5A and 6.5B show the upper surface of the inboard station. The chordwise pressure distribution is characterized by a spatially rapid acceleration from the attachment line Cp of roughly 0.12 to a rooftop level around -0.02, followed by a short adverse-gradient region, then an extended region of gradual acceleration. As expected, the most highly amplified waves found in the initial acceleration region are the stationary crossflow waves. Only the "critical" waves, i.e. those threatening to pass through N = 9, are shown. In figure 6.5A, the leading-edge suction level is just sufficient to prevent any of these waves from exceeding N = 9. The leading-edge suction level in figure 6.5B is slightly higher. These figures illustrate the sensitivity of the critical wave amplification to applied suction. An uncertainty on the order of 0.5 in amplification factor exists due to discretization. In both cases, the growth of the stationary crossflow wave is halted by the peak in the Cp distribution.
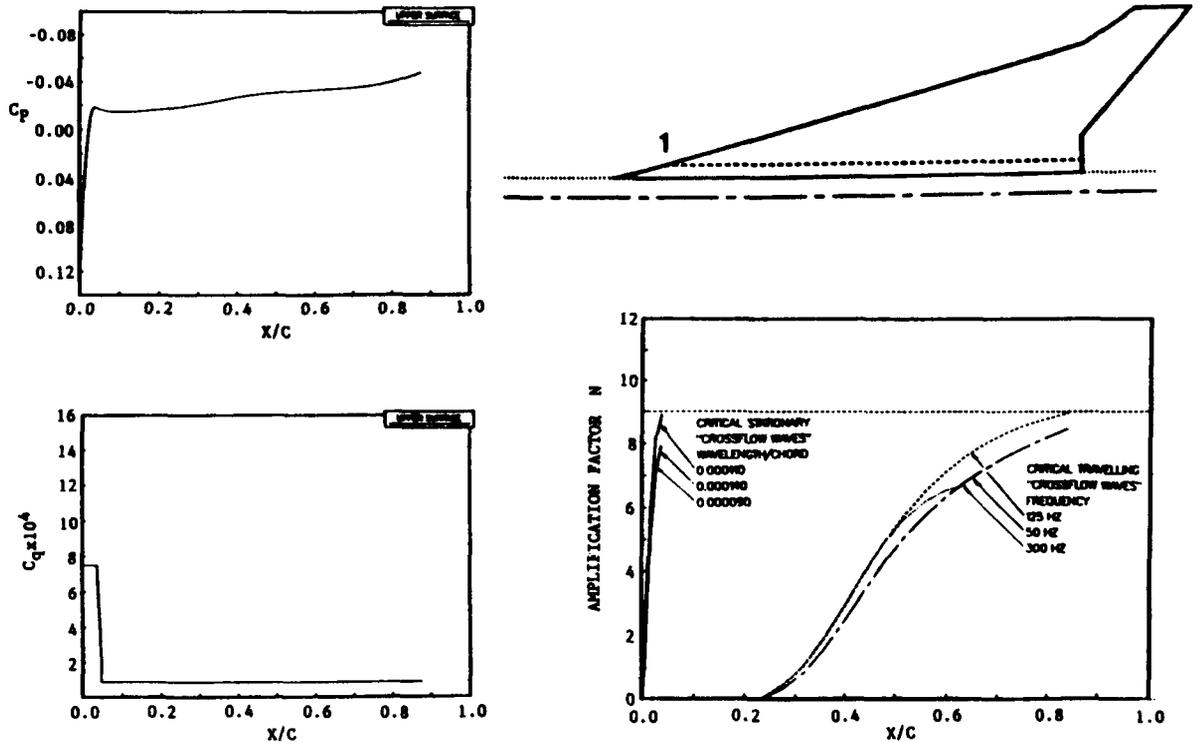
Figure 6.5A BOUNDARY LAYER STABILITY
MODIFIED AST WING - FINAL SUCTION
UPPER SURFACE @ ETA = 0.18
M = 2.2, hp = 58 kft, ALPHA = 2.0 deg

44
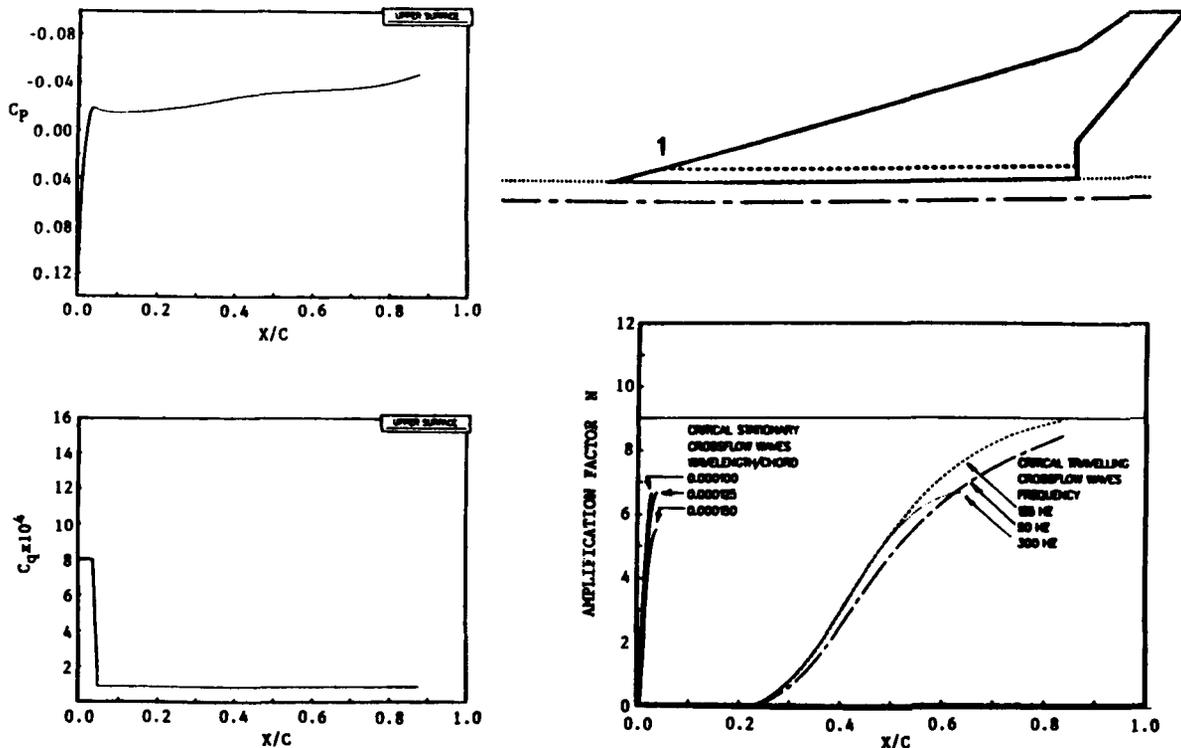
Figure 6.5B BOUNDARY LAYER STABILITY
MODIFIED AST WING - INCREASED L.E. SUCTION
UPPER SURFACE @ ETA = 0.18

The secondary, or sustaining suction level was set by the amplification of travelling crossflow waves in the mild gradient region, so no waves were found in the flat region ahead of X/C = 20%. The suction could, theoretically, be reduced in this region. The favored waves in the mild gradient region at this suction level are relatively low frequency (f = 125 Hz) highly oblique travelling crossflow waves. At lower secondary suction levels the frequency of the most amplified waves was higher, and the waveangles lower (not shown).

Figure 6.6A give stability results for the span station just inboard of the break on the lower surface. The acceleration to the rooftop is spatially more rapid, and the difference between the attachment line Cp (0.12) and the rooftop value (0.03) is less. This reduces stationary crossflow amplification to below the critical level, even without suction. However, the low-gradient region in the first 8 or 10 percent chord gives rise to travelling crossflow waves. The critical wave is found, at this suction level, around 4970 Hz at 75 degrees waveangle. Suction-on velocity component profiles in this region, shown in figure 6.6B, display inflection for waveangles of 65 degrees and above, confirming the identification of these waves as travelling crossflow. The most highly amplified competing waves at higher and lower waveangle are shown in figure 6.6A. The suction required to subdue these waves was retained over the chord, and was sufficient to prevent growth of all waves in the lower gradient region aft of 10% chord. Again, a small suction reduction could have been realized.

45
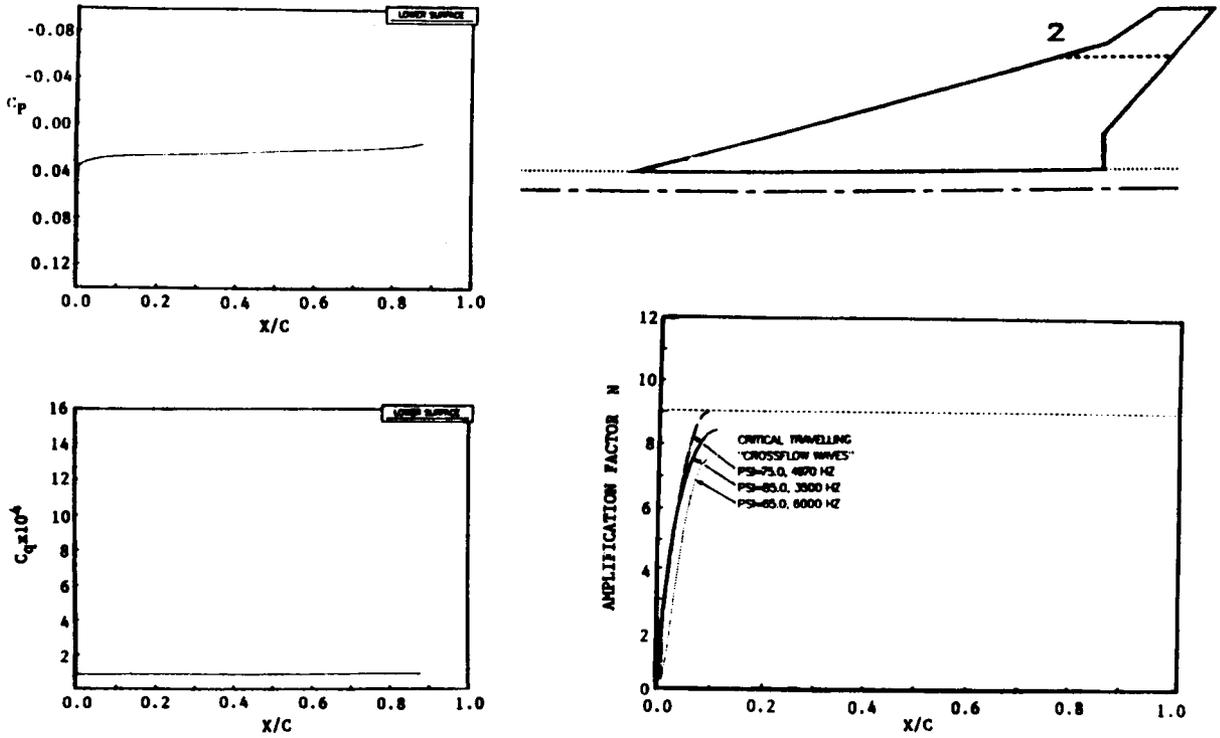
Figure 6.6A BOUNDARY LAYER STABILITY
MODIFIED AST WING - FINAL SUCTION
LOWER SURFACE @ ETA = 0.74
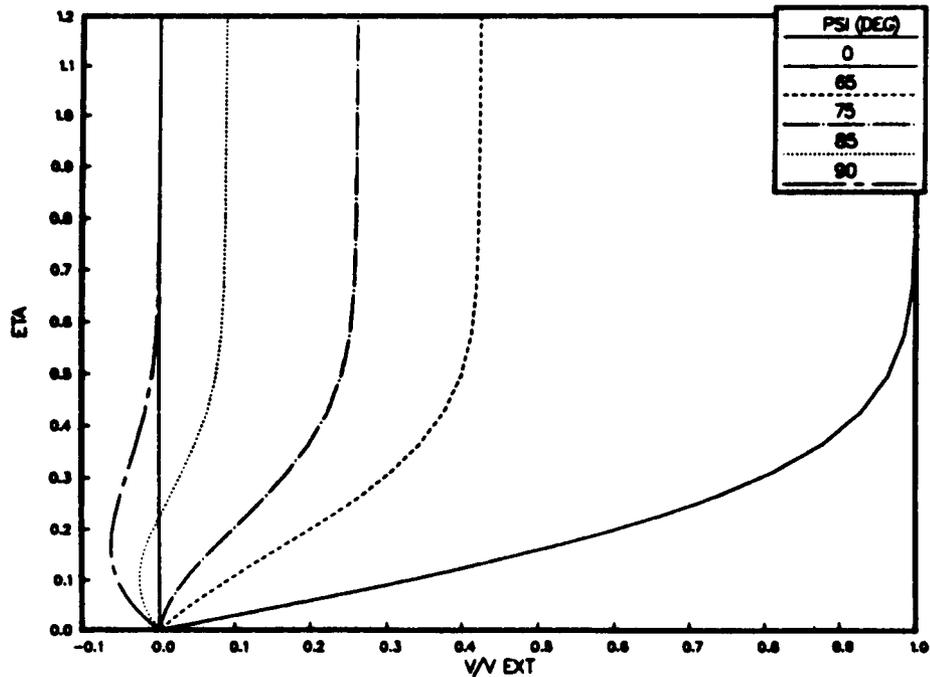
Figure 6.6B COMPONENT VELOCITY PROFILES
MODIFIED AST WING - FINAL SUCTION
LOWER SURFACE @ ETA = 0.74, X/C = 0.03

Figure 6.7A represents perhaps the most interesting case. This station, located on the upper surface just inboard of the sweep break, exhibits all three types of instability. The rooftop velocity level is higher than for the inboard station shown in figure 6.5A, C_p= -0.07 as opposed to -0.02. Stationary crossflow waves are amplified in the initially steep gradient, but so are travelling crossflow waves in the less steep region from about 1% to 5% chord. A stepped suction distribution was used here, resulting in the critical waves shown. Figure 6.7B shows the velocity component profiles at X/C = 0.022 with the suction shown in 6.7A. The clearly inflectional nature of the 85 and 88 degree component profiles identifies the 600 Hz, 87.5 degree wave as travelling crossflow. The very mild adverse region downstream of the velocity peak at 5% chord apparently has a beneficial effect, since the suction level required to stabilize the boundary layer downstream is very small, about Cq = -.00002. The most amplified wave in this region is found at 1000 Hz and 70 degrees. A look at the velocity profiles in figure 6.7C, taken at X/C = 0.31 with nominal suction, shows the virtual absence of boundary layer crossflow at this station, and confirms the identification of this wave as T-S. This is in agreement with Pfenninger and Vemuru[25], and shows the potential that careful design of the wing pressure distribution can have on suction requirements, and hence suction system size, weight, and cost.
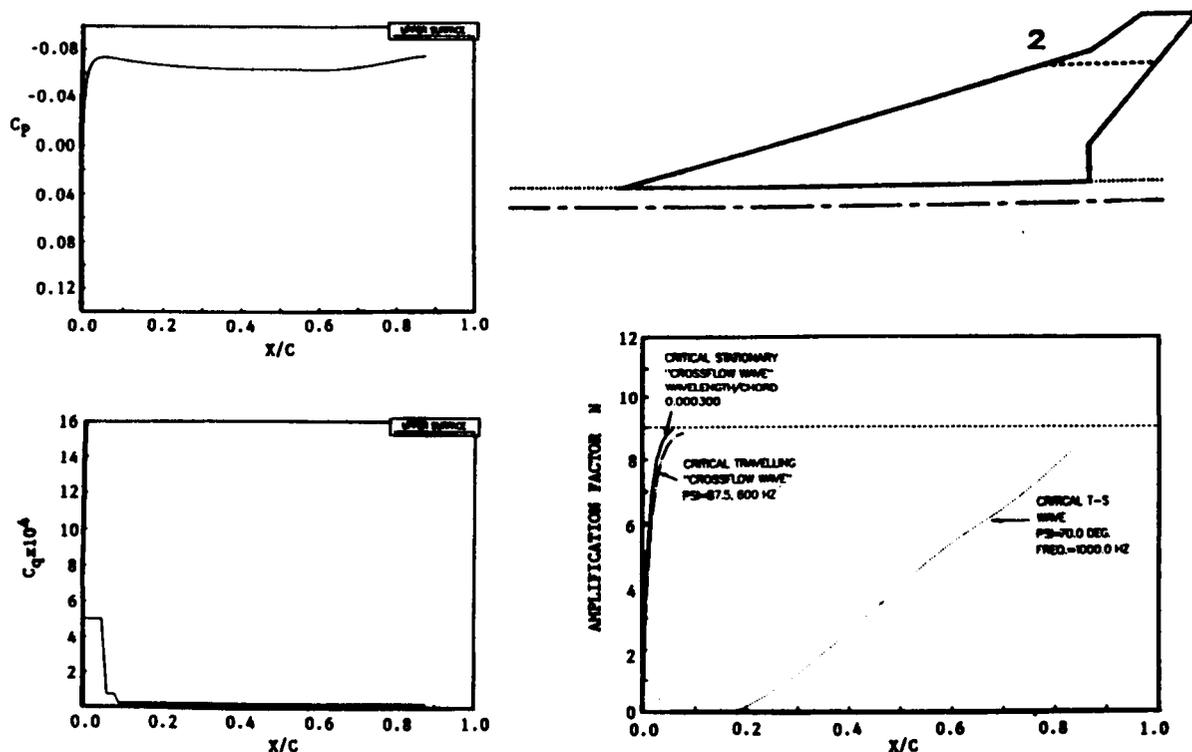
Figure 6.7A BOUNDARY LAYER STABILITY
            MODIFIED AST WING - FINAL SUCTION
            UPPER SURFACE @ ETA = 0.74
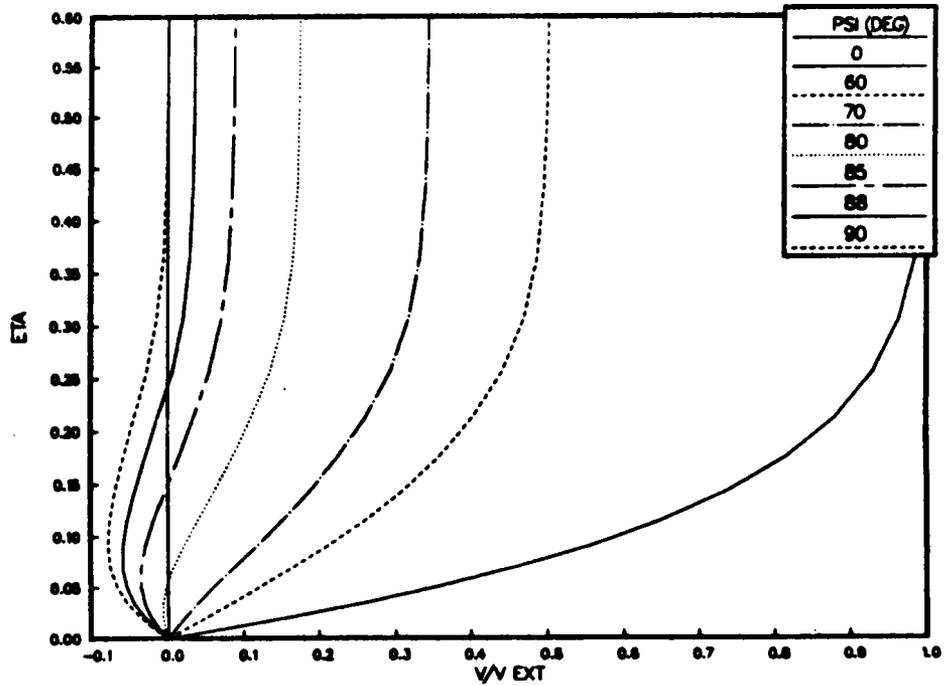
Figure 6.7B   COMPONENT VELOCITY PROFILES
MODIFIED AST WING - FINAL SUCTION
UPPER SURFACE @ ETA = 0.74, X/C = 0.022
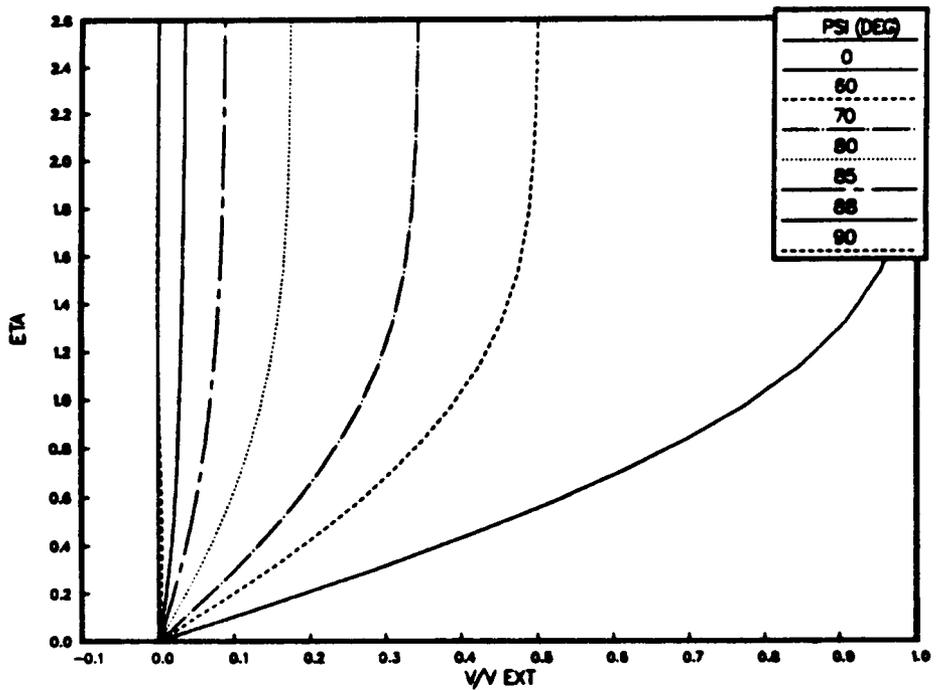
Figure 6.7C   COMPONENT VELOCITY PROFILES
MODIFIED AST WING - FINAL SUCTION
UPPER SURFACE @ ETA = 0.74, X/C = 0.31

48

The required suction levels from the stability analysis were interpolated and integrated over the wing to determine a suction massflow for laminar flow on both surfaces aft to the control surface hingeline. The total suction massflow was 22.3 lbm/sec at initial cruise conditions of Mach 2.2 and 58 kft. For comparison, the total suction massflow computed for the original AST wing used in the feasibility analysis is 23.8 lbm/sec. Although that an. lysis used conservatively high suction levels, the lower surface wingtip could not be laminarized, and had no suction. Although the feasibility of fitting suction ducting into the wing has been established, the design of a ducting system was not seen as appropriate to this study, and was not undertaken.

The skin friction drag was computed on the wing using the Douglas strip-theory boundary layer code, BLP. This program computes both laminar and turbulent boundary layers, with user-specified transition location, and correctly accounts for the effects of wall suction. The laminar skin friction with suction was computed. The inclusion of suction into the viscous drag calculation is important, since it contains what subsonically is accounted for as ram drag. A turbulent calculation with no suction was also made for purposes of comparison.

Wing-body drag due-to-lift, configuration volume wave drag, and trim drag were assumed not to differ from those computed for the original AST. This was deemed appropriate to the scope and intent of the study. The questions of proper wing drag accounting and optimum discharge of suction air have been addressed, and have been found to be significant issues at supersonic speeds. Suction air is assumed to enter through the porous skin, pass through internal ducting to a compressor driven by shaft power extracted from the thrust engines, then pass through ducting to an optimally expanded, aft facing nozzle, where it is ejected. A thermodynamic model has been formulated and used to quantify pumping and nozzle thrust effects for the suction air. This is described in appendix A.

A simple skin-friction estimate of the performance improvement of the laminarized original AST wing is shown in figure 6.8. This was done using flat-plate skin-friction charts. It is given in this section for purposes of comparison with the results of more detailed calculations, shown in figure 6.9. The more detailed calculations utilize a strip-theory boundary layer, and properly account for the effects of pressure distribution, wall suction, and the thermodynamics of the LFC pumping system. Since with a supersonic trailing edge there is no adverse pressure gradient associated with pressure recovery, there is no pressure drag benefit for laminarization, as in subsonic flow. For this reason it was expected that a simple skin friction estimate would be reasonably accurate for the supersonic case. Note the estimated 12% improvement in L/D for full wing laminarization.

Baseline TOGW = 750 000 lbf
5750 nm Mission
LFC weight penalty on suction area:
both surfaces - 2.82 psf
one surface - 1.98 psf

| LAMINAR EXTENT | L/D | L/D INCREASE | ----- RESIZE -------- | |
			TOGW CHANGE	FUEL BURN CHANGE
TURBULENT BASELINE	10.25	-----	-----	-----
BOTH WING SURFACES TO CNTL HINGES, EXCEPT LOWER SURFACE OUTBD & 6 DEG TURBULENT WEDGES. TURBULENT V & H TAIL.	11.35	10.7%	-6.5%	-12.4%
BOTH WING SURFACES TO CNTL HINGES, EXCEPT 6 DEG TURBULENT WEDGES. TURBULENT V & H TAIL.	11.49	12.1%	-7.5%	-14.0%
WING AND V & H TAIL, TO CNTL HINGES, EXCEPT 6 DEG TURBULENT WEDGES.	11.79	15.0%	-9.3%	-17.0%
WING AND V & H TAIL, TO CNTL HINGES. NO TURBULENT WEDGES.	11.99	17.0%	-9.5%	-18.1%

Figure 6.8 LFC BENEFIT ESTIMATE -
ORIGINAL AST WING,
BASED ON FLAT PLATE
SKIN FRICTION CALCULATIONS

The performance benefits for LFC, including the increased skin friction
due to suction and the thermodynamics of the suction system compressor and
exhaust nozzle, were computed and are presented in figure 6.9 for the AST
with the LFC-modified wing. The aerodynamic benefits are based on a 10%
total pressure loss for suction air from the wing surface to the compressor.
A 5% duct loss is assumed between the compressor and nozzle. Realistic
efficiencies of 80% for the compressor and 98% for the nozzle were assumed.
Despite the additional detail, the results of figure 6.9 compare very well
with the simple skin-friction estimates of figure 6.8. The details of the
suction system drag accounting are given in appendix A.

The gross weight and mission fuel burn reductions for the LFC
configurations are the results of sizing calculations. Since the baseline
AST engine sizing was based on a takeoff noise constraint, engine size was
assumed to be proportional to take-off gross weight (TOGW). The weights of
the wing, suction system, and landing gear were proportional to gross weight
as well. The LFC system weight, based on reference 26, was assumed to be
2.82 psf for both-surface suction and 1.98 psf for single-surface suction,
based on suction area. Takeoff wing loading was held constant. Fuselage and
other weights were considered fixed. The decrease in TOGW seen in the
figures is principally due to the fuel reduction. The wing planform areas
are reduced by the same percentages as the TOGW, but the resulting operating
empty weights are found to be in the neighborhood of 0.5% less than that of
the turbulent baseline airplane for all of the cases shown.

Baseline TOGW = 750 000 lbf
5750 nm Mission
LFC weight penalty 2.82 psf
over suction area only.

LAMINAR EXTENT	L/D	L/D INCREASE	RESIZE	
			TOGW CHANGE	FUEL BURN CHANGE
TURBULENT BASELINE	10.25	-----	-----	-----
BOTH WING SURFACES TO CNTL HINGES, EXCEPT 6 DEG TURBULENT WEDGES, TURBULENT V & H TAIL. DISCHARGE AT V_{fs}.	11.52	12.4%	-7.8%	-14.4%
BOTH WING SURFACES TO CNTL HINGES, EXCEPT 6 DEG TURBULENT WEDGES, TURBULENT V & H TAIL. SONIC DISCHARGE.	11.50	12.2%	-7.6%	-14.1%
WING AND V & H TAIL, TO CNTL HINGES, EXCEPT 6 DEG TURBULENT WEDGES, SONIC DISCHARGE.	11.80	15.1%	-9.4%	-17.2%
WING AND V & H TAIL, TO CNTL HINGES NO TURBULENT WEDGES, SONIC DISCHARGE.	12.00	17.1%	-9.6%	-18.2%

Figure 6.9 LFC BENEFIT SUMMARY -
MODIFIED AST WING,
INCLUDING SUCTION AND
PUMPING SYSTEM EFFECTS

7. MACH 4 TRANSPORT - FEASIBILITY

As part of an overall attempt to identify the applicability limits of Laminar Flow Control, and to identify useful trends, the feasibility of laminarizing a configuration with a higher design Mach number was undertaken. The configuration chosen was developed as part of ongoing High-Speed Commercial Transport (HSCT) studies, being done under NASA contract. The configuration is shown in figure 7.1. This configuration was designed for a cruise Mach number of 5.0, and was fully blended, with an inboard wing leading-edge sweep of 80 deg. At the cruise attitude, the lower surface was a section of a cone at zero degrees angle of attack, so that spatial pressure variations would be minimized. The upper surface shape was dictated by practical constraints regarding volume distribution and packaging.
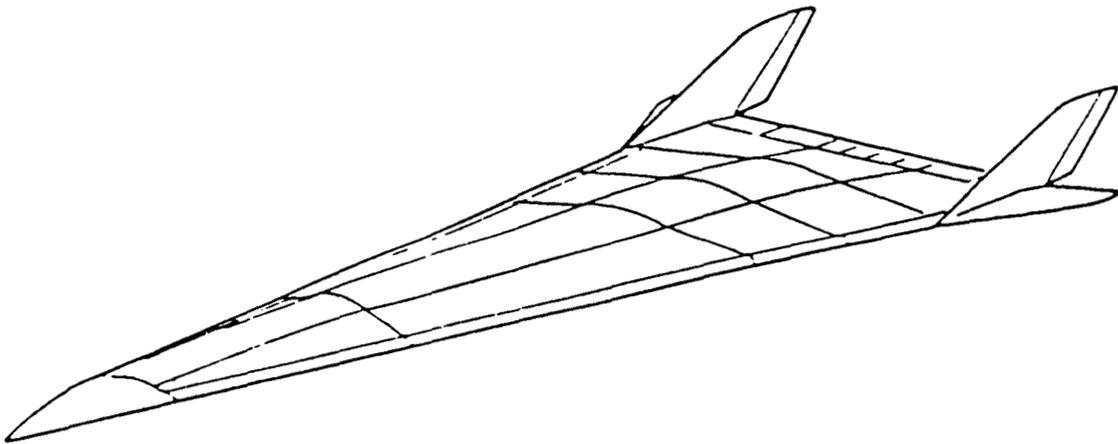
Figure 7.1   DAC HSCT CONFIGURATION

53

The analysis was conducted at a Mach number of 4.0, which was the highest Mach number for which a solution could be obtained from the Kaups-Cebeci boundary layer code. The angle of attack was 4.75 degrees, corresponding to best configuration L/D. The corresponding initial cruise altitude was approximately 85 kft. The configuration was run through the MDC SCRAM Euler code[27] at Mach 4.0 and the design angle of attack. At this Mach number the sonic sweep angle is 75.52 degrees so the 80 degree inboard leading edge is subsonic. Figures 7.2A through 7.2C show the pressure distributions in three selected planes taken at different axial stations on the configuration. Only one side of the configuration is shown. Except in the leading-edge region, an essentially flat design pressure distribution was achieved on the lower surface. The theoretical attachment line pressure coefficient for Mach 4.0 and 80 degrees sweep is .0340. Note that the maximum pressure coefficient is substantially above the theoretical value, and is found on the lower surface inboard of the leading edge at all axial stations shown. These pressure coefficients are, in fact closer to the wedge-flow values corresponding to the local surface incidences relative to the freestream. Comparisons with the calculations of Jones[28] for elliptical cones in supersonic flow indicate that attachment is indeed occurring at the point of maximum pressure coefficient.

The surface velocity field computed by the SCRAM code was used to directly calculate the momentum-thickness Reynolds number along the indicated attachment line in the midspan region. The computed value was 1827. It was felt that this high R_Θ value would preclude laminarization of the lower surface, so further analysis of this configuration was terminated.
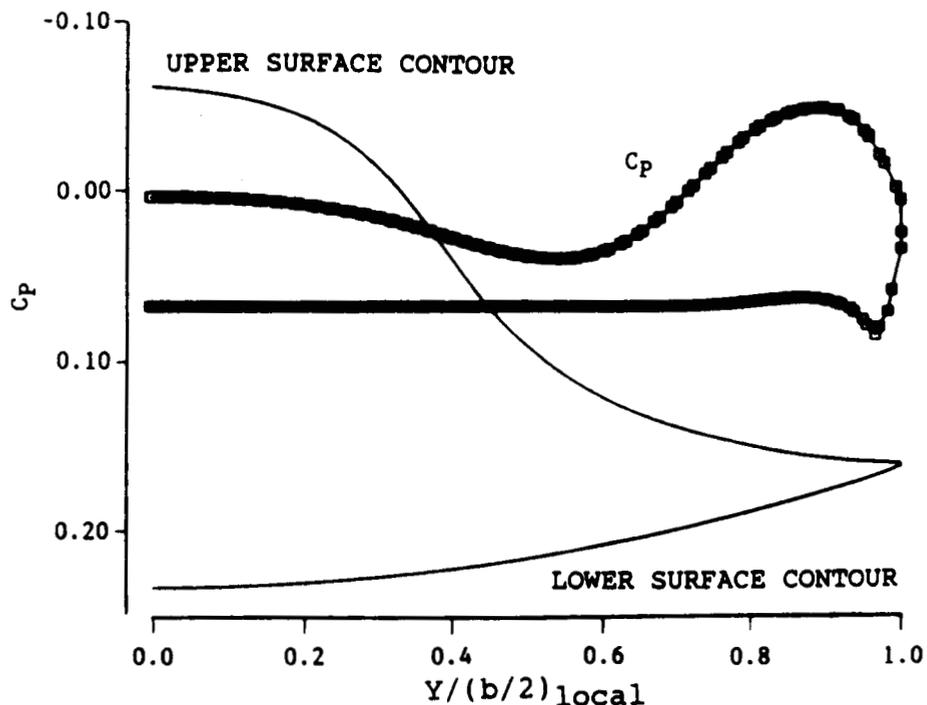
Figure 7.2A   SCRAM EULER SOLUTION FOR HSCT CONFIGURATION
16 PERCENT LENGTH AXIAL STATION
MACH = 4.0, ALPHA = 4.75 deg
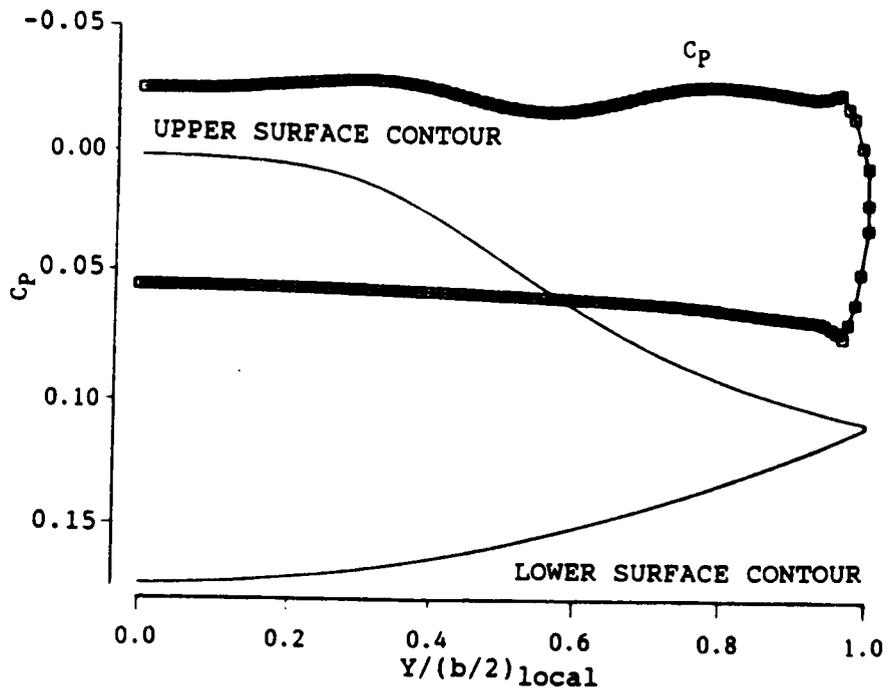
Figure 7.2B   SCRAM EULER SOLUTION FOR HSCT CONFIGURATION
              48 PERCENT LENGTH AXIAL STATION
              MACH = 4.0, ALPHA = 4.75 deg
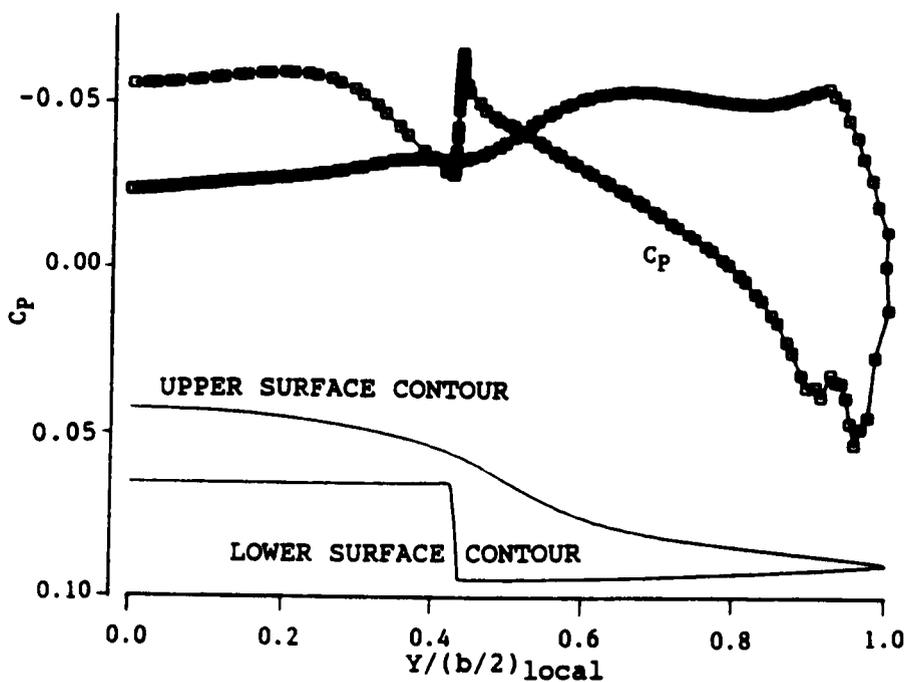
Figure 7.2C   SCRAM EULER SOLUTION FOR HSCT CONFIGURATION
              80 PERCENT LENGTH AXIAL STATION
              MACH = 4.0, ALPHA = 4.75 deg

8. LFC ON SUPERSONIC FIGHTERS

One emerging application of supersonic cruise technology is to fighter aircraft, where efficient supersonic cruise capability can greatly enhance operational utility and survivability. In keeping with the study objective of determining the applicability of LFC to various types of supersonic cruise airplanes, a study of the application of LFC to supersonic cruise fighter airplanes was conducted. The objectives for this part of the study were to determine the feasibility of applying LFC technology to this type of aircraft and to evaluate LFC benefits for typical missions involving significant supersonic cruise segments. The two configurations chosen for study are shown in figures 8.1 and 8.2.
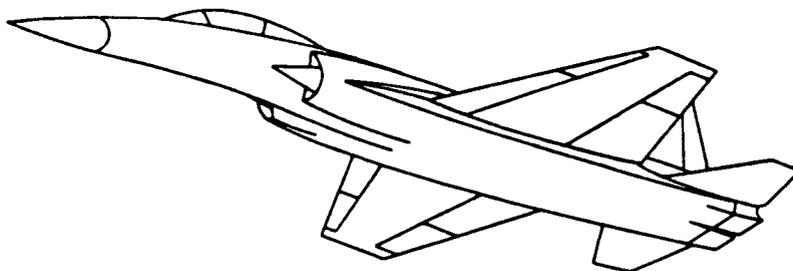
GP83-0447-31

Figure 8.1   SF-1107 SUPERSONIC CRUISE FIGHTER CONFIGURATION
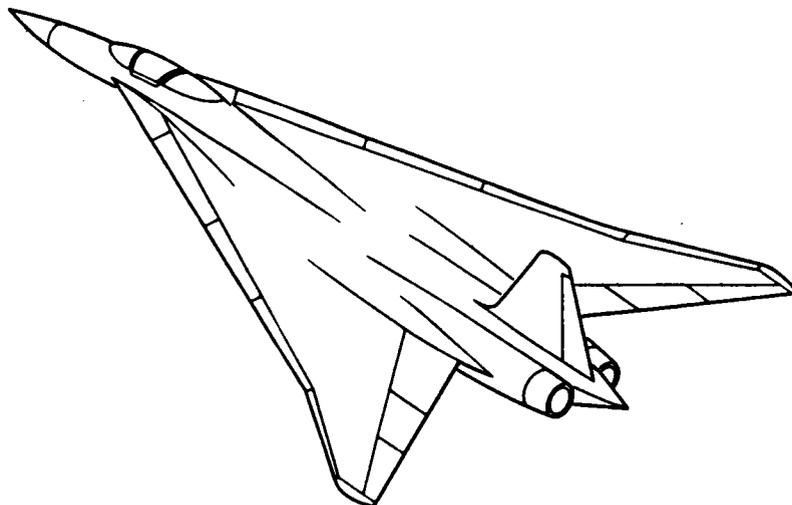
GP83-0447-7

Figure 8.2   SF-1302 SUPERSONIC CRUISE FIGHTER CONFIGURATION

57

The two configurations, designated SF-1107 and SF-1302, are generic examples of fighter aircraft designed to cruise at or near Mach 2.0. The SF-1107 aircraft uses the supersonic wing leading edge approach, while the SF-1302 employs a highly swept subsonic wing leading edge design. A comparison of the physical characteristics of the two configurations is shown in figure 8.3. Their basic missions are to cruise out at subsonic speeds to a prescribed distance from the target, accelerate and climb to Mach 2.0 cruise conditions, dash to and from the target at Mach 2.0 over the prescribed hostile territory, then return to base subsonically. These configurations evolved during a rather detailed advanced design study to investigate the respective sizes of aircraft to meet certain supersonic cruise mission requirements for both low sweep and highly swept wing configurations. They should, therefore, be fairly representative of fighter configurations one might expect to see in the future. It should be noted, however, that the SF-1302 aircraft is significantly larger than the SF-1107 not because it is inherently less efficient, but because it it was designed to a longer mission.

A major part of this study effort was concentrated on the stability of the boundary layer on the two aircraft wings. A detailed analysis of the boundary layer and its stability with and without suction on the two fighter wing configurations was conducted for a cruise Mach number of 2.0 and angle of attack of 4.0 degrees. The inviscid pressures obtained from an Euler code (FLO-67) are used to generate the boundary layer solutions using a modified version of the Kaups-Cebeci code. The boundary layer stability was analyzed with compressible linear stability methods, using the NASA COSAL code. Performance and sizing analyses were conducted to determine the effects of laminarization on the gross weight required to make certain specified missions.

Item		Configuration	
		SF-1107	SF-1302
1. Wing Area	(ft^2)	530	741
2. LE Sweep	(deg)	31	71/61.5
3. Wing Span	(ft)	38.15	37.51
4. Aspect Ratio		2.75	1.89
5. Takeoff GW	(lb)	33,200	37,869
6. Internal Fuel		10,702	13,681
7. Combat Radius on Supersonic Cruise Mission	(NM)	400	500

GP83-0447-56-T

Figure 8.3   A CHARACTERISTICS COMPARISON OF THE SF-1107 AND SF-1302 AIRCRAFT

9. SF-1107 FIGHTER WING

The SF-1107 fighter configuration is shown in figure 8.1. The wing is simple geometrically, consisting of 5% thick symmetric parabolic biconvex sections with no twist. Wing chord varies linearly from 22.50 ft. at the centerline to 5.45 ft. at the tip. Leading edge sweep is 32 degrees. The inviscid flow solutions on the isolated SF-1107 wing were obtained using the FLO-67 Euler code. The pressure distributions were found to be very smooth, which is essential for an accurate stability analysis. The surface pressure distribution at the 50% semispan station is shown in figure 9.1. The corresponding upper surface isobar plot, which is very conical, is shown in figure 9.2. For the parabolic biconvex airfoil in supersonic flow, Cp varies almost linearly with X/C, giving a nearly constant favorable gradient over the chord. Although this stabilizes the boundary layer against low waveangle Tollmien-Schlichting waves, the presence of boundary-layer crossflow caused by isobar sweep causes amplification of high-waveangle crossflow waves.
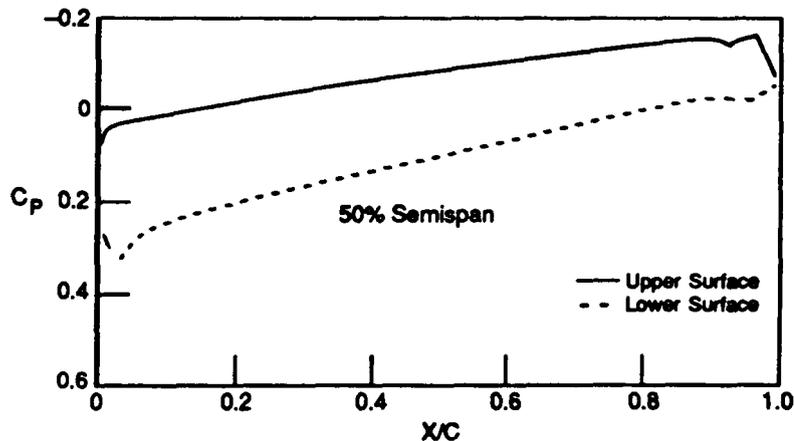
Figure 9.1   SURFACE PRESSURE DISTRIBUTION AT 50% SEMISPAN
              SF-1107 WING WITH BICONVEX SECTION

$M_\infty = 2.0$, $\alpha = 4°$

The boundary layer solutions for this case, obtained using the modified version of the Kaups-Cebeci code, were examined in detail to allow confidence in their subsequent stability characteristics. All boundary layer analyses were conducted for a freestream Mach number of 2.0 and 4 degrees angle of attack, at a standard day altitude of 40 kft. Some sample results of the analyses are shown in figures 9.3 through 9.11. The results shown in these figures are for 50% semispan on the upper surface with no boundary layer suction. Figures 9.3 and 9.4 show very smooth distributions of external velocities, U_E and W_E, obtained from the FLO-67 Euler code, in the polar coordinate system (figure 5.7) used in the Kaups-Cebeci code. For emphasis, the second derivative of Cp with X/C is also shown in figure 9.5. These distributions are plotted against chord fraction, X/C. The smooth distribution of Cp" is necessary for accurate stability calculations.

59
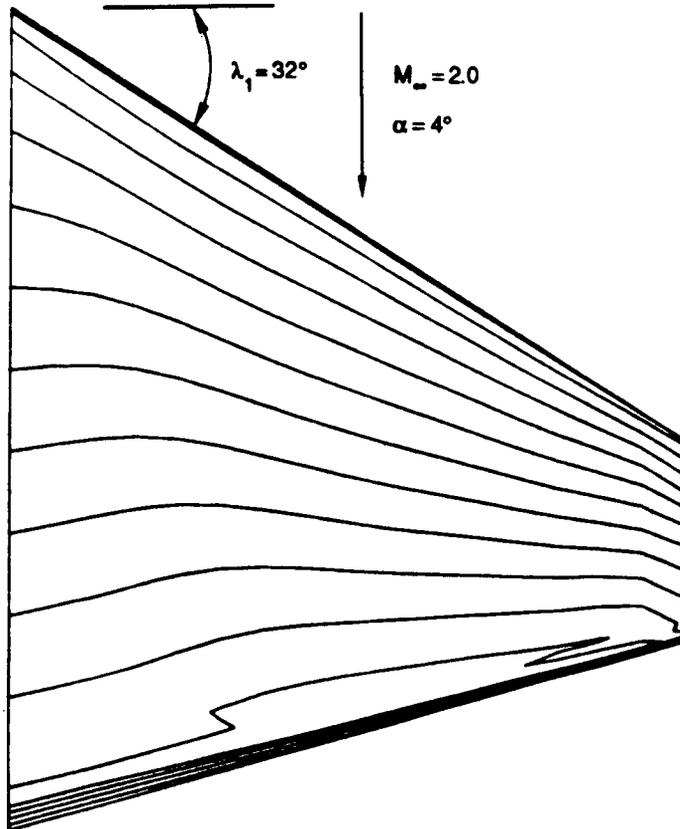
Figure 9.2   UPPER SURFACE PRESSURE CONTOURS, SF-1107 WING
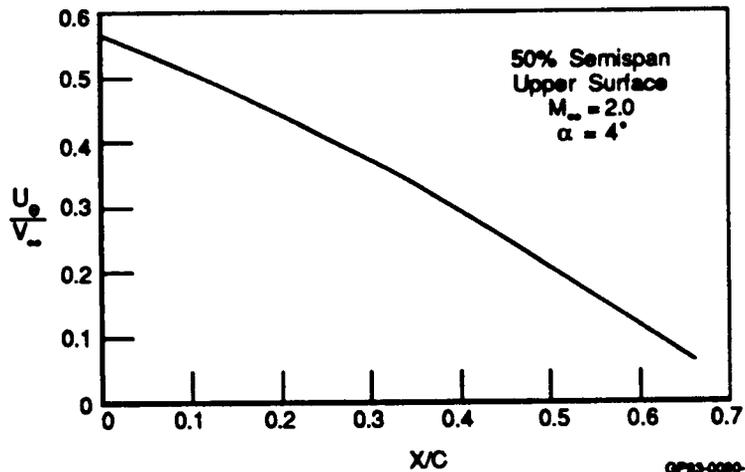
Figure 9.3   DISTRIBUTION OF VELOCITY Ue ON THE UPPER SURFACE
AT 50% SEMISPAN, SF-1107 WING
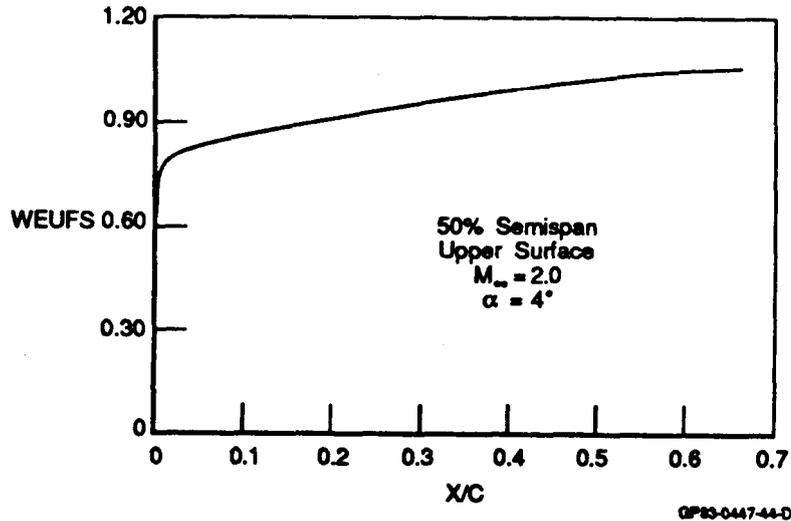
Figure 9.4   DISTRIBUTION OF VELOCITY We ON THE UPPER SURFACE
AT 50% SEMISPAN, SF-1107 WING
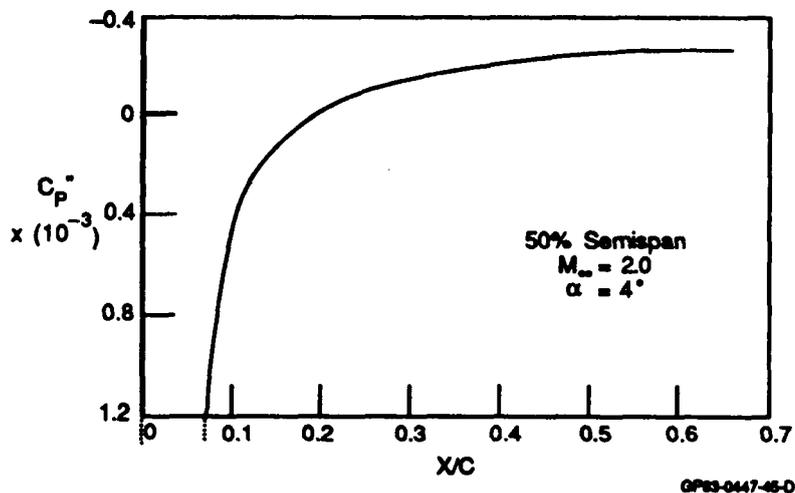
Figure 9.5   SECOND DERIVATIVE Cp" VS. X/C ON THE UPPER SURFACE
AT 50% SEMISPAN, SF-1107 WING

The boundary layer velocity profiles along the radial direction are shown
in figure 9.6 at four different chord fractions ranging from 1% to 51%.
Figure 9.7 shows the high degree of self-similarity of typical consecutive
velocity profiles in scaled coordinates, Y/DELSTX. However a closer
examination indicates that they do not exactly fall on a single curve as
anticipated for zero radial pressure gradient. Figure 9.8 shows that the
second derivative of the radial velocity, u", is well behaved for the middle
and outer regions, but not near the wall. This problem was alluded to in
section 8. The near-wall numerical oscillation is also reflected in the wall
shear stress (Figure 9.9).

61
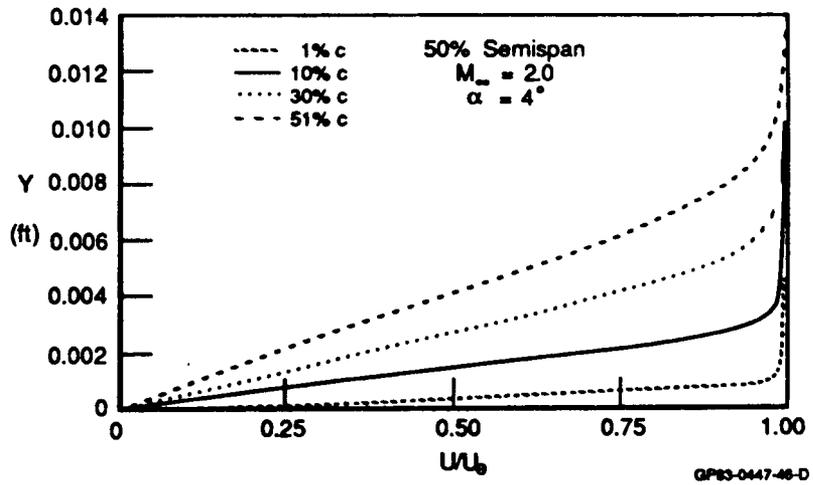
Figure 9.6   BOUNDARY LAYER VELOCITY PROFILES ALONG THE RADIAL
DIRECTION ON THE UPPER SURFACE AT 50% SEMISPAN,
SF-1107 WING, NO SUCTION
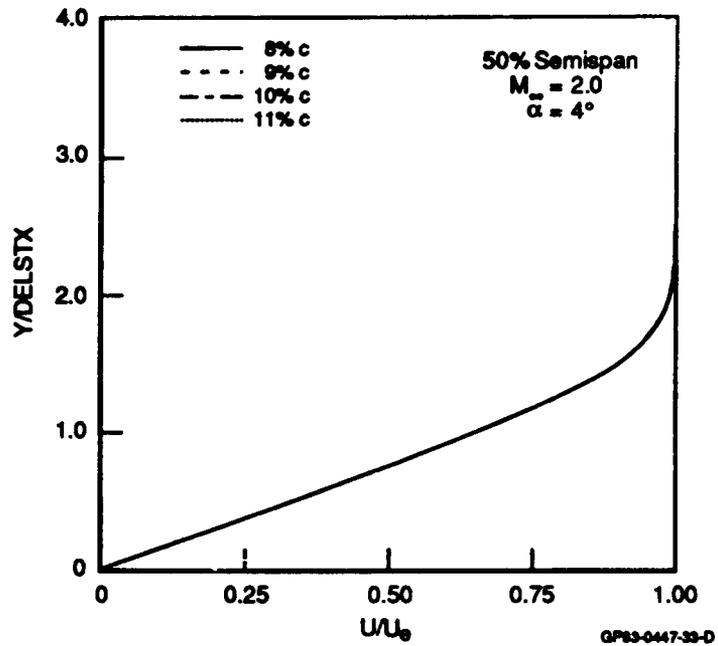
Figure 9.7   CONSECUTIVE VELOCITY PROFILES IN SCALED COORDINATES
AT 50% SEMISPAN, SF-1107 WING, NO SUCTION
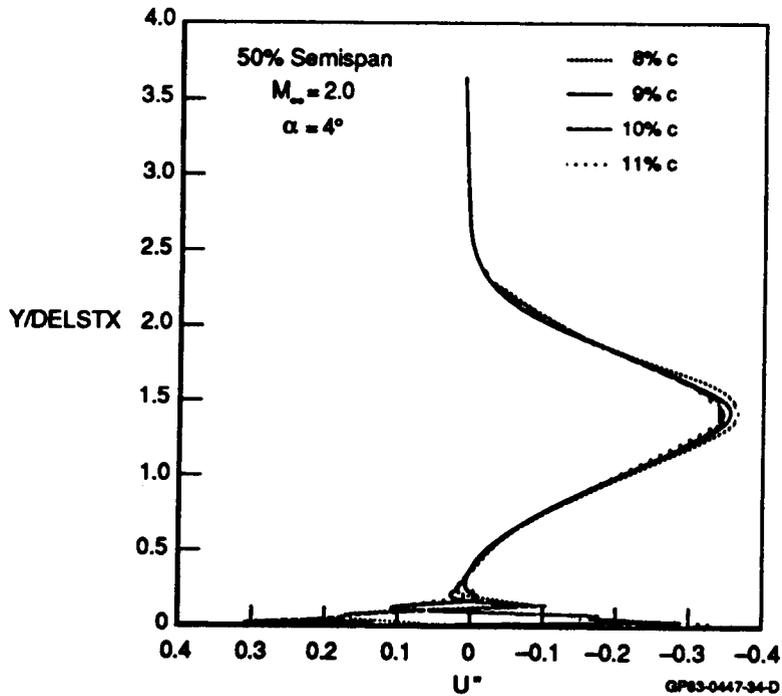
Figure 9.8   SECOND DERIVATIVE OF VELOCITY VS. SCALED NORMAL
              COORDINATES AT FOUR CONSECUTIVE CHORD STATIONS,
              SF-1107 WING, NO SUCTION
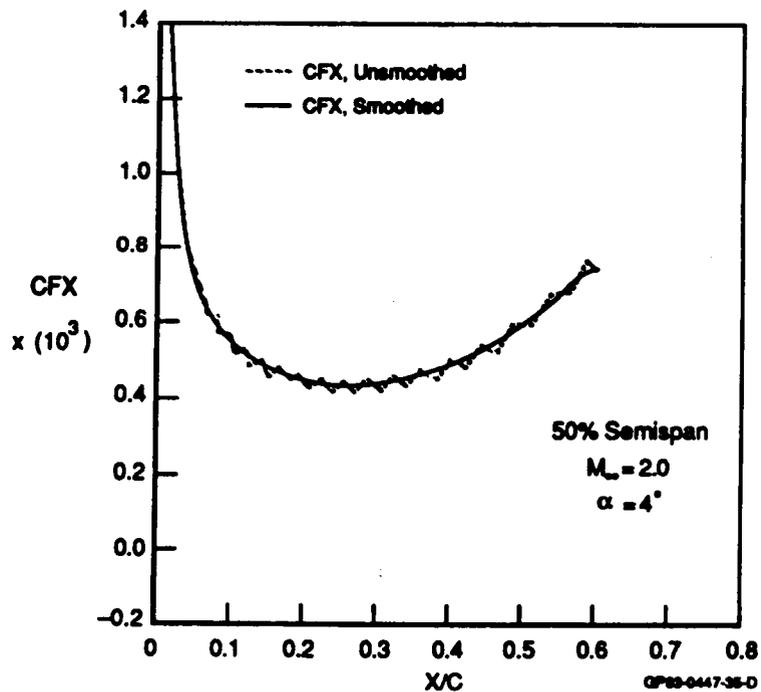
Figure 9.9   WALL SHEAR STRESS VS. X/C AT 50% SEMISPAN,
              SF-1107 WING

These oscillations caused great concern in the early phase of this study, and motivated the addition of a simple averaging scheme to the Kaups-Cebeci code. By averaging each consecutive pair of velocity profiles, all signs of the oscillation dissappear, as shown by the solid line in figure 9.9. Comparison stability analyses conducted with and without the modification have shown no differences in computed N-factors. It should be noted, however, that the oscillations have been observed to increase with Mach number, so the improved code incorporating the averaging scheme would likely have to be used under these conditions.

Prior to conducting stability analyses, the effects of suction on boundary layer velocity profiles were also studied. There are several effects of suction. Suction thins the boundary layer and thereby lowers the effective Reynolds number. This thinning effect is demonstrated in figure 9.10, where the velocity profiles at 25% chord station are plotted against the normal coordinate (Y) for different suction values. With increased suction, the thickness of the boundary layer is reduced considerably. Another effect of suction is to change the boundary layer shape factor. This is quite evident from figure 9.10, which shows that the profile shape also changes appreciably.
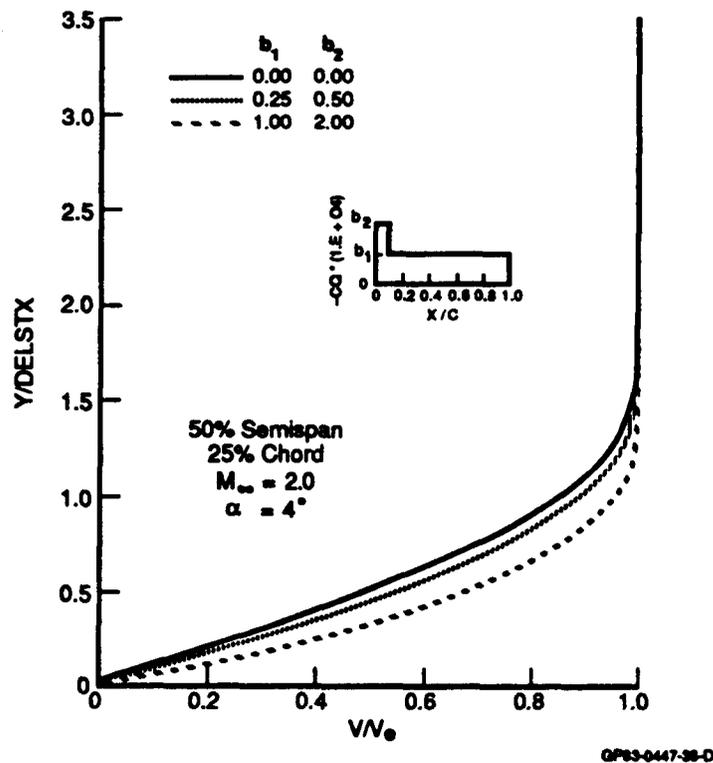
Figure 9.10   EFFECT OF SUCTION ON VELOCITY PROFILES AT 25% CHORD AND 50% SEMISPAN LOCATION, SF-1107 WING

The suction also causes the inflection point of the crossflow profile to move closer to the wall, where the increased viscosity acts to help damp out crossflow waves. This is demonstrated in figure 9.11, where a crossflow parameter, (DELTCF) is plotted against chord fraction for two different suction levels. This crossflow parameter is an integrated value of the crossflow boundary layer thickness. It is quite clear that this thickness is reduced substantially with suction. All of these effects of suction are known to have a stabilizing influence on the boundary layer[29].

A stability analysis of the boundary layer profiles obtained from the Kaups-Cebeci code was performed using COSAL. Analysis with and without suction was conducted to determine the most amplified wave. In this study, both the constant waveangle and constant wavelength options were used, for the reasons outlined in the beginning of section 6. The growth of both stationary and nonstationary crossflow waves was calculated. Both the upper and lower surfaces of the wing were examined in detail. Three spanwise stations (inboard, midspan, and outboard) were analyzed.
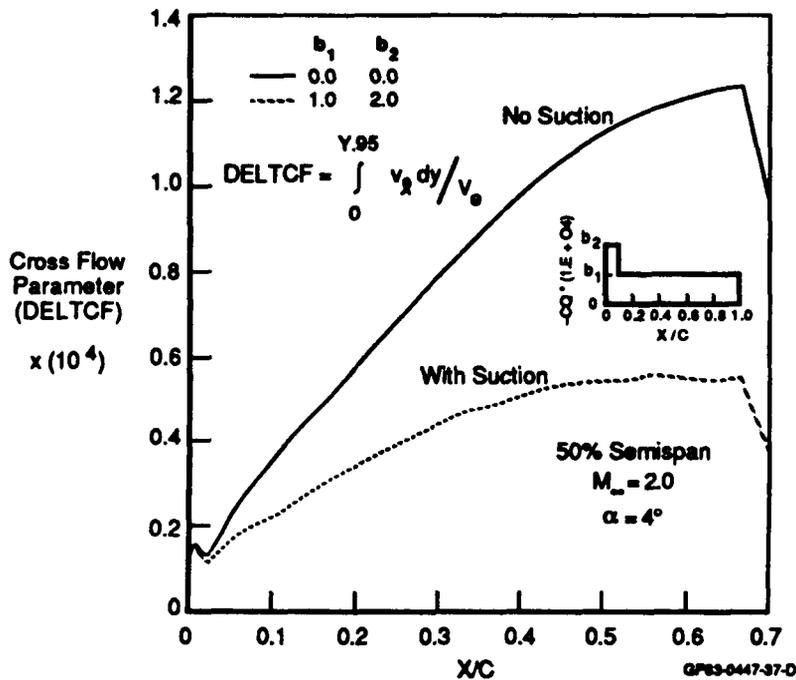
Figure 9.11   EFFECT OF SUCTION CROSSFLOW PARAMETER, DELTCF, AT 50% SEMISPAN LOCATION, SF-1107 WING

For the zero suction case, initially a broad range of frequencies, waveangles, and wavelengths were analyzed to identify the most amplified waves. Figure 9.12 shows the results of a stationary (f = 0.5 Hz) crossflow stability analysis on the upper surface at the midspan station. The N-factors are plotted against X/C for different values of the wavelength-to-chord ratio, (XLENC). An attempt was made to find a band of XLENC for which the growth of these waves could be important, and it appears that the band lies between 0.001 and 0.003. The maximum amplification factor occurs near XLENC = 0.0015.
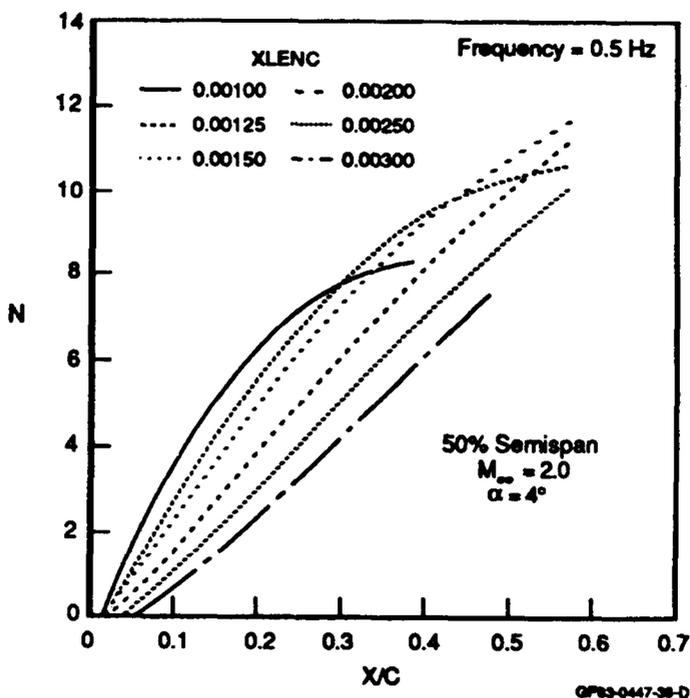
Figure 9.12   STATIONARY CROSSFLOW INSTABILITY WITHOUT SUCTION,
              SF-1107 WING

Figure 9.13 shows a stability chart constructed from the results of many runs for the zero suction case. Frequency is plotted against the local momentum-thickness Reynolds number, R_Θ, where N = 9 was first found, indicating transition. Several wave orientation angles are shown. Since the computed N-factor varies with wavelength, waveangle, and frequency, $R_{\Theta\ N=9}$ as defined here is the dependent variable. It is observed that the minimum $R_{\Theta\ N=9}$ is approximately 1935 (found at approximately the 8% chord station), and the frequency and orientation angle of the corresponding wave are 10-12 kHz and 80 degrees, respectively. The largest N-factors computed are found for frequencies around 5 kHz and PSI = 80 degrees. The corresponding XLENC was around 0.004 (not shown here). Figure 9.14 shows the N-factors for PSI = 80 degrees and several different frequencies. The N-factors first reaches a value of nine at approximately the 8% chord location for f = 10 kHz. This indicates that natural laminar flow could exist only up to the 8% station. For a frequency of 5 kHz, the N-factor reaches a value as high as 23, whereas for higher frequencies the maximum values are considerably smaller. The higher frequency waves have more rapid initial growth, but become stable in a shorter distance from the leading edge, due to the thickening boundary layer.

It is perhaps worth noting here that the results of the linear stability theory may not be too meaningful when computed N-factors are very large, since presumably the boundary layer would have undergone transition, or at least departed the linear region (reference 30). Therefore, more significance should be attached to the question of which wave reaches the critical range of, say, 7 to 12 first. For practical purposes a critical N-factor of 9 is being used in this study.
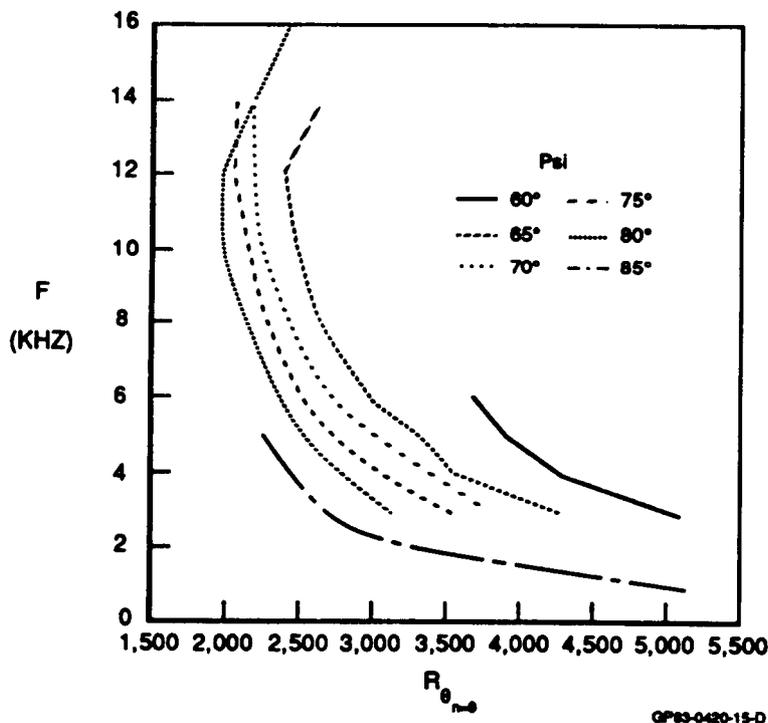
Figure 9.13   FREQUENCY VS. R_Θ CORRESPONDING TO N = 9, NO SUCTION, 50% SEMISPAN, SF-1107 WING
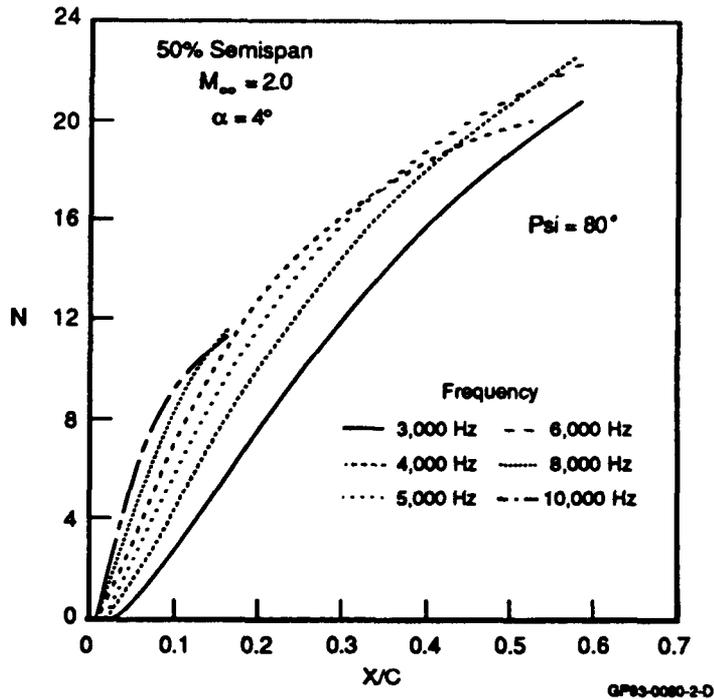
Figure 9.14   AMPLIFICATION FACTOR FOR DIFFERENT FREQUENCIES
NO SUCTION, 50% SEMISPAN, SF-1107 WING

The boundary layer velocity profiles on the wing were analyzed in order
to gain insights into the type of instabilities present at high waveangles as
observed here. The velocity profiles resolved along different wave
orientation angles were examined at several chord stations at the 50%
semispan location. The analysis offered some valuable information about the
development of inflections in the velocity profiles from the leading edge to
the 60% chord station for different wave orientation angles. Figures 9.15
through 9.18 show component velocity profiles at different chord stations,
but no suction, for orientation angles of 70, 80, 85, and 90 degrees
respectively. It is observed that for angles, PSI, of 80 degrees and up,
there is a visible inflection, which becomes deeper and farther above the
surface as waveangle is increased. This analysis indicates that the
mechanism of instability for the critical waves found in the stability
analysis is inflectional, so the waves should be classified as travelling
crossflow waves.
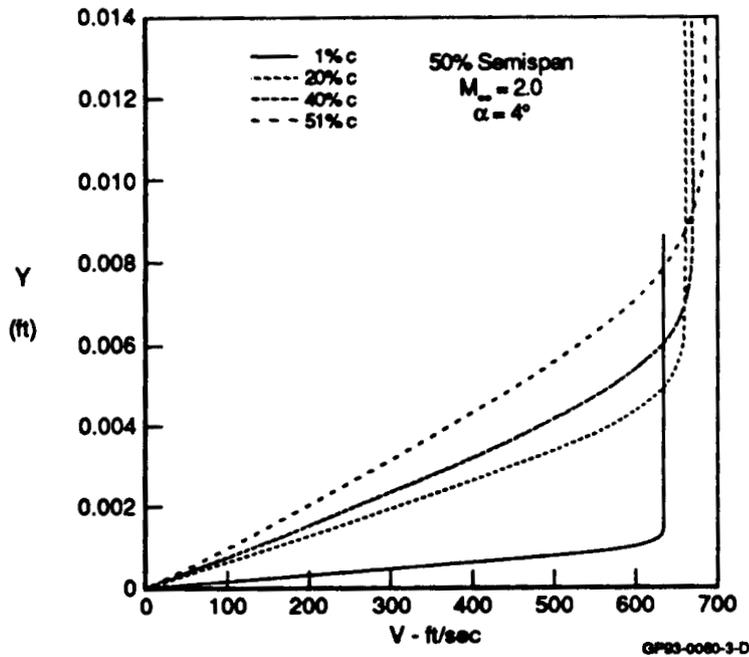
Figure 9.15 BOUNDARY LAYER VELOCITY PROFILES AT PSI = 70 DEGREES, 50% SEMISPAN, NO SUCTION, SF-1107 WING
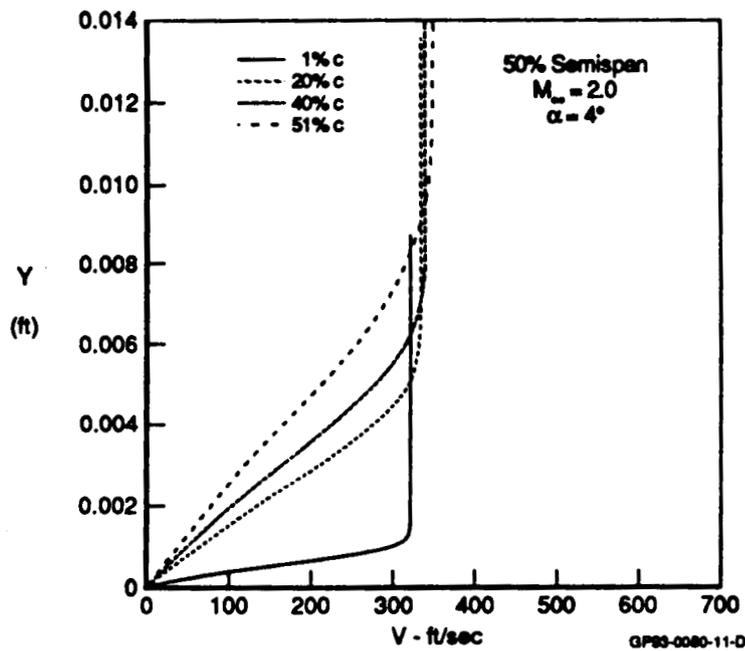
Figure 9.16 BOUNDARY LAYER VELOCITY PROFILES AT PSI = 80 DEGREES, 50% SEMISPAN, NO SUCTION, SF-1107 WING

69
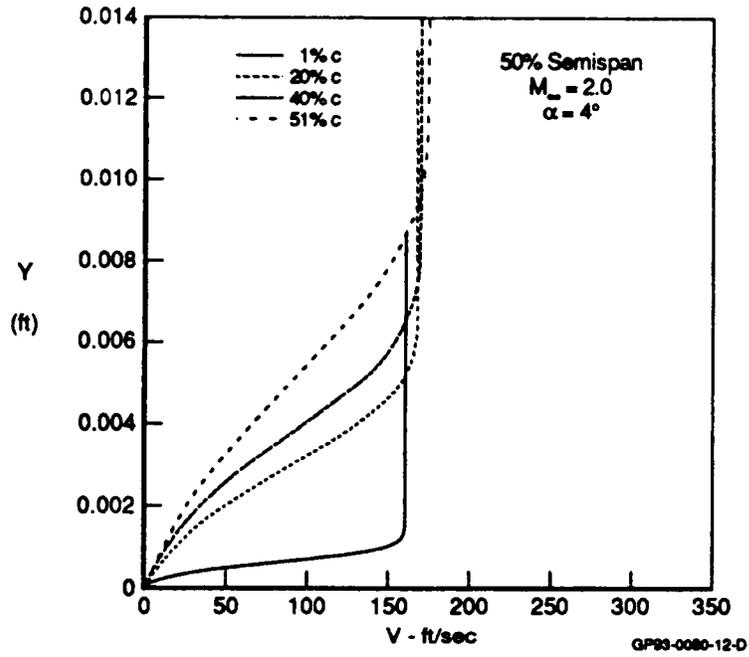
Figure 9.17   BOUNDARY LAYER VELOCITY PROFILES AT PSI = 85 DEGREES,
50% SEMISPAN, NO SUCTION, SF-1107 WING
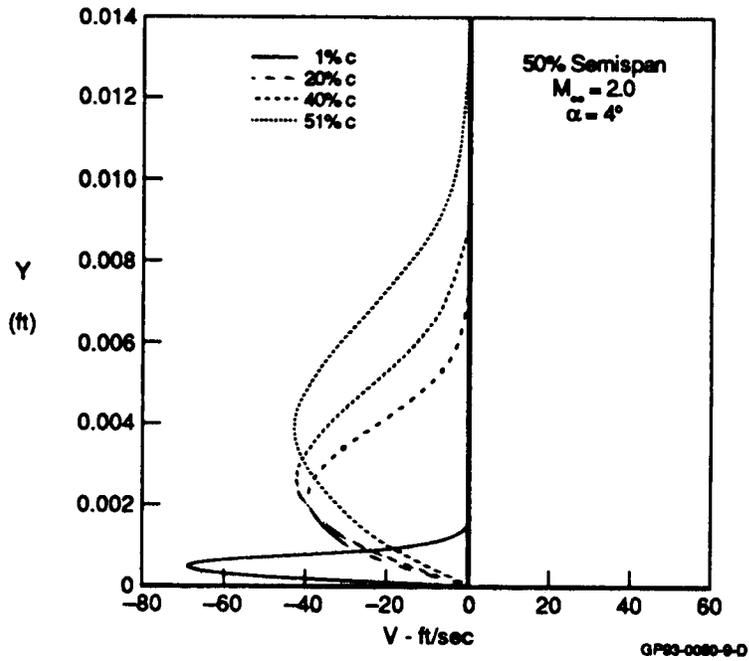
Figure 9.18   BOUNDARY LAYER VELOCITY PROFILES AT PSI = 90 DEGREES,
50% SEMISPAN, NO SUCTION, SF-1107 WING

70

The boundary layer with suction has also been analyzed in detail. In the next several figures are shown the results of the stability analysis with suction. Figure 9.19 shows the effect of suction on the amplification of the 5 kHz, 80 degree wave. This wave had the highest maximum amplification factor with suction off. Note the extent to which growth of this wave can be controlled with relatively low suction levels.

Due to the various adverse aspects of boundary layer suction, such as system weight, increased skin friction drag, etc., the aim is to apply just enough suction so that the N-factors do not grow beyond a value of 9. From this figure it would appear that the suction level corresponding to the label (1.00,0.50), which is one half of that shown in the same figure in the lower right-hand corner, is perhaps sufficient. However, further stability calculations indicated that a higher level of suction was needed (labeled as 2.00,1.00 and shown in the lower right-hand corner of the figure). This distribution was used in several calculations to make sure that the growth of neither stationary nor nonstationary crossflow waves ever reached a value of 9. Some of these results are shown in figures 9.20 through 9.23.
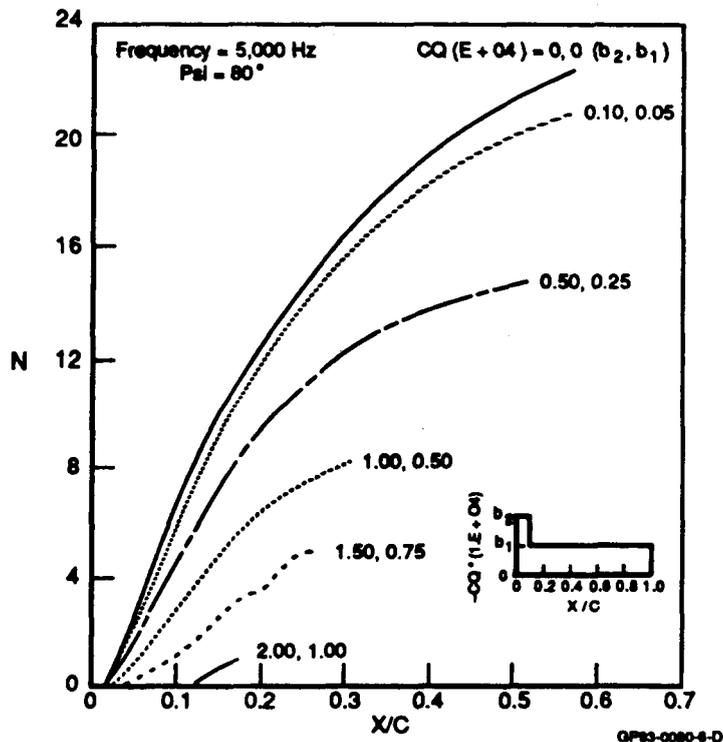
Figure 9.19   EFFECT OF SUCTION ON AMPLIFICATION FACTOR AT PSI = 80
               DEGREES AND F = 5000 Hz, 50% SEMISPAN, SF-1107 WING

One effect of applying suction was a much greater damping of the high frequency waves. For example, compare the effect of applying suction, labeled as (2.00,1.00), on waves of frequency 5 kHz (figure 9.19) with the same at 2 kHz (figure 9.22). In fact, this level of suction results in a shift of the most amplified wave to a lower frequency (from 5 kHz to 2 kHz) when suction, labeled as (2.00,1.00) was applied.

Figure 9.20 shows the amplification factors computed for several different values of PSI, but fixed at a constant frequency of 2 kHz. Calculations are shown here for 2 kHz only, as it corresponds to the most amplified disturbance. The distribution of suction level is also shown in the figure. Once again it is noticed that the largest amplification is found to be for highly oblique waves (87.5 degrees in this case). In fact, the orientation angle of the most amplified wave has increased as a result of suction application. Stationary crossflow calculations are shown in figure 9.21, whereas nonstationary crossflow calculations for 2 and 3 kHz (also done holding wavelength constant) are shown in figure 9.22 and 9.23, respectively. The value of XLENC corresponding to the most amplified wave is found to be about 0.0020 (figure 9.22). It is noted that the effect of suction on the nonstationary crossflow waves is much greater than that on the stationary crossflow waves.
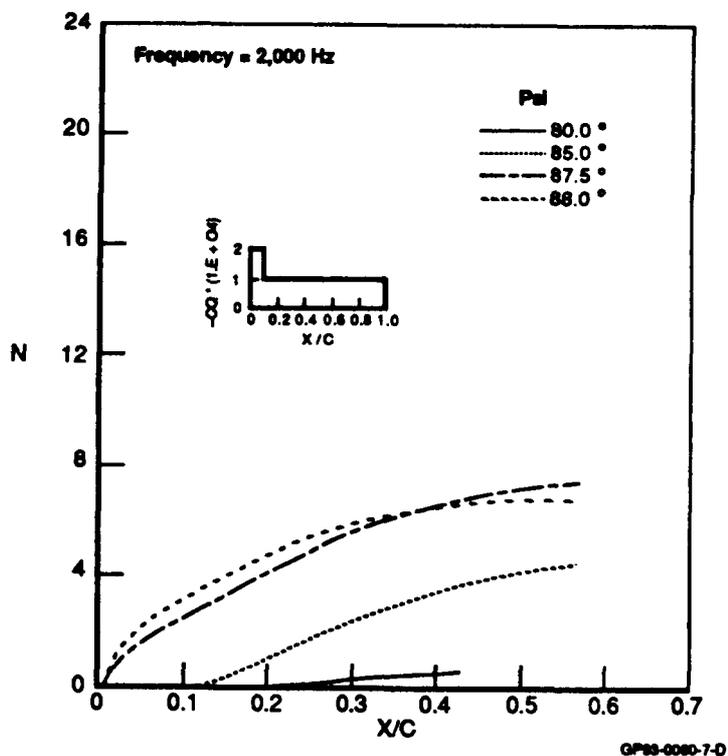
Figure 9.20   AMPLIFICATION FACTOR FOR DIFFERENT WAVE ANGLES WITH
                SUCTION, 50% SEMISPAN, M = 2.0, α = 4 DEG.,
                SF-1107 WING

72
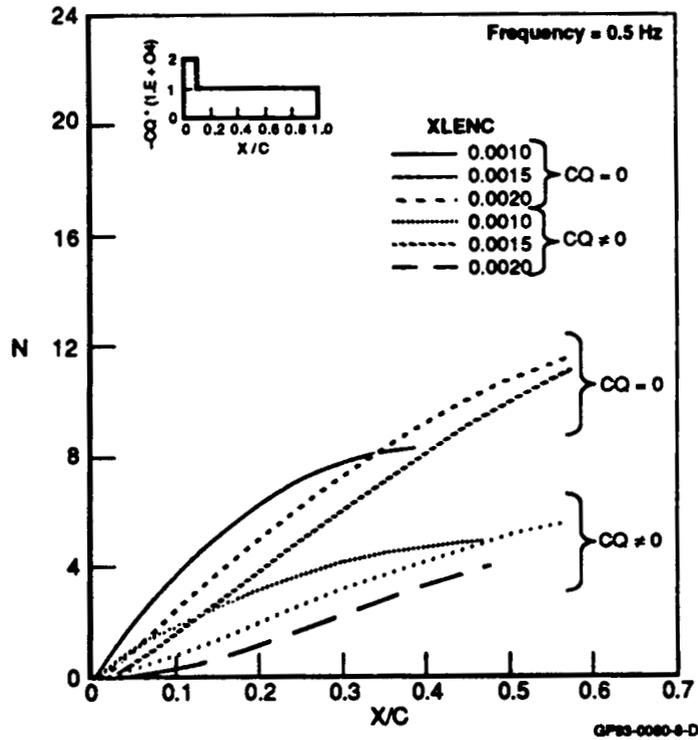
Figure 9.21   EFFECT OF SUCTION ON THE GROWTH OF STATIONARY WAVES
50% SEMISPAN, SF-1107 WING
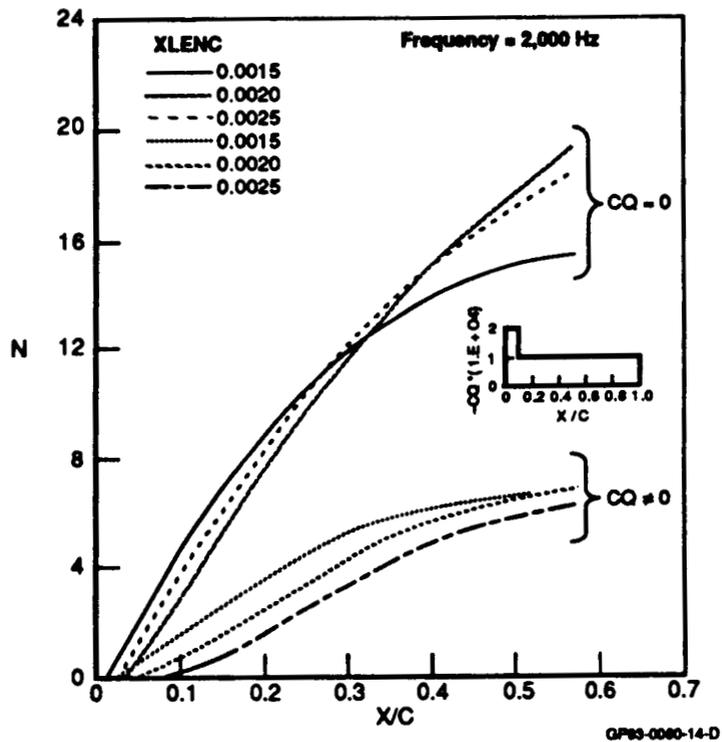
Figure 9.22   EFFECT OF SUCTION ON THE GROWTH OF NONSTATIONARY
CROSSFLOW WAVES, 50% SEMISPAN, M = 2.0, α = 4 DEG.,
SF-1107 WING

73
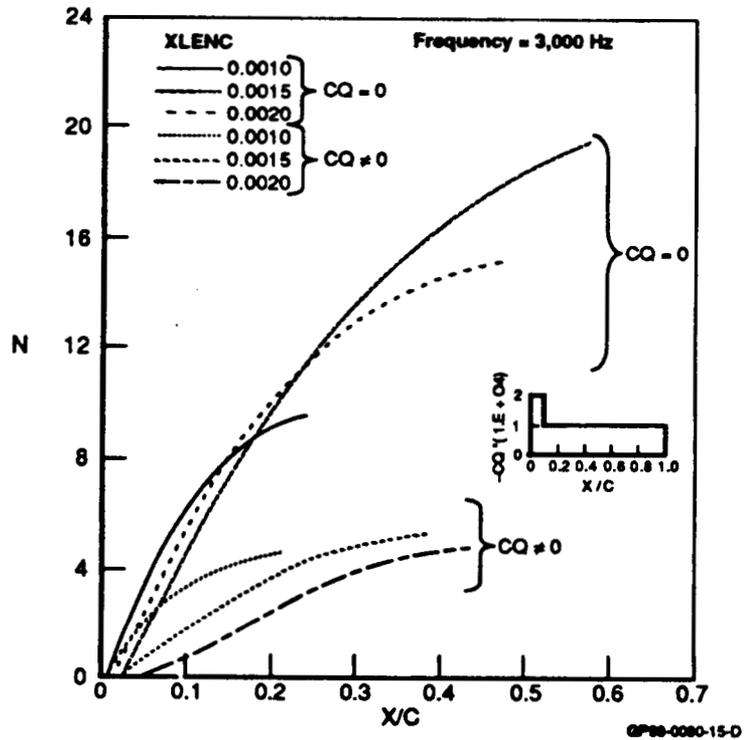
Figure 9.23   EFFECT OF SUCTION ON THE GROWTH OF NONSTATIONARY
CROSSFLOW WAVES, 50% SEMISPAN, SF-1107 WING

An analysis, similar to that shown in figures 9.15 through 9.18, was also
conducted to examine the development of inflections in the boundary layer
velocity profiles with suction. The semispan and chord locations were the
same as in figures 9.15 through 9.18. The results from this analysis are
shown in figures 9.24 through 9.27.
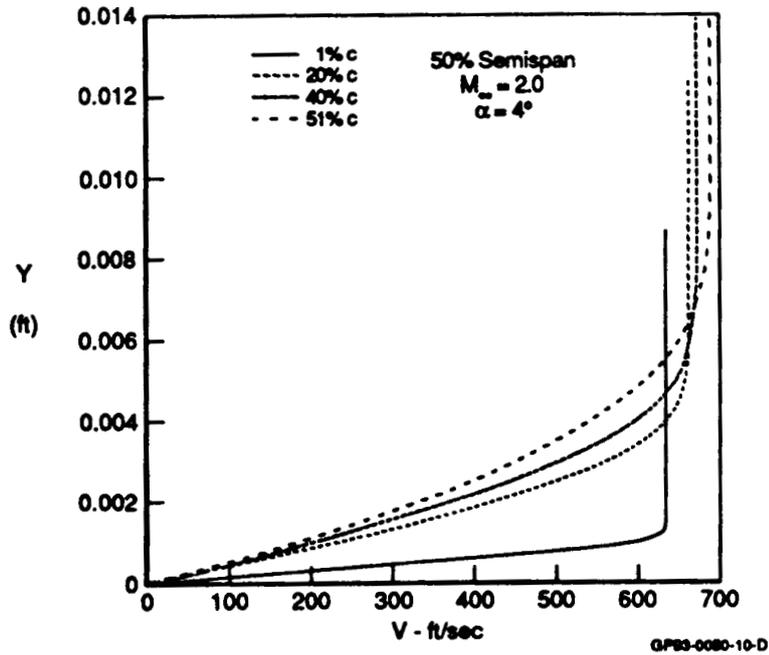
Figure 9.24 BOUNDARY LAYER VELOCITY PROFILES AT PSI = 70 DEG.,
50% SEMISPAN, WITH SUCTION, SF-1107 WING
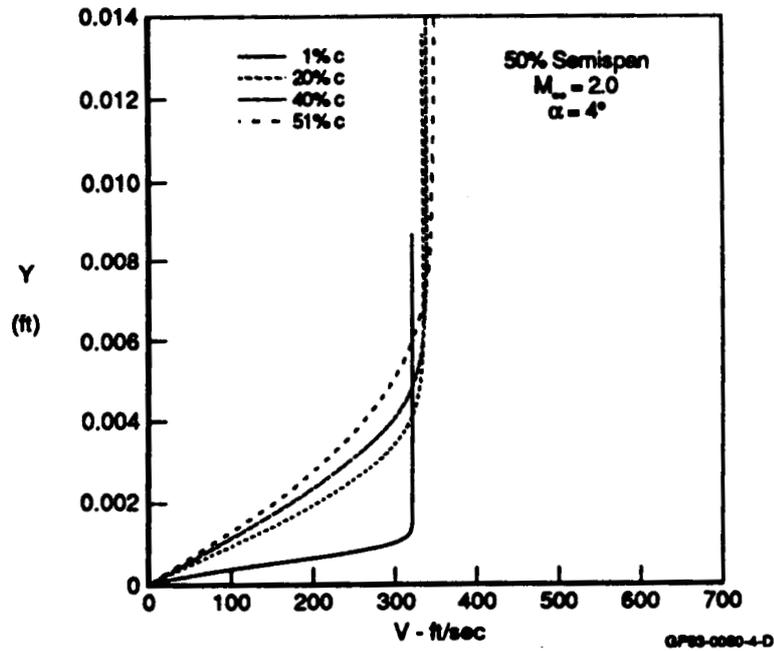
Figure 9.25 BOUNDARY LAYER VELOCITY PROFILES AT PSI = 80 DEG.,
50% SEMISPAN, WITH SUCTION, SF-1107 WING
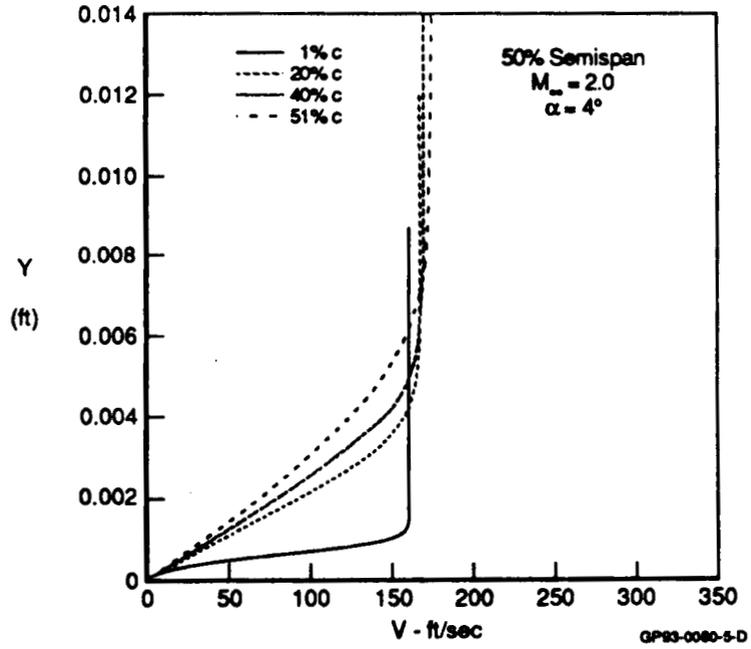
Figure 9.26   BOUNDARY LAYER VELOCITY PROFILES AT PSI = 85 DEG.,
50% SEMISPAN, WITH SUCTION, SF-1107 WING
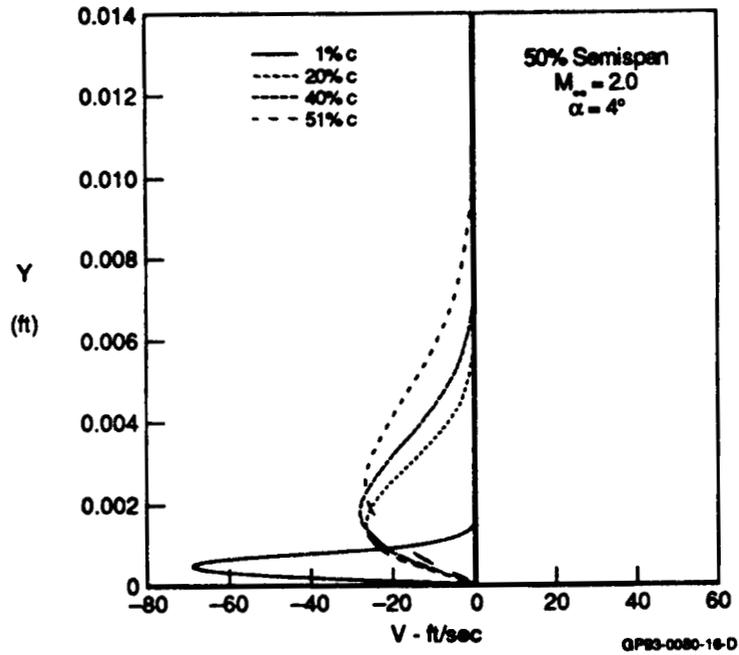
Figure 9.27   BOUNDARY LAYER VELOCITY PROFILES AT PSI = 90 DEG.,
50% SEMISPAN, WITH SUCTION, SF-1107 WING

Not surprisingly, the profiles change considerably when suction is applied. The boundary layer is thinner as expected. Moreover, the inflections are almost absent at PSI = 80 degrees. They do, however, show their presence at 85 degrees and beyond. Once again, this analysis indicates that the highly oblique waves (PSI = 87.5 degrees) corresponding to the largest amplification factor as determined from the stability results, are indeed travelling crossflow waves. One effect of suction, therefore, is to move the visible inflection to higher waveangle.

Similar results have also been obtained at 18.75% and 81.25% semispan locations on the SF-1107 wing. Since the pressure distributions at these locations are very similar to that at the 50% location, calculations were reduced considerably. Knowing the trends of the different wave growths at 50% semispan, the ranges of frequencies, wavelengths and waveangles were bracketed very well. Results for those calculations are not shown here as they were very similar to those at 50% semispan.

Calculations were also performed on the lower surface at the same three span stations. Without suction the transition is predicted to occur very close to the leading edge. This can be expected since adverse pressure gradient exists near the leading edge of the wing for the conditions examined (figure 9.1). With the suction distribution shown in figure 9.19 the predicted location of transition was delayed to 60% chord. If a less favorable pressure gradient had been used, less suction would have been required.

Since the SF-1107 wing has a relatively sharp supersonic leading edge, it was thought that attachment line conditions would not be critical. Calculations have verified this, with computed attachment line momentum thickness Reynolds numbers below 50 for all three span stations.

A performance and aircraft sizing analysis was conducted on the SF-1107 configuration. Distributed suction was applied to both upper and lower surfaces of the wing outboard of the strake, and on both surfaces of the horizontal and vertical tails. On the wing, suction was applied back to the flap hingeline and inboard of the wing tip cap. The entire horizontal tail surface inboard of its tip cap was laminarized, and the vertical surfaces were laminarized back to the rudder hingeline below the tip cap. Fully turbulent flow was assumed on the other surfaces of the aircraft. A breakdown of the wetted areas which were laminarized is given in figure 9.28. The effects of the laminarization on skin friction drag and $C_{D\ min}$ are shown in figures 9.29 and 9.30. Energy maneuverability (EM) and mission performance were calculated for the baseline configuration and for a laminarized version with and without a system weight penalty. The assumed weight penalty was 2.82 lbf/sqft of planform area affected by the laminarization system, taken from reference 26. The effect of LFC performance on system performance is summarized in figure 9.31.

Component	Wetted Area - ft**2		% Laminarized
	Actual	Laminarized	
A. Wing	664	424	64
B. Horizontal Tail	206	192	93
C. Vertical Tail	182.5	120.5	93
D. Total	2.232	736.5	33

GP83-0447-8-T

Figure 9.28   BREAKDOWN OF WETTED AREAS LAMINARIZED, SF-1107 CONFIGURATION
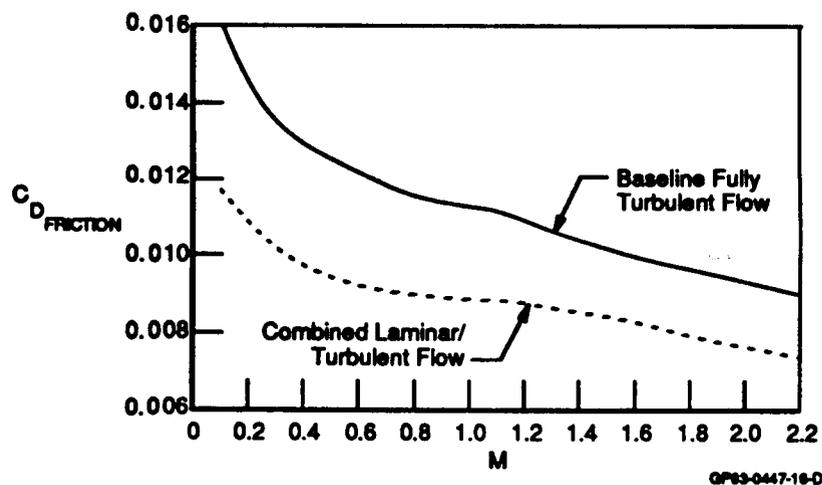
GP83-0447-16-D

Figure 9.29   EFFECT OF LAMINARIZATION ON SKIN FRICTION DRAG COEFFICIENT, SF-1107 CONFIGURATION
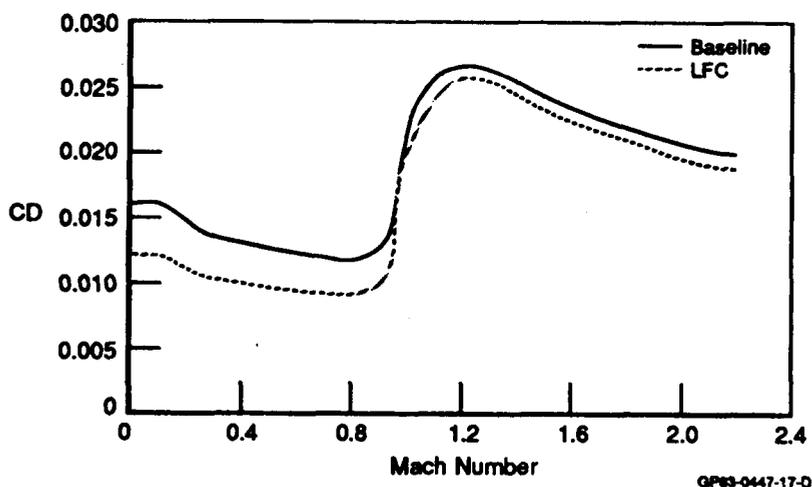
Figure 9.30   EFFECT OF LAMINARIZATION ON MINIMUM DRAG COEFFICIENT
AGAINST MACH NUMBER, SF-1107 CONFIGURATION

Configuration	TOGW	T/W	W/S	FF	Mission Radii - NM		EM Pts 50% Fuel + (4) AMRAAMS				
					Fighter Sweep	CAP	NL Sust - g Mach 0.9 30/Max	NL Sust - g Mach 1.6 30/Max	1 g Ps - fps Mach 0.9 20/Max	Accel - secs Mach 0.6 - 1.2 SL/Max	Accel - secs Mach 0.6 - 1.6 30/Max
Baseline	30,743	1.8	58	0.34	400	208	6.0	9.2	1,248	13.7	25.3
Baseline Size, LFC Drag											
— W/O Wt Penalty	30,743	1.8	58	0.34	484	278	6.1	9.3	1,273	13.3	24.8
— W/ Wt Penalty	31,882	1.75	60	0.33	449	243	5.8	8.9	1,218	13.9	26.0
Sized to Baseline Perf LFC Drag											
— W/O Wt Penalty	28,879	1.8	57.5	0.32	400	211	6.0	9.1	1,257	13.6	25.3 ·
— W/ Wt Penalty	31,131	1.8	57.5	0.31	400	201	6.0	9.1	1,253	13.6	25.3

Figure 9.31   EFFECTS OF LFC ON PERFORMANCE/AIRCRAFT SIZE
SF-1107 CONFIGURATION

In figure 9.31 mission performance is presented for a fighter sweep mission
(figure 9.32), and for a combat air patrol mission (figure 9.33). Also shown
in figure 9.31 is the effect of LFC on aircraft size if the fighter sweep
mission radius is held constant. If Laminarization can somehow be affected
at no weight penalty, the takeoff gross weight is reduced from 30 743 lbf to
28 879 lbf, a size reduction of 6.1 percent. Using the aforementioned
weight penalty, however, the takeoff weight actually increases to 31 131 lbf,
a size increase of 1.3 percent.
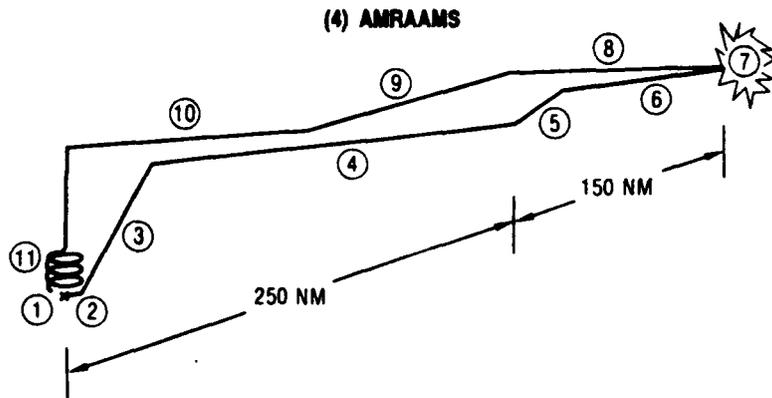
79

(4) AMRAAMS

Mission Definition

① Warmup: 30 min Idle

② Takeoff: Max Power Accel Mach 0 → 0.6
      Credit Distance

③ Minimum Fuel Climb to Optimum Cruise

④ Optimum Cruise

⑤ Climb Accel to Mach 2.0 and Optimum Altitude

⑥ Dash at Mach 2.0

⑦ Combat: 25% Fuel, Fire Missiles

⑧ Dash: At Mach 2.0 and Optimum Altitude

⑨ Decel, Descend: To Optimum Subsonic Mach
      and Altitude

⑩ Optimum Cruise

⑪ 20 min Loiter at Optimum Mach, Sea Level

GP83-0447-11

Figure 9.32   FIGHTER SWEEP MISSION FOR THE SF-1107 CONFIGURATION

(4) AMRAAMS
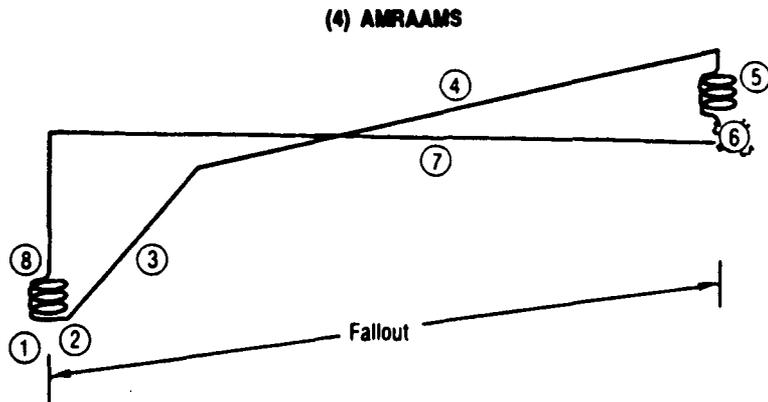
Mission Definition

① Warmup: 30 min Idle
② Takeoff: Max Power Accel Mach 0 → 0.6
③ Minimum Fuel Climb to Optimum Cruise
④ Optimum Cruise
⑤ 2 hr Loiter at Subsonic Corner Speed
⑥ Combat: 25% Fuel, Fire Missiles
⑦ Optimum Cruise
⑧ 20 min Loiter at Optimum Mach,
Sea Level

GP83-0447-10

Figure 9.33   COMBAT AIR PATROL MISSION FOR THE SF-1107 CONFIGURATION

10. SF-1302 FIGHTER WING

The SF-1302 configuration, shown in figure 8.2, features an arrow wing with a subsonic leading edge inboard of the leading edge sweep break at 70% semispan. The leading edge is swept 71.0 degrees inboard of the break, and 61.5 degrees outboard. The wing consists of uncambered NACA 64A005 airfoils inboard of the break, and 5% thick parabolic biconvex airfoils outboard. The gross planform area is 741 sqft. The wing twist was set by a moment constraint. The wing camber suface was not optimized as was that of the AST.

FLO-67 Euler solutions were obtained on the wing at supersonic cruise conditions of 2.0 Mach at 4 degrees angle of attack. The pressure contours on the upper surface are shown in Figure 10.1 while the chordwise pressure distributions at 18.75%, 50%, and 81.25% semispan are shown in Figure 10.2 through 10.4.
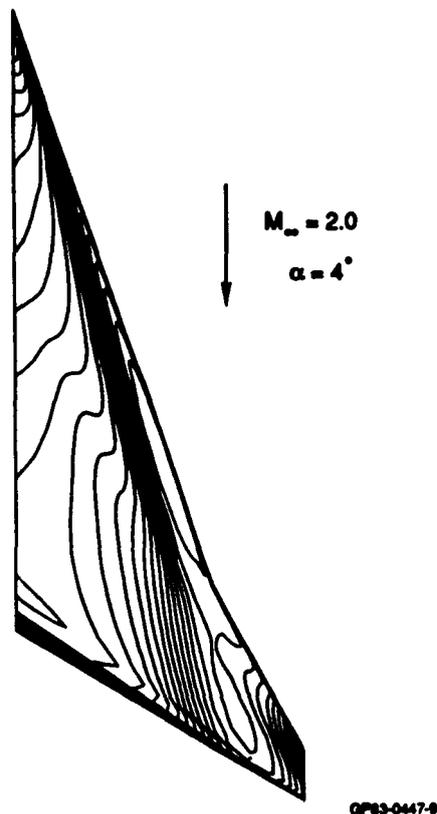
Figure 10.1   UPPER SURFACE PRESSURE CONTOURS, SF-1302 WING

PRECEDING PAGE BLANK NOT FILMED
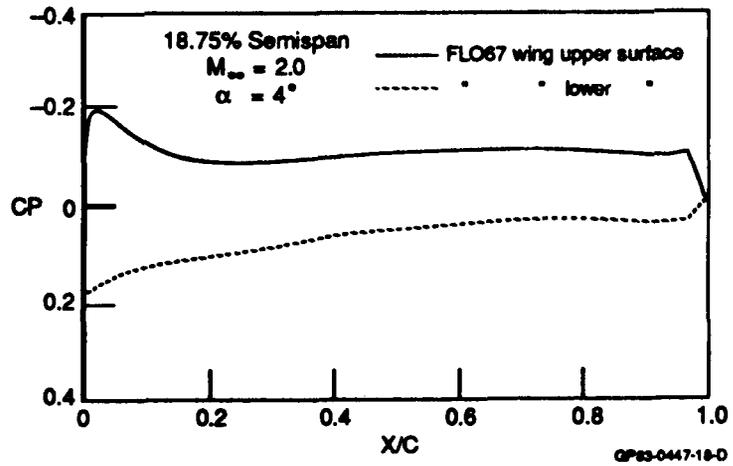
Figure 10.2   PRESSURE COEFFICIENT VS. X/C, 18.75% SEMISPAN
SF-1302 WING
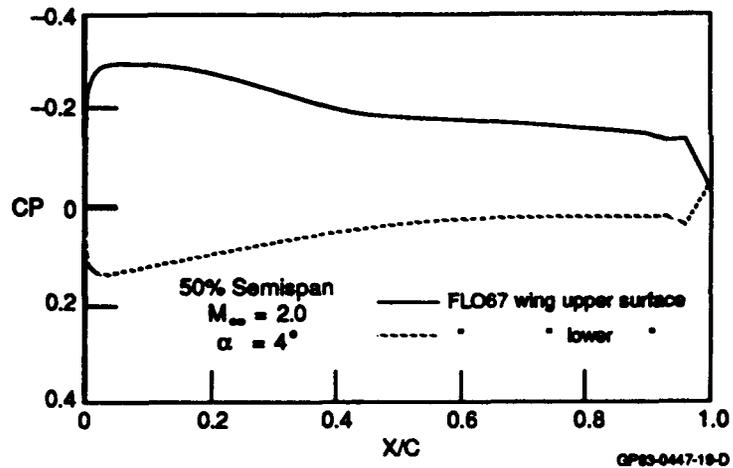
Figure 10.3   PRESSURE COEFFICIENT VS. X/C, 50% SEMISPAN
SF-1302 WING
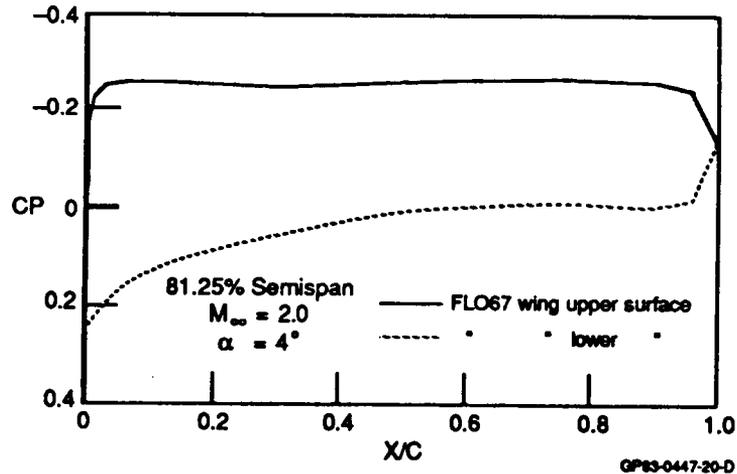
Figure 10.4   PRESSURE COEFFICIENT VS. X/C, 81.25% SEMISPAN
SF-1302 WING

At a Mach number of 2.0, the leading edge of the outboard panel is still
operating in the subsonic regime, since the planform was designed for
reasonable dash performance at 2.2 Mach and above. For the SF-1302 wing, the
upper surface chordwise pressure distribution is decelerating past 3% chord
length. It is noted here that no effort was made to modify the geometry of
the wing in order to tailor the pressure distribution for improved laminar
flow. One point must be kept in mind regarding the conical flow assumption
used in the boundary layer code. The inviscid flow solutions on the SF-1302
wing did not exhibit a high degree of conicality. The extent to which this
affected the stability results can only be determined from comparisons with
COSAL results calculated using a fully 3-D boundary layer code. Such a
stability package was unavailable at the time this study was done.

Attempts were made to run the Kaups-Cebeci boundary layer code on the
upper surface at the 50% semispan station using the pressure distribution
shown in figure 10.3. Without suction, the laminar boundary layer could not
negotiate the the adverse pressure gradient region downstream of roughly the
15% chord station. However, the code was successfully executed with a
suction level of Cq = -.0003

Because of the shape of the upper-surface pressure distribution, and the
high suction levels required to even get a laminar boundary layer solution,
only a cursory stability analysis was carried out. The intent was to roughly
identify how much additional suction would be required for laminar flow with
such a pressure distribution.

Figure 10.5 shows the most amplified stationary crossflow wave found in
the leading edge region at the suction level indicated. This is really the
end result of an iterative process in which various suction levels were tried
and the most amplified waves were found for each level. The maximum
amplification of the critical crossflow wave at this suction level is below
9. This process was explained in detail in section 6.

85
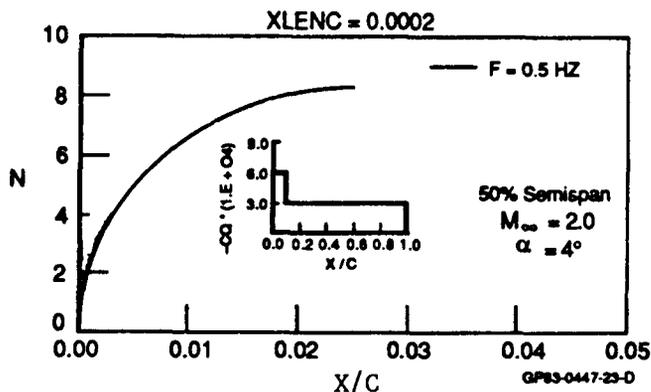
Figure 10.5 CRITICAL STATIONARY CROSSFLOW WAVE,
LEADING-EDGE REGION, SUCTION ON.
50% SEMISPAN, SF-1302 WING

Figure 10.6 shows the critical stationary crossflow wave amplification in the adverse region without additional suction. The suction in the adverse gradient region was then progressively increased until the critical stationary crossflow wave was not amplified beyond N = 9. Figure 10.7 shows the amplification of the critical stationary crossflow wave after the suction was increased. Travelling crossflow waves were not comprehensively investigated, so are not shown, although none were found which were more highly amplified than the stationary wave. Also it is likely that travelling waves would be more attenuated by suction than the stationary waves, since their inflection points have been shown to lie closer to the surface. The amount of suction required to stabilize the boundary layer against stationary crossflow waves, as shown in figure 10.7, is large. This underscores the importance of carefully tailoring the pressure distribution for LFC application.

Difficulty was also encountered in obtaining a boundary layer solution on the lower suface at 50% semispan when the attachment line was assumed to be at the leading edge. It was found that a boundary layer solution could be had if a high level of suction was applied in the leading-edge region. This case is similar to the HSCT case discussed in section 7, in which the attachment line is actually located aft of the leading edge on the lower surface, and the attachment line Cp is higher than the simple-sweep value of .1177. It is anticipated, however, that by suitably modifying the wing geometry, as shown in section 6, the attachment location and pressure distribution could be changed so that both upper and lower surfaces are amenable to laminar flow.

The attachment-line momentum-thickness Reynolds number was computed at the 50% span station, and was found to be 152.5. This value could easily be reduced by slightly increasing the suction level. Therefore, the attachment line instability is again not expected to present any difficulty for an airplane of this size.
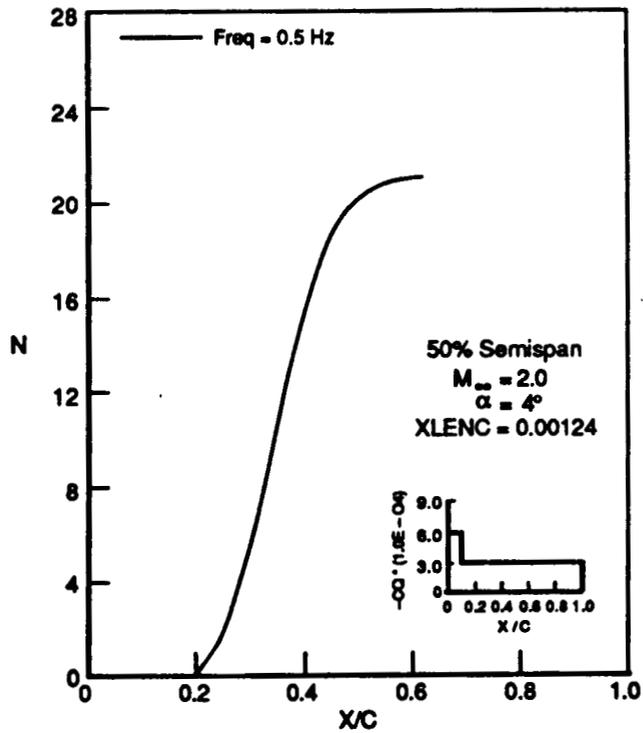
Figure 10.6   CRITICAL STATIONARY CROSSFLOW AMPLIFICATION
               IN THE ADVERSE PRESSURE GRADIENT REGION, WITH SUCTION
               50% SEMISPAN, SF-1302 WING
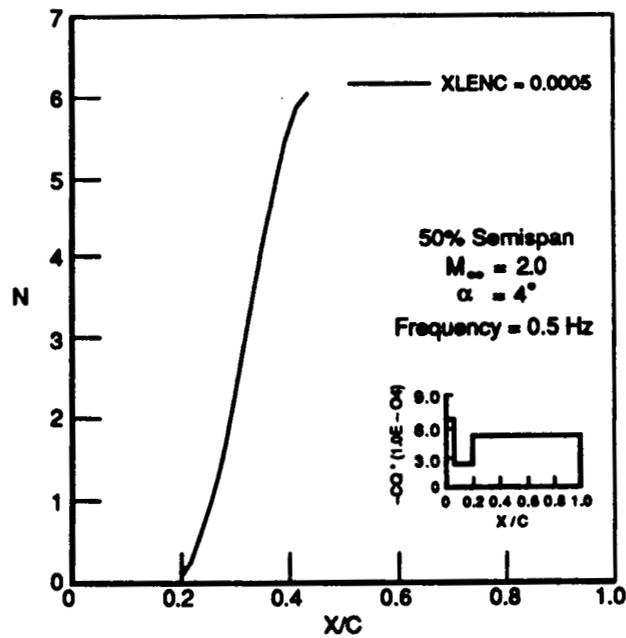
Figure 10.7   CRITICAL STATIONARY CROSSFLOW AMPLIFICATION
               IN THE ADVERSE PRESSURE GRADIENT REGION, INCREASED
               SUCTION, 50% SEMISPAN, SF-1302 WING

A performance and sizing analysis, based on simple skin friction estimates, was conducted for the SF-1302 configuration. Laminar flow was assumed on both upper and lower surfaces of the wing outboard of the engine nacelle - wing intersection and inboard of the tip cap, aft to the trailing-edge flap and aileron hingelines. Laminar flow was also assumed on the vertical tail forward of the rudder hingeline. Fully turbulent flow was assumed on all other surfaces of the aircraft. A breakdown of the wetted areas which were laminarized is provided in figure 10.8.

Component	Wetted Area - ft**2		%
	Actual	Laminarized	Laminarized
A. Wing	1,384	920	66
B. Vertical Tail	274	189	69
C. Total	1,658	1,109	67

GP83-0447-4-T

Figure 10.8   BREAKDOWN OF WETTED AREAS LAMINARIZED, SF-1302 CONFIGURATION

The effects of the laminarization on $C_{D \, min}$ are shown in figure 10.9. The effect of LFC on baseline performance is summarized in figure 10.10. Mission performance was calculated for a fighter sweep mission (figure 10.11). Also shown in figure 10.10 is the effect of LFC on aircraft size when the fighter sweep mission radius is held constant. Under the assumption of no LFC system weight penalty the takeoff gross weight is reduced from 43 622 lbf to 38 292 lbf, a size reduction of 12.2 percent. Using the assumed system weight penalty of 2.82 lbf/sqft (reference 26) the aircraft gross weight reduces to 41 951 lbf, a size reduction of 3.8 percent. It is noted that these sizing effects are significantly greater than similar results on the SF-1107 configuration, which were a 6.1% reduction without the weight penalty and a 1.3% increase in size with it. These differences are attributed primarily to the larger baseline radius requirement of the SF-1302 aircraft (890 nm), as compared to 400 nm for the SF-1107. Since LFC is essentially a cruise technology, the benefit should be expected to improve as the length of the cruise segment increases.

QP83-0447-15-D
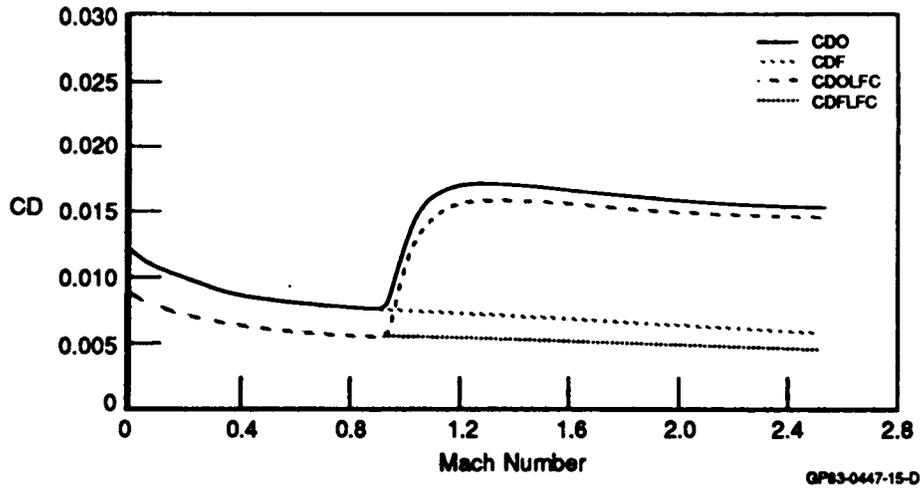
Figure 10.9   EFFECT OF LAMINARIZATION ON MINIMUM DRAG COEFFICIENT, SF-1302 CONFIGURATION

Configuration	TOGW	T/W	W/S	FF	Mission Radii - NM		EM Pts 50% Fuel + (4) AMRAAMS				
					Fighter Sweep	CAP	NL Sust - g		1 g P_s - fps	Accel - secs	
							Mach 0.9 3g/Max	Mach 1.6 3g/Max	Mach 0.9 2g/Max	Mach 0.6 - 1.2 SL/Max	Mach 0.8 - 1.6 3g/Max
Baseline	43.622	1.42	42.2	0.45	890	665	5.8	10.3	1,013	18.2	32.1
Baseline Size, LFC Drag											
— W/O Wt Penalty	43.622	1.42	42.2	0.45	1,070	810	5.9	10.4	1,040	17.1	31.0
— W/ Wt Penalty	45.337	1.37	43.8	0.43	1,010	745	5.6	9.9	990	17.9	32.6
Sized to Baseline Perf LFC Drag											
— W/O Wt Penalty	38.292	1.46	42.2	0.41	890	645	5.8	10.3	1,051	17.1	31.0
— W/ Wt Penalty	41.951	1.47	42.2	0.40	890	625	5.8	10.4	1,059	16.7	30.6

QP83-0447-3-T

Figure 10.10   EFFECTS OF LFC ON BASELINE PERFORMANCE, SF-1302 CONFIGURATION
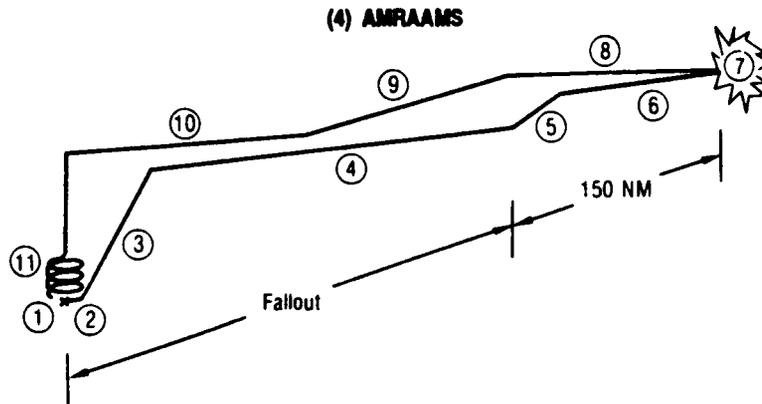
89

(4) AMRAAMS

Mission Definition

①   Warmup: 30 min Idle

②   Takeoff: Max Power Accel Mach 0 → 0.6
       Credit Distance

③   Minimum Fuel Climb to Optimum Cruise

④   Optimum Cruise

⑤   Climb Accel to Mach 2.0 and Optimum Altitude

⑥   Dash at Mach 2.0

⑦   Combat: 25% Fuel, Fire Missiles

⑧   Dash: At Mach 2.0 and Optimum Altitude

⑨   Decel, Descend: To Optimum Subsonic Mach
       and Altitude

⑩   Optimum Cruise

⑪   20 min Loiter at Optimum Mach, Sea Level

GP83-0447-12

Figure 10.11   FIGHTER SWEEP MISSION FOR THE SF-1302 CONFIGURATION

11. CRITICAL TECHNICAL ISSUES

One of the objectives of this investigation was to identify technical issues which would be critical to the successful application of laminar flow control to supersonic airplanes. Accordingly, a list of technical issues was kept and updated as the study progressed. Each of the issues is listed and discussed below. The items are given in prioritized order; those issues whose satisfactory resolution would have the greatest impact on the success of supersonic LFC are listed first.

1. ATTACHMENT LINE CONTAMINATION PROTECTION - One of the important discoveries of this study is that supersonically the payoff for lower-surface laminarization is as large or larger than that for the upper surface. Furthermore, for airplanes similar to the AST in size, the high sweeps make for attachment line R_θ values greater than 100, even with moderate to high suction levels. Even if values of R_θ less than 100 were feasible, a turbulent wedge emanating from an excrescence on or near the leading edge could eliminate laminar flow on a large fraction of the wing area, due to the high sweep and low aspect ratio. It is therefore essential to provide protection against accumulated supercritical excrescences due to insect strikes and other sources of environmental contamination. The leading-edge Kreuger-shield which proved so successful in the (subsonic) Leading-Edge Flight Test experiment[4] is inappropriate, since it is important supersonically to laminarize the lower surface as well the upper surface. Stowing the shield leaves the accreted insect remains on the lower surface leading edge.
   The role leading-edge sweep plays in how well or poorly a wing leading edge collects debris is not well understood. Fortunately, methods now exist to allow this to be studied on a parametric basis. This could be supplemented by parametric testing in environmental tunnels to develop a database for sweep effects at the high sweep end of the spectrum. Applicable data could also be obtained by field observations of leading-edge contamination on various existing supersonic aircraft.
   Once the physics of contaminant accretion are well understood at high sweep angles, systems can be designed to provide protection. Oozing anti-icing or other fluids out of the wing surface is one method that could be employed. Others include spray application of sublimating material prior to takeoff, or using an onboard or ground-based refrigeration system or recirculating cold fuel to cause the appropriate regions of the wing to ice up, using ambient moisture. Although this last idea would be out of the question for a subsonic airplane, there are two good reasons this approach could be acceptable for a highly-swept supersonic configuration: (1) highly-swept wings of necessity exploit separated flow phenomena in low-speed flight, so icing does not present a safety concern, and (2) cruise skin temperatures are sufficiently high to preclude ice retention. A related question is whether there exists a Mach number above which insect remains would simply char off, as in a self-cleaning oven.

2. STEP, GAP, AND ROUGHNESS CRITERIA AT HIGH MACH NUMBER - The viscous
    dissipation occurring in the laminar boundary layer gives rise to
    elevated temperatures near the wall. The resulting increased viscosity
    in the near-wall region should result in improved damping of disturbances
    relative to the incompressible case. From a practical standpoint this
    should mean a relaxation of step, gap and roughness criteria as Mach
    number is increased. The roughness issue is particularly important as it
    relates to how large an excrescence can be and still be subcritical. The
    step and gap issue relates to thermal expansion joints and possible
    leading-edge high lift systems. For the case of transition caused by
    steps and gaps, the mechanism involves the amplification of waves in a
    locally separated boundary layer, as well as pressure jumps associated
    with any shock waves created. The disturbance environment would
    therefore be expected to be of first-order importance. The most useful
    data would therefore come from flight test, where the spurious effects of
    freestream turbulence and tunnel noise would be absent.

3. DEVELOPMENT OF ATTACHMENT LINE TURBULENCE DIVERTERS - In the NASA
    Leading-Edge Flight Test program[4], a leading-edge notch/bump
    successfully diverted boundary layer turbulence emanating from the
    fuselage boundary layer, allowing extensive laminarization along the
    leading edge of the test article. This same problem will need to be
    faced for supersonic laminarization to be successful where subsonic
    leading edges are used, but the notch/bump may not be the best solution
    at supersonic speeds. Alternate solutions include a region of reduced
    sweep and sharpened leading edge in the root region, where the induced
    upwash caused by the highly swept wing leading edge is a minimum. Testing
    on a lifting wing will be necessary in order to arrive at the best
    solution.

4. ATTACHMENT LINE MOMENTUM-THICKNESS REYNOLDS NUMBER CRITERIA AT HIGH MACH
    NUMBER - The increased viscosity in the wall region of high-speed
    boundary layers can have a beneficial effect on the upper critical level
    of attachment line momentum-thickness Reynolds number. Below this
    critical Reynolds number, Tollmien-Schlichting waves do not grow in the
    attachment line boundary layer, but existing turbulence can propagate.
    Above this level attachment line boundary layer transition can occur due
    to amplifying T-S waves. The upper critical value of R_θ, according to
    various sources, including Bacon & Pfenninger[14] is about 240. This
    value is for an incompressible attachment line boundary layer, and has
    not been extended to higher Mach numbers. For correlation purposes, the
    external Mach number component along the attachment line seems a logical
    choice. The upper critical R_θ value is expected to increase with
    attachment line Mach number. The high sweeps of interest in supersonic
    wing design make this an important issue.

92

5. LEADING-EDGE RADIUS EFFECTS FOR SUPERSONIC LEADING EDGES - The detached, curved leading-edge shock waves associated with blunt leading edges create rotational wakes, which can impose an external velocity profile on the boundary layer. The scale of the leading edge bluntness in relation to the boundary layer thickness over the airfoil should have a first-order effect on boundary layer stability characteristics. This problem is amenable to both theoretical analyses and wind tunnel research, and should be pursued.

6. DEVELOPMENT OF SCHEMES FOR LIMITING TURBULENCE SPREAD - For highly swept, low aspect wings, the bodyside turbulent wedge can occupy a large fraction of the wing planform area. If means could be found to reduce the area lost to laminar flow, the laminarization benefit could be improved. Simple-skin-friction estimates for the DAC AST indicate a potential of about .5 in L/D or 28% of the total wing laminarization benefit. A highly swept, aft- and inward-facing step of height comparable to the local turbulent boundary-layer thickness is one possible device for controlling the spread of bodyside turbulence. Whether this or other ideas could be developed into a practical device could be determined by parametric supersonic wind tunnel testing.

7. DEVELOPMENT OF LAMINAR SWEEP-BREAK GEOMETRIES - The geometric transition from highly swept but blunt subsonic leading edge to less swept but sharp supersonic leading edge provides an opportunity for a turbulent wedge to be created, due to abrupt spanwise variation in flow properties. How exactly this can be designed around is not clear at the present. Sharpening up the leading edge as the break is approached from inboard might be expected to work over a narrow angle-of-attack range, but could have other unforseen consequences. Wind-tunnel or flight testing of alternative concepts needs to proceed so this issue can be resolved.

8. FUSELAGE RADIATED NOISE - If the fuselage, and in particular the forebody, is not laminarized, sound waves created by turbulent eddies in the fuselage boundary layer can propagate outward and disturb the wing boundary layer flow, resulting in earlier transition or an increase in suction requirements. Whether or not this in fact proves to be a problem can only be resolved by flight testing, since too many spurious effects are present even in a "quiet" supersonic tunnel.

9. CROSSFLOW IN CONCAVE REGIONS, EFFECTS ON GORTLER INSTABILITY - Low-speed investigations[19,20] have identified beneficial effects of boundary layer crossflow in destroying existing Gortler vortices. How the mechanism responsible for this is affected by compressibility effects is not well understood. Conversely, the effect of streamwise surface concavity on crossflow stability characteristics is not widely understood. Critical analyses and experimental studies at high Mach number need to be undertaken in order to understand these effects.

C-2

10. SENSITIVITY OF ATTACHMENT LINE LOCATION AND R_θ TO ANGLE OF ATTACK -
According to simple-sweep theory, for small angles of attack the rate of
change of leading-edge-normal angle of attack with streamwise angle of
attack is proportional to the secant of the sweep angle. The low section
thickness ratios required for low drag in supersonic flight cause the
local surface curvature to typically fall off rapidly with surface
distance going away from the leading edge on either the upper or lower
surface. The combination of these two effects causes wings with highly
swept leading edges to depart from attached flow at relatively low angles
of attack, and can cause the attachment line momentum thickness Reynolds
number to vary rapidly with angle of attack. An assessment, made on the
modified Mach 2.2 AST wing in the vicinity of the cruise angle of attack,
showed this not to be a problem at the 71 degree leading-edge sweep angle
of this wing. The problem could be significantly worse for higher
sweeps, and should be considered in any LFC design. It is not a problem
for wings having supersonic leading edges, as long as the leading-edge
shock remains attached, since for this case the attachment line travel is
nil.

12. RECOMMENDED RESEARCH PROGRAM

In order for supersonic laminar flow to be rendered a practical technology, each of the technical issues discussed in section 11 must be addressed. Since technology development paths and timelines may vary with available funding levels, the individual tasks comprising the research program recommended here will only be given in a temporal sequence. The program is divided into four categories of endeavor: code development, analysis, wind-tunnel test, and flight test. Where two or more suggested program elements address a common technical issue, the above sequence also defines a sensible temporal sequence, i.e. analysis precedes wind-tunnel test, which precedes flight test, etc. Economy of effort results when several issues can be addressed by one experiment, so this is made use of where applicable. The priorities indicated in section 13 can be applied if sufficient funding is not made available for the entire program, but it is highly recommended that issues 1 through 7 be addressed, as a minimum.

CODE DEVELOPMENT:

1. Continue the development of a fully 3-D, all-speed boundary layer stability package, including the effects of suction, nonadiabatic wall conditions, and allowing attachment line and wedge flow starting solutions. This will be needed for the interpretation of experimental results and for LFC design. The correct accounting for curvature effects as recently incorporated into the COSCUR stability code[22] should be included.

2. Develop a wing-body inverse wing design procedure, in which the wing geometry is determined from input pressure distributions, for the supersonic case which does not make use of small-perturbation assumptions. An inverse Euler would be necessary for supersonic leading edges, where modeling of flow through shock waves is important. Whether or not a potential method is sufficient for subsonic leading edges is not clear, due to the conical shock from the fuselage forebody.

ANALYSIS:

1. Investigate the effect of leading edge sweep on particle catch efficiency in the high sweep angle regime, using particle tracing techniques. Formulate an improved criterion for insect remains deposition. Accumulate a database for insect remains accretion on highly swept supersonic aircraft in operational service. Develop a predictive capability for insect accretion.

95

2. Determine the effect of Mach number on separation bubble length Reynolds number to transition in zero pressure gradient. Combine this information with the existing database to produce an estimated permissible gap criterion as a function of Mach number. Attempt to formulate generalized roughness and step criteria as well.

3. Determine the effect of attachment-line tangential Mach number on the growth of Tollmien-Schlichting waves in the attachment line boundary layer on a swept cylinder with subsonic normal Mach number. Formulate a relationship for the upper critical attachment line R_θ as a function of this Mach number or other significant dimensionless parameters.

4. Perform a parametric 2-D study on the effects of supersonic leading-edge radius on boundary layer velocity profiles and stability, using a full Navier-Stokes code. Downstream of the leading edge, a flat pressure distribution is of the most interest. Perhaps vary Re/1 for a fixed geometry, and look around Mach 2 to 3.5. Identify favorable or unfavorable combinations of Re/1 and leading-edge radius/chord.

5. Perform a study similar to 4. above with swept infinite wings to identify any sweep effects. The most desirable data is in the 40° to 60° sweep range, from Mach 2 to 3.5.

6. Perform a study of crossflow effects in 3-D concave regions at supersonic speeds. This study would be similar to the one done by Kohama[21] but at supersonic Mach number. This would establish any new physics brought about by compressibility effects.

WIND-TUNNEL TESTS:

1. Test a swept cylinder in an environmental tunnel with insects introduced into the flow upstream. Vary the sweep angle and determine the catch efficiency as a function of leading-edge sweep angle and other parameters. The test insects (real or simulated) should cover the range of ballistic coefficients of real insects. The data would be used to corroborate theoretical results, and possibly to improve the theoretical model.

2. If necessary, conduct simple impact tests to determine a normal-velocity criterion for insect remains deposition.

3. Plan and conduct a half-span supersonic test on an appropriate wing planform for the empirical development of the following items:
   1. supersonic turbulence diverters,
   2. laminar sweep-break geometries, and
   3. devices for turbulent wedge minimization.

4. Conduct a series of tests to measure supersonic leading-edge bluntness effects on boundary layer stability and transition. These data would be used to substantiate theoretical analyses (item 5, ANALYSIS).

5. Conduct a supersonic research test to substantiate the results of analysis (item 6) regarding the effects of boundary layer crossflow in concave regions.

6. Use a low-speed tunnel test to develop concepts for contamination-avoidance on the modified wing of whatever airplane is to be used for supersonic LFC flight tests. The 2-D approaches used in the past for subsonic airplanes may not work well enough on a highly swept supersonic wing.

7. Low-speed, subsonic, and supersonic testing may be necessary in order to establish the acceptability of the aerodynamic characteristics of the modified airplane to be used for LFC flight tests.

FLIGHT TESTS:

It is assumed that all flight tests will be conducted using a single modified airplane. The overall objective of the flight testing is to establish that supersonic LFC is in fact achievable and can be made practical.

1. Verify the effectiveness of turbulence diverters, laminar leading-edge sweep break geometry, and turbulent wedge control devices. Establish any limitations in their operation.

2. Conduct a series of tests to establish data for supersonic step, gap, and roughness criteria at different Mach numbers. Determine the validity of theoretical estimates.

3. Verify contamination system effectiveness, and continue development of these technologies.

4. Confirm the correctness of leading-edge radius criteria for the supersonic outer wing panel.

5. Using high-response acoustic sensors, determine the amplitude and frequency spectrum of noise in the laminar wing boundary layer at several key locations. With a loudspeaker mounted at an appropriate axial station on the fuselage, attempt to change measured transition locations by acoustic means. Determine whether or not noise radiated from the fuselage is a concern.

6. Through comparisons with Euler code predictions, verify the extent of attachment line travel with angle of attack on the highly swept subsonic leading-edge part of the wing.

97

13. TEST FACILITIES

13.1 SUPERSONIC WIND TUNNELS:

With the exception of the NASA LaRC 3.0 ft x 7.5 ft subsonic low turbulence wind tunnel, the 8 ft transonic facility at LaRC, the 10 in x 6 in M = 3.5 Beckwith quiet tunnel at LaRC, and the recently activated 1.0 ft quiet trisonic facility at NASA Ames, most wind tunnels in the U.S. are ill-suited for most laminar flow investigations because of test section noise and unsatisfactory turbulence levels. Supersonic wind tunnels tend to be even more noisy and turbulent; however, certain types of laminar flow testing have been successfully completed at supersonic Mach numbers. In the early 1960s, scale model tests were run at Mach numbers from 2.0 to 4.0 in the AEDC tunnel A facility on flat plates, a parabolic nose body of revolution and two swept wing planforms with and without suction to determine whether laminar flow is attainable via suction applied through a series of spanwise slots[7]. Full chord laminar flow was apparently achieved in these tests when suction was applied in this manner.

13.2 FLIGHT TEST VEHICLES:

Several supersonic aircraft could be made available as a supersonic test bed. These would include the F-106, F-15, F-16XL, and F/A-18. Since engines and other aircraft hardware and support equipment may become progressively more scarce on the F-106 aircraft, our study was limited to the three more recent aircraft. Figure 13.1 compares some of the more relevant physical characteristics and performance capabilities of the supercruise study aircraft, the AST, the SF-1302 and SF-1107, with those of the F-16XL, F-15 and F/A-18. The F/A-18 would appear to be less desirable than either the F-15 or F-16XL due to its M_{max} of 1.7 and its low wing sweep which would limit the supersonic flight testing to the supersonic leading edge condition.

Both the F-15 and F-16XL would appear to be reasonable testbeds for supersonic LFC testing. A comparison of the flight test potential of these two aircraft is shown in figure 13.2. The F-15 has a M_{max} = 2.2 capability whereas the F-16XL has M_{max} of approximately 2.0. However the F-16XL offers much improved time at supersonic speeds, and has a planform which is more representative of long range supercruiser concepts. A planform comparison of the candidate testbed aircraft and study fighter aircraft is shown in figure 13.3. The AST planform is geometrically similar to that of the SF-1302, so is not shown. As was noted earlier, the highly swept subsonic leading edge is the approach of choice for long range supercruisers due to better drag due-to-lift characteristics, and since any LFC benefit would otherwise have to overcome the inferior performance of the supersonic leading edge in order to show a net improvement. The high inboard leading edge sweep of the F-16XL is therefore an essential feature. Another valuable feature of the F-16XL is its relatively simple geometry, and location of the inlet below the fuselage. This allows for reduced uncertainty in computing the wing flowfield.

AIRCRAFT	SW (sqft)	$\bar{C}$ (ft)	AR	L.E. (deg.)	--TIME AT M (MIN)-- Mach 1.5	--TIME AT M (MIN)-- Mach 1.8	M_{max}
DAC AST	10 000	64.8	1.84	71/61.5	----	----	2.20
SF-1107	530	15.4	2.75	32	----	----	2.20
SF-1302	630	24.1	1.89	71/61.5	----	----	2.20
F/A-18	400	11.5	3.52	27	11.3	----	1.71
F-15A	608	16.0	3.01	45	9.5	5.6	2.4
F-16XL	663	24.7	1.58	70/50	42	21	2.0

Figure 13.1   COMPARISON OF STUDY AND POSSIBLE TESTBED AIRCRAFT

Aircraft	Flight Test Potential	Notes
F-15	• Supersonic Flight Testing From Mach 1.0 Through Mach 2.2 With Limited Testing at Mach 2.4 • Both Subsonic and Supersonic Leading Edge Testing Possible • Wing Planform Fairly Representative of SF-1107 Supercruise Configuration	• Leading Edge Root Extensions Provide Excellent Location for Suction Pumps and Plumbing • Relatively Thick Airfoil Provides Good Depth in Which to House the Suction Flutes and Plenums Required to Route Bleed Air to Suction Pumps
F-16XL	• Supersonic Flight Testing From Mach 1.0 Through Mach 2.2 • Subsonic Leading Edge Testing • Wing Planform Fairly Representative of SF-1302 Supercruise Configuration and the DAC Supercruise Transport • Testing of Leading Edge Break Is Possible	• Will Probably Be More Available for LFC Testing Than Other Aircraft

GP83-0447-2-T

Figure 13.2   COMPARISON OF POTENTIALS OF F-15A AND F-16XL
AIRCRAFT AS TESTBEDS

100
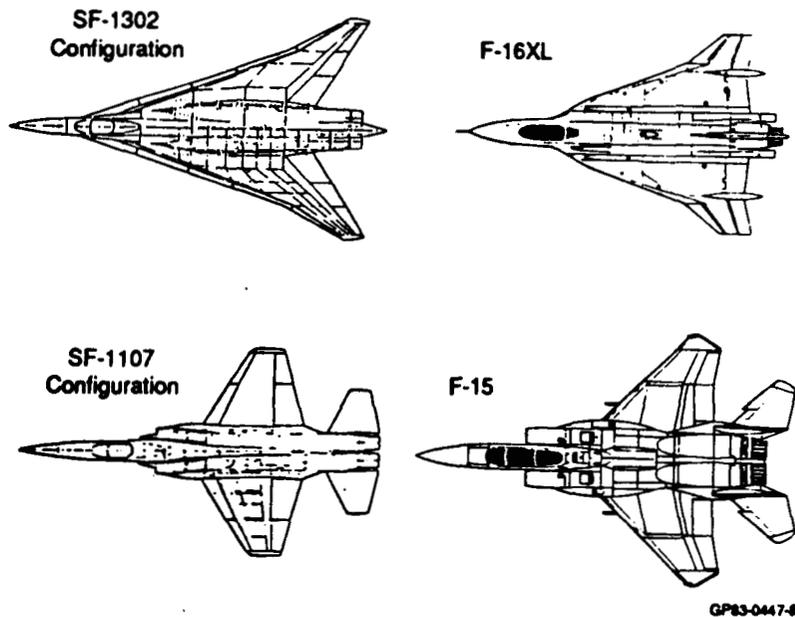
Figure 13.3   PLANFORMS OF STUDY AND POSSIBLE TESTBED AIRCRAFT

Dynamic similarity to transport scale aircraft is partially served by the high dynamic pressure capability of fighter aircraft, which allows high unit Reynolds numbers. Specific similarity issues like the attachment line can readily be resolved by design of the glove test article. A possible glove concept is shown in figure 13.4. The local leading edge unsweep near the bodyside allows experimentation with various supersonic turbulence diverter concepts. The presence of a leading-edge sweep break and supersonic leading-edged wingtip provide an opportunity to probe laminarization issues related to this type of geometry, an added plus. If hardware problems can be resolved, the F-16XL is the clear choice for a supersonic LFC testbed.

101
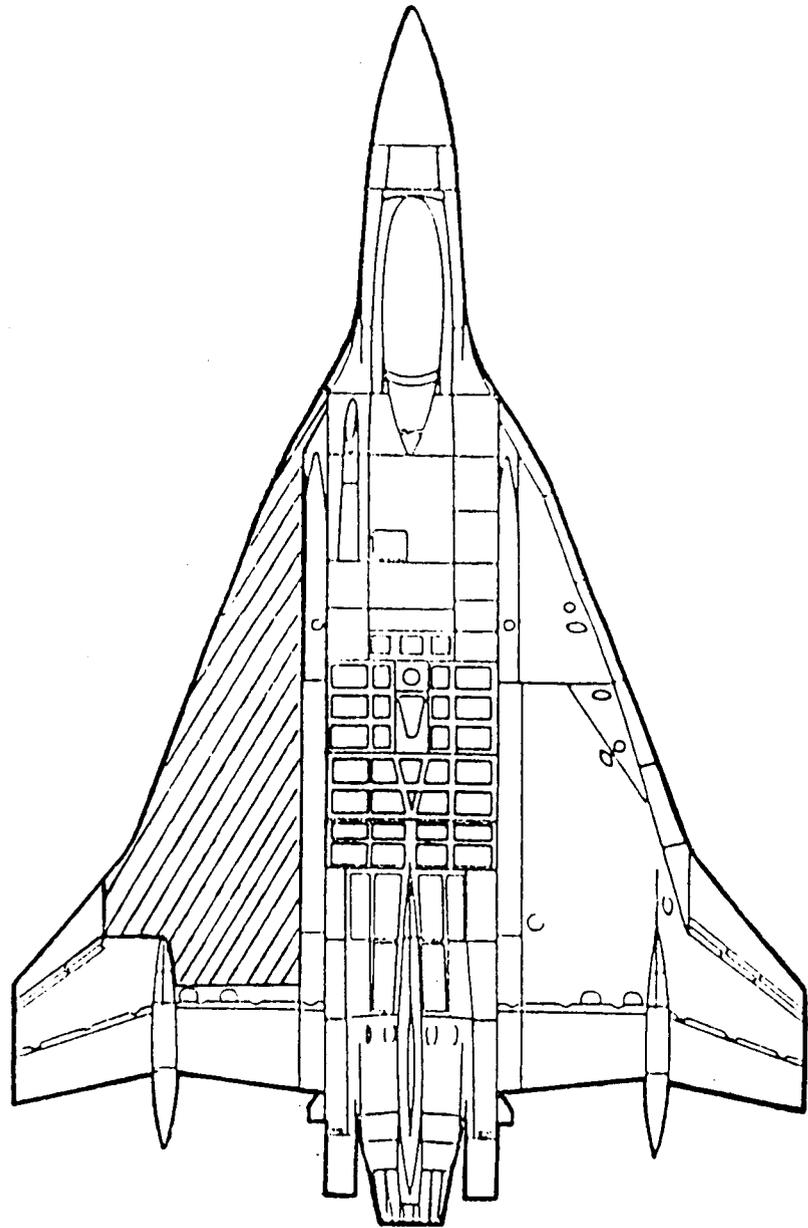
Figure 13.4   F-16XL WITH LFC GLOVE

14. CONCLUDING REMARKS

This study represents a first attempt to apply Laminar flow control methodologies developed for subsonic and transonic swept wings to the problem of achieving extensive regions of laminar flow on airplanes designed to cruise efficiently in the supersonic regime. As such, it tested and extended the capabilities of the current methods, pointed to needed improvements, and indicated technical areas ripe for theoretical and experimental investigation.

The results of this study indicate that supersonic LFC is technically feasible, and is a viable way of providing substantial fuel burn and sizing improvements. Significant technical issues remain, however, which need to be pursued vigorously. If commercial supersonic transports remain the technological hostages of arbitrary regulations on such things as jet noise and sonic boom, this study will at least have added to our general LFC knowledge base. Significant spinoffs include an improved way of calculating the attachment line momentum-thickness Reynolds number, a complete understanding of proper LFC drag accounting and pumping system thermodynamics, and some important insights into the nature of T-S and crossflow waves in 3-D boundary layers.

The weight, cost, and maintenance requirements of the LFC suction system comprise the bulk of the economic risk as seen by airframe manufacturers and operators. These are all minimized when suction massflow is minimized. In both subsonic and supersonic cases this requires careful and precise control of the wing pressure distribution. Particularly at higher Mach numbers, control of low levels of boundary layer crossflow is the key to minimizing suction. To accomplish this for the supersonic case requires aerodynamic design capability beyond what is currently available.

Although for subsonic and transonic wing design, inverse methods, in which the designer specifies the desired pressure field, and the corresponding wing geometry is computed, have achieved a high degree of sophistication and accuracy, the same cannot be said for supersonic wing design methods. State-of-the-art Euler codes currently operate only in the forward or analysis mode; no 3-D inverses exist. For the potential methods, due to the elegance with which velocities are represented, the creation of inverse design codes has proven to be relatively straightforward, yet no such simplifications appear to apply to the Euler formulations. The Euler is a necessity if shock waves or vorticity exist in the region of interest. However, it is not clear that vorticity behind curving shockwaves is a significant effect in the supersonic flow over a wing-body configuration, if the body is sufficiently sharp and slender, and the wing leading edge is either subsonic or sharp. It may therefore be possible to get the desired capability without going to a full Euler inverse. Since the influence of the fuselage on the wing pressure field is substantial in supersonic flow, it is necessary to design the wing in the presence of the fuselage. While developing this design capability is a difficult task, it is within the realm of possibility, and would move us closer to the goal of designing optimum configurations, allowing the minimization of economic risk associated with the application of LFC technology.

103

REFERENCES

1. Graf, D.A.: "High-Speed Commercial Transportation and the Pacific Rim Focus", Douglas Paper 7960, presented to Commercial Aviation in the Pacific Rim Conference, Hong Kong, September 14-16, 1987.

2. Wagner, R.D., Maddalon, D.V., Bartlett, D.W., and Collier, F.S.: "Fifty Years of Laminar Flow Flight Testing", presented to SAE Aerotech '88 Aerospace Technology Conference and Exposition, Anaheim, California October 3-6, 1988.

3. Harvey, W.D. and Bobbitt, P.J.: "Toward Lower Drag With Laminar Flow Technology", ICAS-88-4.1.2, Presented to 16th Congress of the International Council of the Aeronautical Sciences, Jerusalem, Israel, August 28 - September 2, 1988.

4. Anon.: "Research in Natural Laminar Flow and Laminar-Flow Control", NASA CP-2487, Proceedings of Symposium held at Langley Research Center, Hampton, Virginia., March 16-19, 1987.

5. Groth, E.E.: "Low Drag Boundary Layer Suction Experiments on a 5% Thick Biconvex Airfoil Section at M = 2.23 and 2.77", Northrop Report NAI-58-195 or BLC-105, March 1958.

6. Pate, S.R. and Brillhart, R.E.: "Investigation of Boundary-Layer Transition on Swept Wings at Mach Numbers 2.5 to 5", AEDC-TDR-63-109, July 1963.

7. Groth, E.E., Pate, S.R., and Nenni, J.P.: "Laminar Flow Control at Supersonic Speeds", AGARDograph 97, Part IV, Section B, May 1965.

8. Bushnell, D.M., Malik, M.R., and Harvey, W.D.: "Transition Prediction in External Flows via Linear Stability Theory", Presented to IUTAM Symposium Transonicum III, Gottingen, West Germany, May 24-27, 1988.

9. Srokowski, A.J., and Orszag, S.A.: "Mass Flow Requirements for LFC Wing Design", AIAA Paper 77-1222, August 1977.

10. Dagenhart, J.R.: "Amplified Crossflow Disturbances in the Laminar Boundary Layer on Swept Wings with Suction", NASA TP-1902, November 1981.

11. Malik, M.R.: "COSAL - A Black Box Compressible Stability Analysis Code for Transition Prediction in Three-Dimensional Boundary Layers", NASA CR-165925, May 1982.

12. Jameson, A.: "A Vertex Based Multigrid Algorithm for Three-Dimensional Compressible Flow Calculation", presented at the ASME Symposium on Numerical Methods for Compressible Flow, Anaheim, California, December, 1986.

105

13.   Kaups, K. and Cebeci, T.: "Compressible Boundary Layers with Suction
       on Swept and Tapered Wings", J. Aircraft, Vol. 14, 1977.

14.   Morkovin, M.V.: "Instability, Transition to Turbulence and
       Predictability", AGARDograph No. 236, 1978.

15.   Bacon, J.W. and Pfenninger, W.: "Transition Experiments at the Front
       Attachment Line of a 45 degree Swept Wing with a Blunt Leading
       Edge", Technical Report AFFDL-TR-67-33, June 1967.

16.   Shapiro, A.H.: The Dynamics and Thermodynamics of Compressible
       Fluid Flow, Vol II, pp. 706-709, The Ronald Press Co., New York,
       Copyright 1954.

17.   Anon.: "Supersonic Cruise Research '79", NASA CP 2108, Proceedings
       of a Conference held at Langley Research Center, Hampton, Virginia,
       November 13-16, 1979.

18.   Douglas Aircraft Co.: "Technology Study for Advanced Supersonic
       Cruise Vehicles", NASA CR-165723, June 1981.

19.   Halsey, N.D. and Zaretsky, B.: "Grid Generation for NASP
       Configurations", MDC report in preparation.

20.   Collier, F.S. Jr. and Malik, M.R.: "Stationary Disturbances in Three
       Dimensional Boundary Layers Over Concave Surfaces", AIAA-87-1412,
       Presented to AIAA 19th Fluid Dynamics, Plasma Dynamics, and Lasers
       Conference, June 8-10, 1987.

21.   Kohama, Y.: "Three-Dimensional Boundary Layer Transition on a Curved
       Wall", Presented at the IUTAM Symposium on Turbulence Management and
       Relaminarization, Bangalore, India, January 19-23, 1987.

22.   Collier, F.S. Jr., Bartlett, D.W., and Wagner, R.D.: "Curvature
       Effects on Swept Wing Boundary Layer Stability-Theory and
       Experiment", Presented to SAE Aerotech '88, Anaheim, California,
       October 3-6, 1988.

23.   Reshotko, E. and Beckwith, I.E.: "Compressible Laminar Boundary
       Layer over a Yawed Infinite Cylinder with Heat Transfer and
       Arbitrary Prandtl Number", NASA TR-1379, 1958.

24.   Fischer, M.C., "Spreading of a Turbulent Disturbance", AIAA Journal,
       Vol. 10, No. 7, pp. 957-959, July 1972.

25.   Pfenninger, W. and Vemuru, C.S.: "Design aspects of Long Range
       Supersonic LFC Airplanes with Highly Swept Wings", SAE Technical
       Paper 881397, Presented at SAE Aerotech '88, October, 1988.

26.   Douglas Aircraft Co.: "Evaluation of Laminar Flow Control Systems
       Concepts for Subsonic Commercial Transport Aircraft", NASA
       CR-159251, June 1983.

27.   Verhoff, A. and O'Neil, P.J.: "Accurate, Efficient Prediction Method
        for Supersonic/Hypersonic Inviscid Flow", McAir Paper 87-006,
        Presented at the AIAA 19th Fluid Dynamics, Plasma Dynamics and
        Lasers Conference, Honolulu, Hawaii, June 8-10, 1987.

28.   Jones, D.J.: "Numerical Solutions of the Flow Field for Conical
        Bodies in a Supersonic Stream", National Research Council of Canada
        Aeronautical Report LR-507, July 1968.

29.   Lekoudis, S.G.: "Stability of Three-Dimensional Compressible
        Boundary Layers over Wings with Suction", AIAA paper No. 79-0265,
        January 1979.

30.   Hefner, J.N., and Bushnell, D.M.: "Status of Linear Boundary-Layer
        Stability Theory and the e^N Method, with Emphasis on Swept-Wing
        Applications", NASA TP-1645, April 1980.

APPENDIX A

LFC DRAG ACCOUNTING AND
PUMPING SYSTEM THERMODYNAMICS

The intent of this appendix is to explain the logic behind a system of drag accounting and a pumping system thermodynamics algorithm for LFC which was developed and used in the course of this study on supersonic LFC. The entire algorithm is applicable to the subsonic case with essentially no modification, and allows optimization of the LFC pumping system for minimum total fuel flowrate. This approach, unlike earlier ones, makes no idealizations, allowing correct and detailed accounting for all loss mechanisms.

Figure A1 shows the control-volume momentum equation. According to this equation, the drag can be computed either using the control volume approach, as is commonly done subsonically, or by integrating pressure and skin friction over the surface in the appropriate fashion. The important message of this figure is that viscous drag + pressure drag = wake drag + suction ram drag. The control volume approach is abandoned for the supersonic case, since pressure drag is relatively easy to calculate, and the control volume momentum integration is much more cumbersome due to shocks, expansions, etc. For the supersonic case, if the control volume approach is not used one should not expect to see a ram drag. As will be shown, the suction ram drag is accounted for as part of the viscous drag.

Figure A2 shows the variation of various drags with suction for a laminar flat plate. The calculations were made using Cebeci & Kaups' strip-theory boundary layer program, BLP, which is a well proven and trusted code at DAC. Plotted versus suction coefficient are the four drags, each computed independently in the correct fashion. Note that the sum of viscous drag and pressure drag is identical to the sum of wake drag and suction ram drag, as the control-volume momentum equation demands. A subsonic wing section would be expected to have similar characteristics, since the pressure drag is small.

Figure A3 shows the various drag components computed <u>for one side</u> of a symmetric biconvex airfoil at Mach 2.2 and zero angle of attack. Note that the pressure drag is almost unaffected by the boundary layer, either transition location or wall suction, so the suction ram drag component is essentially accounted for in the viscous drag component entirely. If the wake drag is backed out by subtracting the suction ram drag from the total drag, the result is physically reasonable, as comparison with the flat plate result (figure A2) shows. The much higher wake drag is expected, due principally to total pressure losses in the shocks.

109

EFFECT OF AIRFLOW ON WING SECTION = EFFECT OF WING SECTION ON AIRFLOW

$$\Sigma \vec{F} \qquad = \qquad \frac{\partial}{\partial t} \iiint_{CV} \rho \vec{v} \, dV \; + \; \oiint_{CS} \vec{v}\left(\rho \vec{v} \cdot d\vec{A}\right)$$

EQUIVALENT
TO

RAM
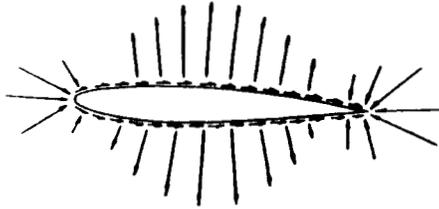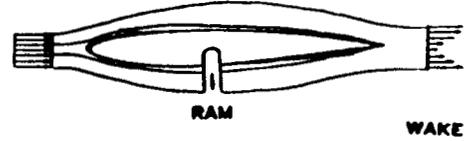
WAKE

$$D_{TOTAL} = D_V + D_P \qquad\qquad \textbf{EQUIVALENT} \qquad\qquad D_{TOTAL} = D_{RAM} + D_{WAKE}$$
TO

EFFECTS OF INCREASED
SUCTION ARE SEEN AS
INCREASED C_F.
VERY SMALL EFFECT ON D_P

THERE EXISTS NO DRAG
THAT CAN BE NEATLY CATEGORIZED
AS SUCTION RAM DRAG!

BETTER FOR SUPERSONIC CASES

EFFECTS OF INCREASED SUCTION
ARE DECREASED WAKE DRAG
& INCREASED SUCTION RAM DRAG

BETTER FOR SUBSONIC CASES

Figure A1   LFC WING DRAG ACCOUNTING

MACH = 0.22   Re = 50 million
Cd visc + Cd pres = Cd suction ram + Cd wake ??

● VISCOUS (INTEGRATED Cf)
— WAKE + SUCTION RAM

SUCTION RAM (2 × Cq)

WAKE (SQUIRE-YOUNG)

PRESSURE (= 0)

DRAG COEFFICIENT, Cd

SUCTION COEFFICIENT, Cq
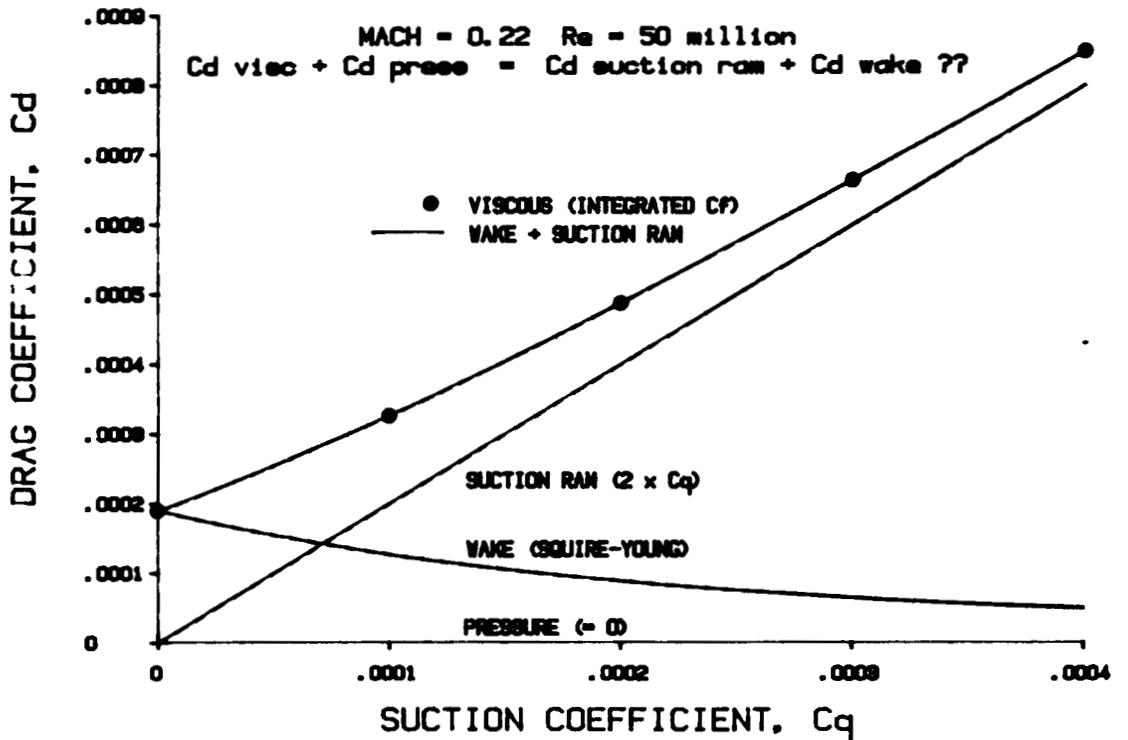
Figure A2   FLAT PLATE DRAGS VS. SUCTION

110

ONE SURFACE MACH = 2.2 Rc = 29 million
t/c = 2.5% @ 65% CHORD

EFFECT OF TRANSITION LOCATION

EFFECT OF SUCTION
SUCTION & L.F. TO 65% CHORD
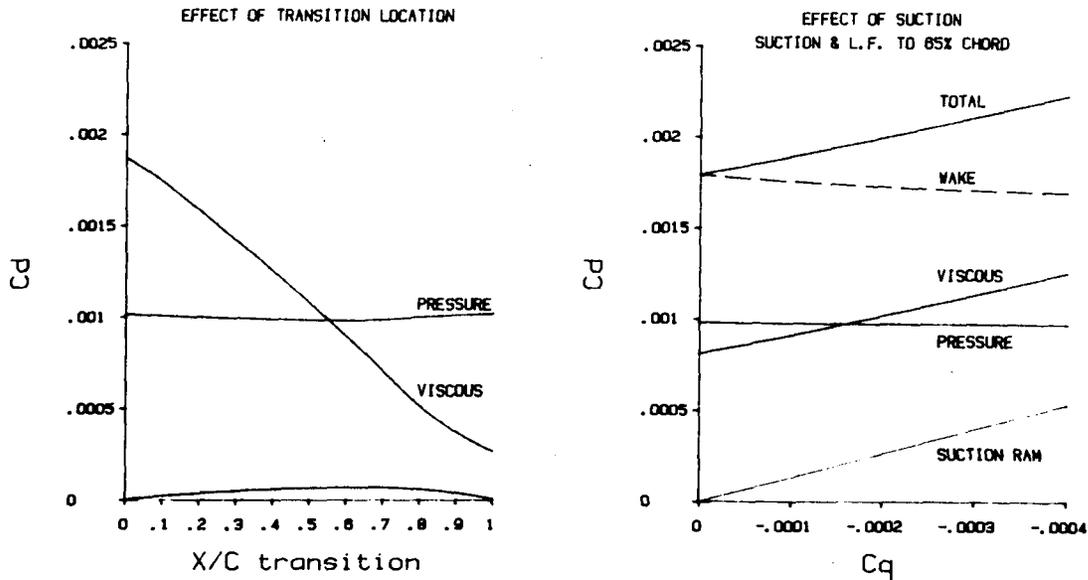
Figure A3   SUPERSONIC SYMMETRIC AIRFOIL

For both subsonic and supersonic cases, the additional drag due to
suction equals the product of suction massflow with freestream velocity.
Whether this is accounted for inside the pumping system calculation or
externally as part of the aerodynamic drag is entirely arbitrary; the end
result of the calculations is identical. In this analysis, the additional
drag due to suction is left as part of the aerodynamic drag, so no momentum
loss terms appear in the pumping system thermodynamic analysis. Separating
the ram drag from the thermodynamic analysis is acceptable at any speed since
the suction airflow is set by laminarization requirements, and does not vary
with engine thrust. With the pumping system rid of the ram penalty, it can
look exceptionally good in comparison to the thrust engines. With this
accounting system, the pumping system functions as a rocket engine with a
fixed massflow supply of free propellant. Of course, work must be done on
this air. Just how much work is optimal is the subject of the thermodynamic
analysis.

111

In the thermodynamics analysis, the suction air is brought in through the porous skin, passes through ducting to a compressor, and then is ejected aft through an optimally expanded nozzle. An important indicator of performance is what we have termed the pumping system efficiency, defined as the ratio of nozzle thrust power to system input shaft power. Inasmuch as this definition is identical to that of a propeller efficiency, it is useful to consider simple actuator-disk momentum theory as a guide to interpreting the correctness of the thermodynamic model. This is summarized in figure A4 below. The ideal actuator disk differs from a real propeller in that the exit flow has no swirl, so only axial velocities are considered. Also the input shaft power is equal to the rate of production of kinetic energy of the air passing through the disk. In the figure, the ideal actuator disk efficiency is derived for two cases: the typical propeller, in which the velocity into the disk is the freestream velocity, and the LFC pumping case, in which this velocity is zero. The speed used in computing the thrust power is still the freestream velocity. For the propeller case, the ideal propulsive efficiency has a theoretical maximum of 2 at zero exit velocity, but the disk only produces net thrust for exhaust velocities greater than freestream. The efficiency is therefore always less than 1 if the disk is producing thrust. For the LFC pumping case, we are only concerned with gross thrust, since the momentum inflow into the disk is zero. The ram drag penalty for collecting the suction air has already been paid elsewhere in the form of increased drag over the wing surface. For this basic reason, the ideal propulsive efficiency is higher. In the thermodynamic model, the pumping system efficiency should reflect this. We should expect the thermodynamic model to recover the dependence shown by the upper curve in the figure, if all component efficiencies are set to 1, and there is no pressure drop in the ducting or skin.

DEFINE PUMPING SYSTEM EFFICIENCY, $\eta_{PS} = \dfrac{T\,V_{fs}}{P_{in}} = \eta_{prop}$

IDEAL ACTUATOR DISK: NO SWIRL => P_{in} = RATE OF INCREASE OF PROPELLANT K.E.

PROPELLER: $V_i = V_{fs}$

$$\eta = \frac{\dot{M}\,(V_e - V_i)\,V_{fs}}{\dot{M}\,(V_e^2/2 - V_i^2/2)} = \frac{2}{\dfrac{V_e}{V_{fs}} + 1}$$

LFC PUMPING SYSTEM: $V_i = 0$

$$\eta = \frac{\dot{M}\,V_e\,V_{fs}}{\dot{M}\,V_e^2/2} = \frac{2}{V_e/V_{fs}}$$
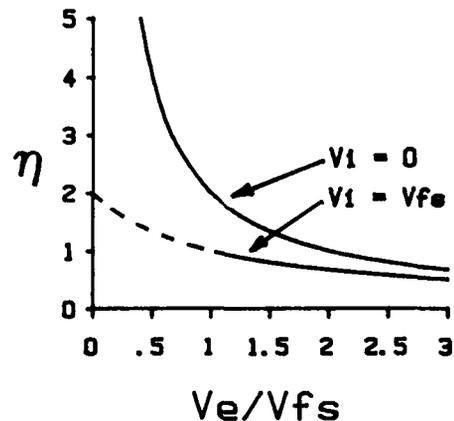
Figure A4   LFC PUMPING SYSTEM MODEL - IDEALIZED

112

Figure A5 shows some sample results from the pumping system thermodynamics calculation. The solid curve (labelled "ideal") demonstrates that the thermodynamic model does indeed recover the actuator disk result under zero loss conditions. The results shown in the figure assume that pump power is extracted from the main thrust engines, so the pumping system input power is shaft power. The level at which the pumping system's overall efficiency equals that of the thrust engines depends on the product: PSFC * V / TSFC. With the values used in this example, the break-even point occurs at an ordinate value of 1.0, which is equivalent to saying that the thermal efficiency for extracted power is equal to the thrust engine's overall efficiency, a conservative assumption. A better assumption is that the thermal efficiency for shaft power extraction is equal to the thermal efficiency of the installed engine. In any event, if the power comes via an engine-mounted alternator and electric motor, the electomechanical conversion efficiencies will lower the pumping system efficiency proportionally.

The amount of total pressure loss between the wing skin and the compressor has a first-order effect on the pumping system performance. The average collection pressure is also an important driver with high collection pressure having a favorable effect. The average collection Cp was taken as 0 for these curves. For maximum suction system performance, the wing suction surface should be divided into two or three collection pressure "zones". Air from each zone could be pumped to a different optimum pressure ratio, and discharged through a separate nozzle. It is important to realize, however, that the optimum pumping system performance as indicated above pertains to the system in isolation. The optimum performance for the LFC airplane is addressed below.
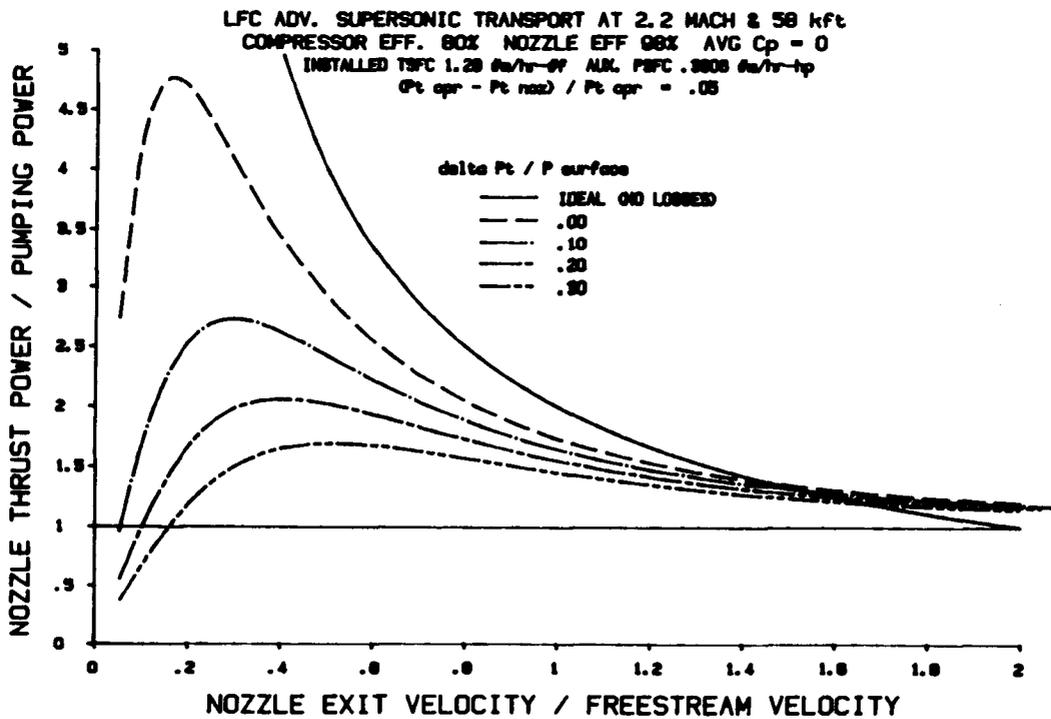

Figure A5 THERMODYNAMIC PERFORMANCE OF LFC SYSTEM

Optimum performance for the airplane is achieved when the pumping system is operated such that airplane overall fuel flow is minimized. This is explained in figure A6. The total fuel flowrate is expressed in terms of a thrust specific fuel consumption (TSFC) times the total thrust required, plus a power specific fuel consumption (PSFC) times the total auxiliary shaft power required. Note that the LFC system nozzle thrust reduces the propulsive fuel flow. With some rearrangement, and the introduction of the pumping system efficiency, an expression is obtained which represents the drag equivalent of the fuel flow increment due to the suction system. This appears in drag coefficient form as the second additive term in the denominator of the boxed expression for airplane L/D. This equivalent drag increment is negative if the pumping system efficiency is greater than the quantity: (PSFC * V) / TSFC. This is satisfied when the curves in figure A5 lie above the solid horizontal line, and means that in terms of fuel flow, the nozzle thrust has paid for the pumping power with some excess thrust left over. Examination of the ideal (zero loss) case reveals that the magnitude of this effective drag reduction is always less than the additional skin friction drag due to suction. This is because some power is necessary to drive the compressor, and is one reason it is desirable to minimize the suction flowrate in LFC design.

The straight breakeven line on the plot of figure A5 is somewhat of an idealization, since both TSFC and PSFC would be expected to vary with shaft power extraction, as well as thrust and flight conditions. In this connection, an accurate model of the thrust engine cycle would be a necessary part of any detailed analysis.

ASSUMPTION : SUCTION AIR IS COMPRESSED, THEN EJECTED AFT THROUGH A NOZZLE.

WANT TO MINIMIZE TOTAL FUEL FLOW :

$$\dot{M}_f = TSFC\ (\ D_{TOTAL} - T_{NOZZLE}\ ) + PSFC\ (\ P_{PUMP}\ )$$

$$\dot{M}_f = TSFC\ (\ D_{TOTAL} - T_{NOZZLE} + \frac{PSFC}{TSFC}\ P_{PUMP}\ ) = TSFC\ (\ D_{EFFECTIVE}\ )$$

INTRODUCE PUMPING SYSTEM EFFICIENCY : $\eta_{PS} = \frac{NOZZLE\ THRUST\ POWER}{PUMP\ INPUT\ POWER} = \frac{T_{NOZ}\ V}{P_{PUMP}}$

$$D_{EFF} = D_{TOTAL} + (\ \frac{PSFC}{TSFC} - \frac{\eta_{PS}}{V}\ )\ P_{PUMP}$$

SO.

$$\boxed{L/D_{EFF} = \frac{C_L}{C_{D\ TOTAL} + \left(\frac{PSFC\cdot V}{TSFC} - \eta_{PS}\right)\frac{P_{PUMP}}{S\cdot q\cdot V}}}$$

NOTE: IF $\eta_{PS} > \frac{PSFC\cdot V}{TSFC}$,

A NET FUEL SAVINGS RESULTS FROM ANY SUCTION SYSTEM NOZZLE THRUST! MORE FUEL EFFICIENT THAN THRUST ENGINES!

Any fuel flow minimum will occur when the fuel-equivalent drag increment is its most negative value. The presence of pumping power in the expression for fuel-equivalent drag increment means that the LFC airplane optimum nozzle exit velocity, if it exists, is higher than would be indicated by the maximum of the appropriate pumping system efficiency curve.

The fuel-equivalent drag increment is plotted in figure A7 for the same conditions as figure A5 for each skin-and-ducting total pressure loss. This represents, in drag coefficient form, the extent to which the pumping system nozzle thrust exceeds the drag equivalent of the LFC pumping power. For an ideal case, in which compressor and nozzle efficiencies are unity, and there are no total pressure losses in the system, the optimum exists at an exit velocity ratio of unity, if (PSFC * V)/TSFC = 1. If (PSFC * V)/TSFC < 1, the optimum is found at higher exit velocity ratio.

For the realistic example there is no optimum, although all of the curves show a stationary region slightly above an exit velocity ratio of unity. This is due to the greater heating of the air in the nonisentropic compressor. This effect only becomes pronounced at the higher velocity ratios, where nozzle total temperature plays an increased role in determining the thrust.

Lastly, a program, written in IBM BASIC-A has been created and is included as figure A8. The approach taken is to set the freestream conditions, compressor and nozzle efficiencies, total pressure losses, collection pressure coefficient, etc. and parametrically vary the nozzle total pressure ratio, Pt3/Ptfs. The nozzle is assumed to be optimally expanded, and aimed directly aft.
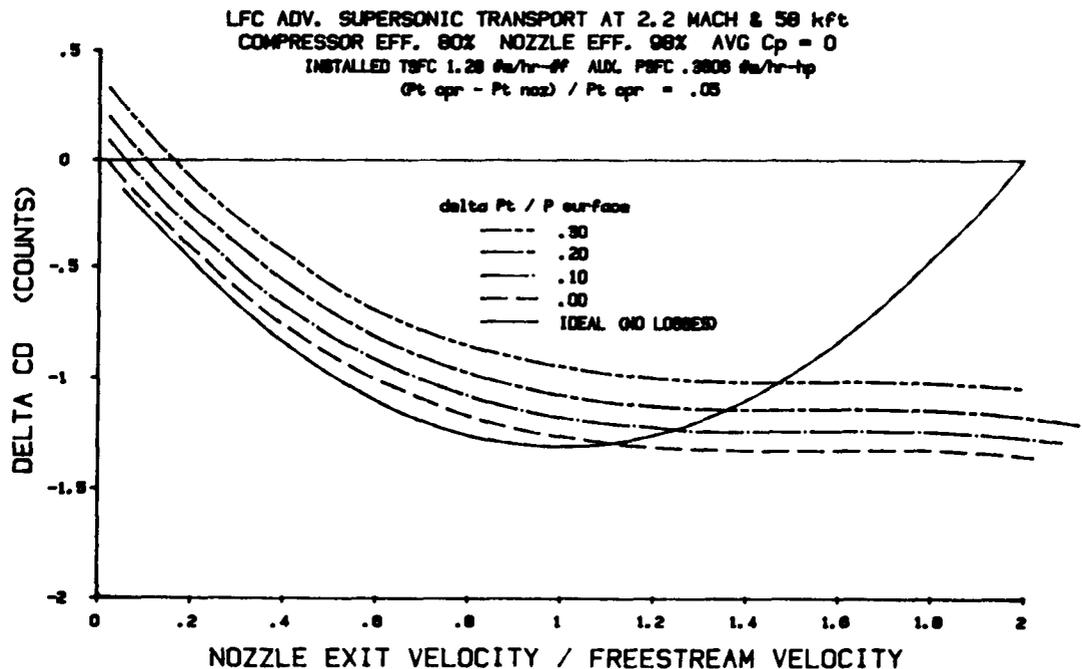

Figure A7   FUEL-EQUIVALENT DRAG INCREMENT DUE TO LFC PUMPING

115

```
10   PRINT "PROGRAM LFCEXH BAS"
20   PRINT "LFC PUMPING SYSTEM THERMODYNAMICS AND DRAG ACCOUNTING"
30   PRINT ""
40   PRINT "ASSUMPTIONS:"
50   PRINT "LFC COMPRESSOR IS DRIVEN ELECTRICALLY OFF OF MAIN THRUST ENGINES "
60   PRINT "LFC EXHAUST NOZZLE IS OPTIMALLY EXPANDED AND AIMED DIRECTLY AFT "
70   PRINT ""
80   PRINT "STATIONS:  1-SKIN, 2-CPR IN, 3A-CPR OUT, 3-NOZ IN, E-NOZ EXIT"
90   PRINT ""
100  PRINT "-- SET KEYBOARD ALL CAPS --"
110  CP=6007.1:R=1716.3:TF=390
120  VRAM=0                            :REM VRAM=VR=VF IF RAM CHARGED TO PUMPING SYS
130  EA=1:EM=1
140  PRINT ""
150  PRINT "EDIT PGM LN 130 TO CHG ALTERNATOR OR MOTOR EFFICIENCY. DEFAULT=1.0"
160  PRINT "FOR DIRECT SHAFT DRIVE SET ALT EFF=1. USE MOTOR EFF AS GEARBOX EFF "
170  PRINT ""
180  PRINT "****** INITIAL INPUTS ************"
190  INPUT "COMPRESSOR EFFICIENCY (DECIMAL FRACTION) = ";EC
200  INPUT "NOZZLE EFFICIENCY = ";EN
210  INPUT "FREESTREAM MACH NUMBER = ";M
220  INPUT "WING SURFACE-TO-COMPRESSOR LOSS. (P1-Pt2)/P1 = ";R1DP
230  INPUT "COMPRESSOR-TO-NOZZLE LOSS. (Pt3A-Pt3)/Pt3A = ";RDP3
240  INPUT "AVG SURFACE Cp = ";PC
250  IF PC<(-1/(.7*M^2)) THEN PRINT "GIVEN Cp IS BELOW VAC LIMIT":GOTO 240
260  INPUT "SPECIFY SKIN TEMP. OVERRIDING ADIABATIC WALL? (Y/N) ";TS
270  IF TS="Y" THEN INPUT "Tskin (R) =";T1
280  INPUT "CHARGE RAM DRAG TO PUMPING SYSTEM? (Y/N) ";RS
290  PRINT "****** RECURRING INPUTS ************"
300  INPUT "Ptnoz/Ptfs = ";R3FP
310  VF=M*SQR(1.4*R*TF)                          :REM Vfs
320  IF RS="Y" THEN LET VR=VF
330  RTF=1+.2*M^2                                :REM TTfs/Tfs
340  RPF=RTF^3.5                                 :REM Ptfs/Pfs
350  P1RF=1+PC*.7*M^2                            :REM Psrf/Pfs
360  T2T=TF*((1-SQR(.72))*P1RF^(1/3.5)+SQR(.72)*RTF)   :REM TT2=Tsrf=Taw
370  IF TS="Y" THEN LET T2T=T1
380  PEPT3=1/(R3FP*RPF)                          :REM Pfs/Pt3
390  P2TF=P1RF*(1-R1DP)                          :REM Pt2/Pfs
400  P3TF=1/PEPT3                                :REM Pt3/Pfs
410  PA3TF=P3TF/(1-RDP3)                         :REM Pt3A/Pfs
420  PR3A2=PA3TF/P2TF                            :REM Pt3A/Pt2
430  T3T=T2T/(1-1/EC*(1-PR3A2^(-1/3.5)))         :REM Tt3
440  IF PEPT3>1 THEN PRINT "TOO LOW.":GOTO 300
450  VE=SQR(2*EN*CP*T3T*(1-PEPT3^(1/3.5)))       :REM EXH VELOC
460  EPS=EA*EM*EC*VF/(CP*T2T)*(VE-VR)/(PR3A2^(1/3.5)-1):REM NZL THRSTPWR/CPR PWR
470  WMC=CP*(T3T-T2T)/32.1739                    :REM CPR W/M (ft-#f/#m)
480  RVEF=VE/VF                                  :REM NZL VELOC RATIO
490  TE=T3T-VE^2/(2*CP)                          :REM NZL EXIT STATIC TEMP
500  ME=VE/SQR(1.4*R*TE)                         :REM NZL EXIT MACH
510  PRINT "****** OUTPUTS *********************"
520  PRINT USING "COMPRESSOR PRESS RATIO = ###.####";PR3A2
530  PRINT USING "COMPRESSOR Tt OUT = #####.# deg R";T3T
540  PRINT USING "COMPRESSOR WORK/MASS = #######. ft-lbf/lbm";WMC
550  PRINT USING "NOZZLE Pt / Pfs = ###.####";P3TF
560  PRINT USING "NOZZLE EXIT MACH NUMBER = ##.####";ME
570  PRINT USING "NOZZLE Vexit / Vfs  = ##.####";RVEF
580  PRINT USING "NOZZLE THRUST POWER / COMPRESSOR POWER  =####.###";EPS
590  IF DS><"Y" THEN PRINT "****** END OF OUTPUTS ************"
600  IF DS="Y" THEN 720
610  INPUT "COMPUTE FUEL-EQUIV DELTA Cd  AND NOZZLE A exit? (Y/N)";DS
620  IF DS="Y" THEN 660
630  INPUT "NEW Pt noz /Pt fs ? (Y/N)";NS
640  IF NS><"N" THEN 290
650  GOTO 10
660  INPUT "TSFC OF THRUST ENGINES (#m/hr-#f) = ";FT
670  INPUT "PSFC FOR AUX POWER EXTRACTION (#m/hr-hp) = ";FP
680  INPUT "WING REFERENCE AREA. S ref (sqft) = ";S
690  INPUT "FS PRESSURE (PSFA) = ";PF
700  Q=.7*PF*M^2
710  INPUT "SUCTION MASSFLOW (#m/SEC) = ";MS
720  DCD=(FP/(FT*550)-EPS/VF)*WMC*MS/S/Q                    :REM PMP SYS CD INCR
730  AE=MS/32.1739*SQR(R*T3T)*(1+.2*ME^2)^3/(P3TF*PF*SQR(1.4)*ME)  :REM EXIT A
740  PWRC=MS*WMC/550
750  IF DS="Y" THEN PRINT "****** OUTPUTS ************"
760  PRINT USING "FUEL-BURN EQUIV CD INCREMENT = ##.########";DCD
770  PRINT USING "NOZZLE EXIT AREA = ####.### SQFT";AE
780  PRINT USING "COMPRESSOR SHAFT POWER INPUT = #####.# hp";PWRC
790  IF DS = "Y" THEN PRINT "****** END OF OUTPUTS ************"
800  GOTO 630
810  END
```

Figure A8   ALGORITHM FOR SUCTION SYSTEM DRAG ACCOUNTING

116

APPENDIX B

CALCULATION OF ISENTROPIC EQUIVALENT C_p FOR SUPERSONIC LEADING EDGES

For the case of the supersonic leading edge, the presence of a leading edge shock changes the nature of the external flow, particularly in the leading edge region. The Kaups-Cebeci conical boundary layer code computes external velocities from the input pressure coefficients, under the assumption of isentropic external flow. This is appropriate to the subsonic and transonic conditions for which the code was designed. On the attachment line, the total external velocity is known to have no component perpendicular to the attachment line, so the direction of the external velocity is known. From this point aft, the direction of the external total velocity vector is reckoned station-by-station, using the condition of irrotationality of flow in planes parallel to the local surface.

If the leading edge is supersonic, pressure coefficients computed using an Euler code will be correct for purposes of determining lift and drag, but will cause the K-C code to compute incorrect total velocities, since the isentropic assumption is violated by the presence of a leading-edge shock wave. One way of computing correct external flow velocities is to input to the K-C code the equivalent isentropic pressure coefficients corresponding to the correct but nonisentropic values computed by the Euler code. This approach was taken in the current study. The assumption used was that all air entering the boundary layer would have passed through the leading-edge-normal part of a detached shock, yawed to the onset supersonic stream by the leading edge sweep angle. Shock curvature near the leading edge is ignored. A simple program was written in IBM BASIC-A to compute the equivalent isentropic C_p values for input to the Kaups-Cebeci code. A listing of the program is given in figure B1.

```
10  PRINT "EQVISEN.BAS: EQUIVALENT ISENTROPIC CP FOR K-C B.L. INPUT"
20  PRINT "FOR SUPERSONIC LEADING EDGE"
30  REM ASSUMES ALL B.L. AIR TO PASS THRU L.E. NORMAL PART OF
40  REM DETACHED L.E. SHOCK.  SHOCK CURVATURE EFFECTS IGNORED.
50  PRINT "IDENTIFIERS: FS = FREESTREAM, 1 = JUST DOWNSTREAM OF SHOCK,"
60  PRINT "            L = LOCAL, N = LEADING-EDGE NORMAL, 2 = SQUARED"
70  PRINT ""
80  G=1.4                                              :REM GAMMA
90  INPUT "FREESTREAM MACH =";MFS
100 INPUT "L.E. SWEEP (DEG) =";SWPLED
110 SWPLER=SWPLED*3.141593/180                 :REM CONVERT TO RADIANS
120 MNFS2=(MFS*COS(SWPLER))^2                  :REM FS NORMAL MACH SQD
130 P1OPFS=1+2*G/(G+1)*(MNFS2-1)               :REM SHOCK PRESS RATIO
140 T1OTFS=1+2*(G-1)/(G+1)^2*(G*MNFS2+1)/MNFS2*(MNFS2-1) :REM SHOCK TEMP RATIO
150 M1N2=(1+(G-1)/2*MNFS2)/(G*MNFS2-(G-1)/2)     :REM DOWNSTREAM NORMAL MACH SQD
160 M1P2=(MFS*SIN(SWPLER))^2/T1OTFS   :REM DOWNSTREAM MACH PARALLEL TO L.E. SQD
170 M1TL2=M1N2+M1P2                             :REM DOWNSTREAM TOTAL MACH SQD
180 INPUT "PHYSICAL CP =";CP
190 IF MNFS2<=1 THEN CPS=CP:PRINT "SUBSONIC NORMAL FLOW":GOTO 250
200 ML2=2/(G-1)*((1+(G-1)/2*M1TL2)/((1+G/2*MFS^2*CP)/P1OPFS)^((G-1)/G) -1)
210 REM ABOVE IS LOCAL TOTAL MACH CORRESPONDING TO THE GIVEN CP.
220 TLOT1=(1+(G-1)/2*M1TL2)/(1+(G-1)/2*ML2)                :REM T LOCAL / T1
230 VLVFS2=ML2/MFS^2*TLOT1*T1OTFS          :REM VELOC RATIO (LOCAL TO FS) SQD
240 CPS=2/(G*MFS^2)*((1-(G-1)/2*MFS^2*(VLVFS2-1))^(G/(G-1)) -1)   :REM ISEN CP
250 PRINT USING "ISENTROPIC EQUIV CP =###.######";CPS
260 PRINT ""
270 INPUT "GIVE NEW CP (Y/N)?";CP$
280 IF CP$<>"N" THEN 180
290 GOTO 90
300 END
```

Figure B1   ALGORITHM TO COMPUTE EQUIVALENT ISENTROPIC
C_p FOR STABILITY ANALYSES, SUPERSONIC
LEADING EDGE CASE

Report Documentation Page

1. Report No.	2. Government Accession No.	3. Recipient's Catalog No.
NASA CR-181817		

4. Title and Subtitle		5. Report Date
Feasibility and Benefits of Laminar Flow Control on Supersonic Cruise Airplanes		July 1989
		6. Performing Organization Code

7. Author(s)	8. Performing Organization Report No.
A.G. Powell, S. Agrawal, and T.R. Lacey	
	10. Work Unit No.

9. Performing Organization Name and Address	505-60-41-01
McDonnell Douglas Corporation 3855 Lakewood Blvd. Long Beach, California 90846	11. Contract or Grant No.
	NAS1-18037
	13. Type of Report and Period Covered

12. Sponsoring Agency Name and Address	Contractor Report
National Aeronautics and Space Administration Langley Research Center Hampton, VA. 23665-5225	14. Sponsoring Agency Code

15. Supplementary Notes
Langley Technical Monitor: Dal V. Maddalon Final Report

16. Abstract

An evaluation was made of the applicability and benefits of Laminar Flow Control (LFC) technology to supersonic cruise airplanes. Ancillary objectives were to identify the technical issues critical to supersonic LFC application, and to determine how those issues can be addressed through flight and wind-tunnel testing.

Vehicle types studied include a Mach 2.2 supersonic transport configuration, a Mach 4.0 transport, and two Mach 2 - class fighter concepts. Laminar flow control methodologies developed for subsonic and transonic wing laminarization were extended and applied.

No intractible aerodynamic problems were found in applying LFC to airplanes of the Mach 2 class, even ones of large size. Improvements of 12 to 17 percent in lift-drag ratio were found. Several key technical issues, such as contamination avoidance and excresence criteria were identified, and recommendations are made for their resolution. A need for an inverse supersonic wing design methodology is indicated.

17. Key Words (Suggested by Author(s))	18. Distribution Statement
Laminar Flow Control Supersonic Cruise Airplanes Feasibility Benefit	Unclassified - Unlimited Subject Category 05

19. Security Classif. (of this report)	20. Security Classif. (of this page)	21. No. of pages	22. Price
Unclassified	Unclassified	119	